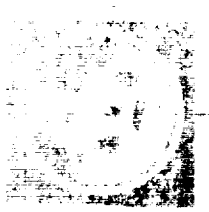

(R) FINAL REPORT
UNDER

Contract Number NAS8-11191

STUDY TO DETERMINE SUITABLE HIGH TEMPERATURE, HIGH ALTITUDE, TOTAL TEMPERATURE SENSORS

REC Report 11652B

Date: 5 November 1965

by

Richard V. DeLeo

and

A.E. Saari

Engineering [illegible]

[illegible] FINAL REPORT

[illegible]

Contract Number NAS8-11101

STUDY TO DETERMINE SUITABLE HIGH TEMPERATURE, HIGH ALTITUDE, TOTAL TEMPERATURE SENSORS

REC Report 71652B

1. INTRODUCTION.

Most atmospheric immersion type total temperature sensors are designed to measure total temperature under steady state conditions. Sensing element design for present units provide fast time constants. The units in flight follow the total temperature with fair accuracy and hence develop high temperatures at Mach number above 4.0. Generally, the construction of the units limits operation to 1500°C. The present units operating above Mach number 3.0 or above altitude of 100,000 feet require a correction of systematic errors due to radiation, conduction, time constant and recovery factor. The accuracy of the systematic correction decreases as the altitude and Mach number are increased.

Work by REC under a previous contract NAS8-5274 indicated the following results:

(1) Analysis of flight test data on present total temperature sensors indicated that accuracy of ±4% could be obtained up to 45 Kms. of altitude.

(2) Large radiation errors could be suppressed if slow time constant sensing elements were provided.

(3) Dynamic matching for temperatures of sensing element and radiation shield appear practical, thus, further suppressing radiation errors.

(4) Due to practical size limitations, heat transfer occurs by air gap conduction between radiation shield and sensing element. This occurs at Reynolds number less than 50. This effect further increases the need for dynamic matching of temperature response between radiation shield and sensing element.

The current investigation has the following objectives:

(1) Using the criteria developed under first phase investigation, continue the analysis and design of a practical sensor configuration.

(2) Conduct preliminary experiments at REC to check expected performance.

(3) Conduct supersonic wind tunnel experiments in a government operating facility with heated flow.

(4) The final phase also consists of fabricating four prototype units for delivery to NASA.

2. DESIGN OF PROTOTYPE TOTAL TEMPERATURE SENSOR CONFIGURATION

Many of the factors affecting the design of total temperature sensor configuration were analyzed under previous Contract NAS8-5274. Final recommendation and conclusions regarding this design are listed below for convenience.

(a) Sensing element shall be oriented parallel to the direction of air flow within the sensor.

(b) Mach number inside the radiation shield and at the sensing element shall be approximately 0.3.

(c) Diameter of the sensing element shall be about 2 mm.

(d) Sensing element should be located approximately 25 mm. from the leading edge of the shield.

(e) The shield construction should be double wall type with an evacuated air space.

(f) The use of boundary layer suction holes is optional.

In addition it was indicated that a parallel flow sensing element was superior to the cross flow sensing element also analyzed on the base of the following:

(a) The cross flow sensing element loses heat by radiation through the open ends.

(b) Recovery factor for parallel flow sensing elements is higher.

(c) Conduction error for parallel flow element is minimized by having an extended length between the sensing element and the rear mounting portion.

(d) Dynamic matching is easier to accomplish for parallel flow element. Heat transfer coefficients are given by similar expressions for sensing element and radiation shield.

2.1 Heat Transfer Considerations.

The relative axial position of the sensing element inside of the shield determines the amount of heat loss by radiation through the open end of the shield. Calculations were performed to determine this heat loss as the distance varied from 5 to 37.5 mm. Details of heat transfer are given in Appendix A at the end of this report. The calculated radiation and convective heat transfer rates and their ratio were calculated. The results are presented as Figure 1 for the following flight conditions.

Altitude	70 Km
Internal Mach numbers	0.333
Recover Temp.	2440°R
Wall Temp.	2330°R
Emissivity	0.08
Reynolds No.	40.0

Test results utilizing a special apparatus, Reference 1, indicated that conduction of heat may occur between the sensing element and the radiation shield. The amount of conduction or temperature error was not significant at Reynold's number above 100 but became significantly larger within decreasing Reynolds number. At a Reynold's number of 40 the error introduced by heat conduction has been considered with results plotted in Figure 2.

The effect of increasing the distance of sensing element from leading edge of the shield is two fold. First, a reduction of radiation heat loss is effected. Second, an increase in air gap conduction occurs. For example, from Figure 1 radiation heat transfer becomes about 5% of the conduction at 25 mm. Air gap conduction, Figure 2, is about 15 per cent of the temperature difference between the sensing element and the radiation shield. If effort is made to match the time constants of the sensing element and the radiation shield this effect can be minimized. The temperature difference between these components should be insignificant as shown in Figure 3. The location of approximately 25 mm. was selected for sensing element location.

2.0 Analysis of Temperature Sensor Theory in Continuum and Rarefied Gas Flow.

A knowledge of the recovery factor and the heat transfer coefficients is essential for the reduction of flight test data. The data obtained from the sensor is essentially the dynamic response of the sensing element, when subjected to varying conditions during the flight. Most of the flight will probably occur such that the dynamic response can be calculated from continuum flow equations. For flights above 60 kilometers, the rarefied atmosphere at the sensing element will influence the heat transfer coefficients. A flow transition to slip flow occurs and the relevent slip flow equations must be used. Figure 4 shows a plot of Nusselt number against modified Reynolds number, Z.

$$Z = \frac{\sqrt{Re\ Pr}}{2.63M} \qquad (1)$$

where

Re = Reynolds Number

Pr = Prandtl Number = 0.73

M = Mach Number = 0.30

The Mach number at the sensing element has been chosen to be 0.3 in all these calculations. The variation of Z with altitude is also shown in Figure 4.

In continuum flow the local heat transfer coefficient at a distance x from the leading edge is given by

$$Nu = 0.332\ Re^{0.5}\ Pr^{0.333} \qquad (2)$$

where, Nu and Re are based on the distance x.

The average heat transfer coefficient over a length x is obtained by integrating Equation (1). The resulting expression is

$$Nu = 0.664\ Re^{0.5}\ Pr^{0.333} \qquad (3)$$

This relation is shown as a dashed line in Figure 1.

The average heat transfer coefficient in slip flow is given by the expression (Reference 6),

$$St = \frac{0.38}{M\,Z^2}\left[\exp.\,(Z^2)\ \text{erfc.}\,(Z) - 1 + \frac{2}{\sqrt{\pi}}\,Z\right] \qquad (4)$$

where, $St = \dfrac{Nu}{Re\ Pr}$

This is shown as a solid line in Figure 4. The transition to free molecule flow from continuum flow occurs between $Z = 3.27$ and 32.7. In this range a line has been drawn to smoothen the Nu-variation from the two flow regimes. This line is expressed by

$$Nu = 0.865\ Re^{0.448} \qquad (5)$$

From this the local heat transfer heat transfer coefficient is given by

$$Nu = 0.387\ Re^{0.448} \qquad (6)$$

The dynamic response of the sensing element was calculated under the following flow conditions:

Flow parallel to the sensing element.

Diameter of the sensing element = 2.00 mms.

Mach Number in the shield = 0.3

Distance from the leading edge = 37.5 mms.

The procedure for calculating the response is described in detail in Reference 1. Adopting this procedure the dynamic response was calculated using both the continuum and slip flow relations (Equations (2) and (6)). The results have been tabulated in Table I. It is seen from the Table that the dynamic response changes negligibly when the slip flow equations are used. Based on these calculations, it has been decided touse the continuum flow equation throughout the flight trajectory.

2.3 Physical Requirement.

Material used for fabrication of the sensing element and shields should have the following properties.

(a) Ability to withstand and retain its mechanical strength at high temperatures.

(b) Good resistance to oxidation, corrosion, and other atmospheric action.

(c) Ability to take high polish, thus reducing emissivity thereby reducing the heat trasfer to and from the surface.

(d) Physical properties, especially the specific heat and its variation with temperature, should be known.

(e) Material should be readily available, not prohibitively expensive.

Materials were analyzed taking into account the above requirements. We finally decided to construct both the sensing element and the radiation shields from 347 SST. This material may not be operated to as high a temperature as others. Considering that initial units are prototypes, it appears that this material would be very practical. Temperature sensor would be limited to approximately 1400°C. The product of density times specific heat determines time response of the sensing element. Variation of this product for three stainless steel materials is shown in Table II. These data are necessary for the prediction of the time constants of the sensing element. More details are included in the next section. The sensing element is actually chromel alumel thermocouple which is insulated from the 347 stainless shell by use of aluminum oxide insulation AL_2O_3. Properties of the aluminum oxide are also important. The graph of variation of the product of density times specific heat with temperature for aluminum oxide and 347 stainless are shown in Figure 5. The product of the two materials is similar over an extended temperature range, 500-2200°R, as indicated.

3. PROTOTYPE SENSOR CONFIGURATION.

A sketch of one of the prototype sensors is shown in Figure 6. The sensor consists of a 347 SST shield housing and a sensing element assembly. The element assembly consists of a 347 SST rod with an embedded chromel-alumel thermocouple, and a 321 SST stem (or element support tube) containing chromel-alumel wires supported by aluminum oxide (alumina) insulators. The stem design minimizes conduction errors, maintains high insulation resistance at elevated temperatures, and provides adequate lead wire support.

Three different prototype element assemblies were fabricated and designated as types A, B, and C. Types A and B, shown in Figure 7 (REC Drawing No. 503-101) share the same element configuration,

but have different transition sections between element and stem. Type A element is attached to the stem by four 302 SST support wires, each welded to the element on one end and secured to the stem with a refractory cement on the other, designed to minimize heat conduction between the element and stem. Type B element consists of a tapered transition section which was fabricated integral with the element. This conventional mounting provides a hermetically sealed unit which is more rugged than type A element. Type C element, the third prototype element assembly, is shown in Figure 8 (REC Drawing 103-109), and consists of an element with a diameter almost double that of element types A and B (0.125 in. diameter for type C as compared to 0.065 in. diameter for both types A and B). Type C element was designed to provide time constants that are about half as fast as the time constants for type B element. A phtograph of a sensor housing and elements A and B are shown in Figure 9.

Three prototype sensor housings have internal flow of Mach 0.1. Each housing consists of two parts, of which one was cooled, the other heated for an interference fit assembly. Two housings were of the configuration shown in Figure 6 and both were designated as shield B. The third prototype housing was similar dimensionally to shield B except that the inside diameter of the shield was 0.760 in. (instead of 0.787 in.) and the four air exit ports were 0.155 in. diameter each (instead of 0.163 in. diameter). The inner shield thicknesses of 0.026 in. for shield C and 0.013 in. for shield B were designed to provide dynamic temperature response matching with the corresponding elements. The matched shield for element C was designed from the established sensor B configuration. This was accomplished by maintaining a constant surface area to volume ratio for both sensing element and inner shield, holding equal shield diameters and element lengths for each sensor. The reduced simplified ratio specify that the ratio of inner shield thicknesses for both sensors equals the corresponding ratio of sensing element diameters.

4. THEORY AND EXPERIMENTAL DETERMINATION OF TIME CONSTANTS.

4.1 Analytical Prediction of Time Constants of the Sensing Element.

A knowledge of the time constant of the sensing element is essential in analyzing the flight test data. Under conditions of constant velocity and small temperature difference, the time constant will remain unchanged, but the following parameters vary during a flight and thus influence the time constants:

(a) Specific heat of the element material.

(b) Density of the element material.

(c) Specific heat of air.

(d) Density of air

(e) Viscosity of air.

(f) Thermal conductivity of air.

(g) Velocity in the shield.

The above factors vary appreciably with temperature but negligibly with pressure (except the density of air). In these calculations the weak pressure dependence is neglected.

At any instant of cooling (or the heating) of the sensing element, the energy balance can be written as

$$hA\ (T-T_a) = -wC_p \frac{dT}{dt} \qquad (1)$$

where,

h = convective heat transfer coefficient; B/hr-ft^2-°F

A = area of surface of the element, ft.^{2}

T = temperature of the element at time t, °R

T_a = ambient temperature, °R

w = mass of the sensing element, lbs.

C_p = specific heat of the material of the element, B/lb-°F

t = time, hr.

The above equation includes the heat transfer by convection to the sensing element and the heat transfer as related to the mass specific heat and time rate of change in the sensing element temperature.

Let $\theta = T - T_a$ the temperature excess. Then Equation 1 becomes:

$$\frac{d\theta}{dt} = -\frac{hA}{wCp}\,\theta \qquad (2)$$

The solution to Equation 2 can be written as:

$$\theta = \theta_o \text{ Exp. } \left(-\frac{hA}{wCp}\right) t \qquad (3)$$

where θ_0 is the temperature excess at zero time. (exp. signifies an exponent.) Differentiating (3) again we get:

$$\frac{d\theta}{dt} = \theta_o \left(-\frac{hA}{wCp}\right) \text{ e Exp. } \left(-\frac{hA}{wCp}\right) t \qquad (4)$$

Taking the ratio $\dfrac{\theta}{d\theta/dt}$ from Equations (3) and (4) we get:

$$\frac{\theta}{d\theta/dt} = \left(-\frac{wC_p}{hA}\right) \qquad (5)$$

The parameter wC_p/hA is known as the time constant.

For a circular cylinder parallel to the flow direction $\dfrac{wC_p}{hA}$ can be further simplified as follows:

$$\frac{w}{A} = \frac{\rho(d^2/4)L}{\pi dL} = \frac{\rho d}{4} \qquad (6)$$

where, ρ = density of the material of the element, lb/ft^3

d = diameter of the element, ft.

L = length of the element, ft.

The expression for the convective heat transfer is:

$$h = 0.332 \left(\frac{k}{x}\right) \left(\frac{xV\rho}{\mu}\right)^{0.5} (P_r)^{0.333} \qquad (7)$$

where, k = thermal conductivity of air, $B/hr\text{-}ft\text{-}^\circ F$

x = distance from the element leading edge, ft.

V = velocity, ft/hr.

ρ = density of air, lb/ft^3

μ = viscosity of air, lb/ft-hr.

P_r = Prandtl number of air, dimensionless

The velocity V can be expressed in terms of Mach number as

$$V = aM \qquad (8)$$

where, a = velocity of sound, ft/hr.

M = Mach number of flow inside the shield.

Combining Equations (6), (7) and (8) we get:

$$\frac{wCp}{hA} = \frac{d}{4} (\rho C_p)_{Mat'l.} \left[\frac{1}{0.332 \left(\frac{k}{x}\right) \left(\frac{xV\rho}{\mu}\right)^{0.5} (P_r)^{0.333}} \right] \quad (9)$$

Using the perfect gas law the density can be expressed in terms of pressure and temperature. Then the following expression results:

$$\frac{wC_p}{hA} = \left(\frac{d}{4}\right) \left[\frac{(\rho C_p)_{Mat'l} (R)^{0.5}}{0.332 \left(\frac{M}{x}\right)^{0.5} (p)^{0.5} \left(\frac{a}{\mu T}\right)^{0.5} (P_r)^{0.333} k} \right] \quad (10)$$

where, R = gas constant of air, ft

P = pressure, lb/ft^2

The above equation can also be written as follows:

$$\frac{\theta}{d\theta/dt} = \frac{d}{4(0.332)} \left(\frac{Rx}{M}\right)^{1/2} \left(\frac{H}{Q}\right)_p^{1/2} \quad (11)$$

where, $H = (\rho Cp)_{Mat'l} = f(Tw)$ = temperature dependent parameter of sensing element material properties, $Btu/ft^3-{}^\circ R$

$Q = (a/\mu T)^{1/2} Pr^{1/3} k = f(T_o + T_w)/2$ = temperature dependent parameter of air properties, $Btu\ lb^{1/2}-{}^\circ R^{1.5}-hr.$

Temperature dependent properties, References 2 and 3, are listed in Table III. The air properties which are listed for 0.01 atmosphere pressure, are independent of pressure through a temperature of 2240°R. H is a function of the element wall temperature, Tw. Q is a function of the average temperature of Tw and the total temperature To. The expression has three distinct terms; one, the geometrical constant $(d/4) \times 0.5/0.332$; second, the pressure dependence $1/p^{0.5}$; third, the temperature dependent term, $(\rho C_p)_{Mat'l}/(a/\mu T)^{0.5} (P_r)^{0.333} k$.

The geometrical constant, including R and M, has been calculated for the following conditions:

d = 1.65 mms. = 0.0650 in.

x = 13.0 mms. = 0.5305 in.

M = 0.333

The expression for the time constant becomes:

$$\tau = \frac{\theta}{d\theta/dt} = \frac{0.8953 (\rho C_p)_{Mat'l.}}{p^{1/2} \left(\frac{a}{\mu T}\right)^{1/2} Pr^{1/3} k} \quad (12)$$

where $\tau = \frac{\theta}{d\theta/dt}$ = time constant, sec.

ρ = density of sensor material, lb/ft^3

C_p = specific heat of sensor material, Btu/lb. -°F

p = pressure, atmospheres

a = speed of sound, ft/sec.

μ = air viscosity, lb/ft-sec.

Pr = Prandtl number of air, dimensionless

k = thermal conductivity of air, Btu/hr-ft

Equation (12) is based on the local (or point) value of the heat transfer coefficient and is plotted versus temperature as the solid curve in Fig re 10. The dashed curve represents the theoretical time constant based on the average value of the heat transfer coefficient. The average value of the heat transfer coefficient is twice as large as the local value, and t.e time constant is based on the entire 1.091 inch element length instead of the 15.0 mm distance from the element leading edge. The time constants based on average values are 0.680 times as large as those based on local values.

The theoretical time constants based on both local and average heat transfer coefficients are plotted in Figures 11 and 12 for a sensor with internal Mach number of 0.1 at 1.0 atmosphere pressure. Time constant remains relatively constant for temperatures up to 1500°F. The theoretical time constants are also listed in Table III.

4.2 Description of High Temperature Flow Apparatus.

The high temperature internal flow apparatus for testing sensors, illustrated in Figure 13, consists of three major components: a tube furnace; a water cooled heat exchanger; and a Beach-Russ vacuum pump. Photographs of the apparatus are presented in Figures 14 and 15. For main flow operation, room air enters the adjustable inlet valve and is heated in the tube bundle located inside the furnace. For room temperature air flow operation, air enters through two lines located downstream of the furnace. Either operation mode, main flow or room temperature air, can be selected by a single switch which controls two normally open solenoid valves for room temperature air and one normally closed solenoid valve for the main flow inlet. Three adjustable hand valves control desired test pressure settings for either operation mode. The air reaches the test section and flows

through the test sensor, the reference sensor, and eight 1/32 inch diameter bleed holes located in the sensor mounting plate to minimize nonuniform air temperatures. Heated air is cooled by the heat exchanger before exhausting through the vacuum pump.

Automatic temperature control of the 3400 watt Hevi-Duty electric tube furnace is provided by a West Gardsman on-off controller monitored by an iron-constantan thermocouple on the surface of the furnace duct assembly. A mercury relay switch activates the tube furnace.

The Perfex single pass heat exchanger contains 1/4 inch diameter brass tubing. Water coolant enters the higher temperature upstream end of the heat exchanger and discharges through the downstream end.

An 18 inch long tube bundle consisting of about 312 1/8 inch O.D., 0.105 inch I.D., tubes provides a heat sink for heating air during main flow operation. The tube can supply constant high temperature air during a test run for the length of time required to reduce the heat sink capacity by about one-half. The tube bundle, ducting, and flanges are constructed of 321 SST.

The test unit and the reference sensor (REC Model 103T sensor) are supported by a sensor mounting plate, Figure 13. A photograph of the sensors and mounting plate is shown in Figure 16. The sensor leads are brought out through the plate to external instrumentation,

4.3 Experimental Results in High Temperature Flow Apparatus:

Instrumentation for experimental determination of time constants in the high temperature internal flow apparatus is pictured in Figure 14 and includes a Sanborn paper strip pen recorder to measure sensed temperatures and a U-tube mercury manometer to measure pressures. An absolute pressure reading Merriam manometer, (specific gravity, 1.04) in conjunction with a direct reading Hastings vacuum gage and a small vacuum pump for evacuating the absolute board, was used for low pressure measurements. An ice bath provided the 32°F reference junction temperatures for the test thermocouple leads.

The test runs in the flow apparatus normally involved the following procedure. The furnace was operated at the desired controller temperature until heat saturation in the tube bundle was reached. Valve positions were preset to the desired test pressure in both main flow and room air temperature flow lines. The strip recorder was turned on and checks were made on established scale factors. The rapid switch from room air flow to heated main air flow provided the stepped temperature change from low to high temperature. Downstream pressure was monitored to assure a downstream to upstream pressure ratio of 0.528 or less, required for sonic flow to exist at the sensor exit ports. The test run was continued until recovery temperature was reached. A typical sensor temperature trace is shown in Figure 17.

Sensor time constant was determined from the temperature trace by the initial slope method, Figure 17, in which the time constant is the elapsed time for the initial slope to intersect the sensor recovery temperature. Conditions before the stepped temperature change are stable and the time constant determined at the beginning of the temperature transient is the most reliable value. As the test run progresses, secondary heat transfer effects may introduce errors which are not measurable.

Experimental time constants for various combinations of three sensor housings and three element assemblies were determined from tests in the high temperature flow apparatus. The experimental results are presented on logarithmic plots, Figures 18 through 23, in which data agrees with the theoretical slope of -1/2. Temperature variation in time constant data was neglected for high temperature flow tests. The housings and elements were previously described in detail, paragraph 3.

Experimental time constants for types A, B, and C elements, housed in a type B housing defined as shield no. 1, are shown in Figures 18, 19, and 20. Types A and B element configurations are similar except for the means of attaching the element to the stem: type A is wire supported and type B incorporates a tapered section. Results for both are similar, indicating negligible conduction differences due to means of element support. Subsequent testing was limited to type B element because of its more rugged construction.

Experimental results for type B element (or type A element) can be compared to theoretical values given in Figure 12 for which the element configurations are similar. The experimental time constant of 9.15 sec. at 1.0 atmosphere pressure, Figure 19 is 48 and 23 percent less than the theoretical values based on the local and average heat transfer coefficient, respectively. Figure 20 shows results for type C element, which has a diameter of about double that of type B element, housed in shield number 1 (type B housing). The time constant is 15.8 sec. at 1.0 atmosphere pressure.

A second type B housing, defined as shield number 2 was fabricated for type C element. Figure 21 shows a comparison of type C element in similar shields number 1 and number 2 at relatively low test temperatures, resulting in slightly faster responses for the element in shield number 2 (14.3 sec. at 1.0 atmosphere pressure).

A pair of sensors was tested in a supersonic tunnel, for which data is presented in a later section (paragraph 6.2). The time constants involved in the data reduction included those from Figures 19 and 21, for element B in shield number 1, and element C in shield number 2, respectively, resulting in a time constant ratio of 1.6. It appeared necessary to rerun tests at a later date in the same supersonic tunnel, incorporating a different means of providing the stepped temperature change. (Data is presented in paragraph 6.3). Another housing designated as type C housing, shield number 3, was designed to match the dynamic temperature response of element C. Element C time constants of 16.5 and 14.3 sec. at 1.0 atmosphere pressure, in matched and unmatched shields (shield number 3 and shield number 2) are compared in Figure 22. The matched shield produced slower time constants as expected. The time constants involved in the data reduction of the second set of supersonic test runs included those from Figures 19 and 22, for element B in shield number 1, and element C in the matched shield number 3, respectively, resulting in a time constant ratio of 1.8.

Figure 23 shows three repeat curves, all of which are involved in supersonic data reduction. The data points are the results of four temperature step conditions consisting of two high temperature

steps (stepped temperature change from low to high temperature) and two low temperature steps. The high temperature step data agrees with previous corresponding data, curves of which are shown in the figure. The low temperature step time constants for element B, Figure 23, are significantly faster than the high temperature step data. Since a different flow path was involved (room air flow through the two cooling lines), additional tests were run after a temporary modification to the flow apparatus. In these tests the furnace was not used. A wire heater wrap was applied to one of the two cooling lines and the other cooling line was closed off. Low temperature steps provided by room air directed through the unheated tube bundle produced slower time constants (not shown) which agreed with the high temperature step data. The results indicate that air flow through the cooling lines produces turbulent flow at the sensor resulting in much faster time constants than those obtained using main flow air through the tube bundle.

5. THEORY OF TEMPERATURE AND PRESSURE PREDICTIONS.

5.1 Theory of Total Temperature Predictions.

The theoretical time constant equation (equation (12), para. 4.1) can be rewritten as follows:

$$\tau = C \left(\frac{H}{Q}\right) p^{-1/2} \qquad (15)$$

where, $\tau = \dfrac{\theta}{d\theta/dt}$ = time constant, hr.

C = geometrical constant by definition
$= (D/1.328)(Rx/M)^{1/2}$, $ft^2/°F^{1/2}$

$H = (\rho Cp)_{Mat'l}$, $Btu/ft^3-°F$

$Q = (a/\mu T)^{1/2} Pr^{1/3} k$, $Btu/lb^{1/2}-°F^{1.5}-hr.$

p = pressure, lb/ft^2

An expression for total temperature, T_o, can be written by solving the above equation for two sensors, B and C. Assume element recovery temperature, T_w, equals T_o. Substitute $\tau = (T_o-T_w)/(dT/dt)$, or $\theta = T_w-T_o$, and $\gamma = dT/dt$.

$$T_o = \frac{T_{w_C} - T_{w_B}\left(\frac{\gamma_C}{\gamma_B}\frac{C_C}{C_B}\frac{Q_B/H_B}{Q_C/H_C}\right)}{1 - \left(\frac{\gamma_C}{\gamma_B}\frac{C_C}{C_B}\frac{Q_B/H_B}{Q_C/H_C}\right)} \tag{14}$$

The ratio C_C/C_B is an experimental constant determined from sensor calibration data in the high temperature flow apparatus. The solution of equation (1) for two sensors is:

$$\frac{C_C}{C_B} = \frac{\tau_C}{\tau_B}\frac{(Q_C/H_C)}{(Q_B/H_B)} \tag{15}$$

When sensors B and C are calibrated at the same test conditions, the temperature dependent parameters cancel, leaving the required constant ratio equal to the ratio of the time constants. The following equation can be written by substituting $\tau = (T_o - T)/\gamma$ in the above equation.

$$\frac{\gamma_C}{\gamma_B} = \left(\frac{T_o - T_{w_C}}{T_o - T_{w_B}}\right)\frac{C_B}{C_C}\frac{(Q/H)_C}{(Q/H)_B} \tag{16}$$

If the temperatures were varied while holding the ratio $(T_o - T_{w_B})/(T_o - T_{w_c})$ constant, γ_B/γ_C will vary with the temperature dependent ratio involving Q and H. Therefore, it is reasonable to assume that the slope ratio γ_B/γ_C in equation (16) cannot be experimentally determined without including temperature effects, and:

$$\left(\frac{\gamma_C}{\gamma_B}\right)_{Test} = \frac{\gamma_C}{\gamma_B}\frac{(Q/H)_B}{(Q/H)_C} \tag{17}$$

Substituting in equation (14) results in the total temperature prediction equation:

$$T_o = \frac{T_{w_C} - T_{w_B}\left[\left(\frac{\gamma_C}{\gamma_B}\right)_{Test}\left(\frac{C_C}{C_B}\right)\right]}{1 - \left[\left(\frac{\gamma_C}{\gamma_B}\right)_{Test}\left(\frac{C_C}{C_B}\right)\right]} \tag{18}$$

The ratio C_C/C_B is normally determined experimentally. However, it is possible to calculate the ratio from the geometry of the sensors. The constant "C" by definition (equation 13) is:

$$C = \frac{d}{4(0.332)} \left(\frac{Rx}{M}\right)^{1/2}$$

The ratio for two sensors is:

$$C_C/C_B = (d_C/d_B)\ (M_B/M_C)^{1/2} \qquad (18B)$$

where: d = diameter of the element

M = Mach number of flow inside the shield

5.2 Theory of Predicting Total Pressure or Total Temperature with a Single Sensor

Total pressures can be predicted from a single sensor provided total temperature is known, and conversely, total temperature can be predicted provided total pressure is known. The required equations are obtained from equation (13)

$$T_o = T_w + \gamma C(M/Q)p^{-1/2} \qquad (19)$$

$$p = C^2 \left[\tau (Q/M)\right]^{-2} \qquad (20)$$

where constant C is:

$$C = \tau(Q/M)_p^{1/2} \qquad (21)$$

An additional consideration must be introduced to the subject predictions involving a single sensor that was unnecessary for T_o predictions where the constant "C" appeared in ratio form for the required pair of sensors. A correction factor for air turbulence is necessary to relate calibration results in the flow apparatus to test results in the wind tunnel. Turbulence factor corrects a calculated Reynolds number to an effective Reynolds number. Since time constant varies inversely with the square root of Reynolds number in T_o predictions (equation 9) and directly with constant "C", the required correction factor is as follows:

$$F = \frac{\tau \text{ (wind tunnel)}}{\tau \text{ (flow apparatus)}}$$

The corrected constant "C" is then the constant "C" from equation (21) multiplied by the factor "F". It is this corrected constant "C" which is required in equations (19) and (20) for pressure and temperature predictions.

6. RESULTS OF WIND TUNNEL TESTS.

6.1 Test Facility and Summary of Test Conditions.

Two series of supersonic wind tunnel tests were performed in the Gas Dynamic Wind Tunnel, Hypersonic (E) of the von Karman Gas Dynamics Facility (VKF), Arnold Engineering Development Center (AEDC), Air Force Systems Command (AFSC). Dynamic temperature responses were measured at nominal Mach 8, nominal stagnation pressures of 400, 500 and 600 (first and second series of tests), and 900 psia, at nominal stagnation temperatures of 900°F for both series of runs. The difference between the two series of tests involved the method of cooling the sensors (between 50 and 150°F) before they were subjected to the stepped temperature change. Summaries of the first and second series of supersonic wind tunnel test conditions are presented in Tables IV and V. Test details are available in AEDC letter reports, References 4 and 5.

6.2 First Series of Wind Tunnel Tests.

The first series of supersonic tests at AEDC involved cooling the sensors by supplying nitrogen gas through two pairs of 1/4 inch O.D. lines through the sting and sensor mount, directing two cooling jets through the base of each sensor. The cooling gas was shut off when stable tunnel conditions were established. The sensing elements were then subjected to the heated air flow which provided the stepped temperature change. The sting supported dual sensor mount is shown in Figure 24.

Results of the first series of supersonic tests are shown in Figures 25 through 36. Predicted total temperatures, shown in Figures 25 through 30, are based on equation (18), using $C_C/C_B = 1.6$ (paragraph 4.3). Predicted temperatures based on $C_C/C_B = 1.7$ are also shown for comparison. Predicted temperatures are within 100°F of measured stagnation temperature at 20 sec. into the run for the 400 and 500 psia runs, Figures 25 through 28. Predictions to within 100°F

for the 900 psia runs occur about 7 sec. earlier, Figures 29 and 30. Temperature predictions are erratic during the first six seconds of the test runs.

All test runs exhibit the typical trends of parameters plotted in Figures 31 through 36 for the 400 psia run. Time history of measured sensor temperatures and tunnel stagnation temperatures are shown in Figure 31. The time rates of temperature change for each sensor are shown in Figure 32. Time constants for the selected run are shown in Figure 33 and the three repeat runs in Figure 34 indicate that the selected run is representative of all four 400 psia runs. Time constants remain at a fairly constant value throughout the time histories. Constant "C" in Figure 35 was calculated from equation (21) for the test data, and the trends are similar to time constant data. The ratio C_C/C_B for the selected run, shown in Figure 36, decreases to a constant value of about 1.6, in 40 sec. The variation in ratio C_C/C_B can be attributed to unrealistic initial conditions during the stepped temperature change.

6.3 Second Series of Wind Tunnel Tests.

The second series of supersonic tests involved an improved means of providing the initial condition. The model was fully retracted from the airstream and cooled to a uniform temperature by several jets of gaseous nitrogen. The model was then injected into the airstream in about 1 second by a pneumatically operated inject mechanism. Figure 37 shows the model mount which was attached to the inject mechanism. The inject method provided a more realistic means of initiating the test runs than was provided in the first series of supersonic runs during which the sensing element and the inside of the housing were cooled by jets of nitrogen directed through the aft end of the sensors. Although radiation heat transfer effects between the sensing element and shield were not expected to be significant, the first series runs appeared to result in unrealistic performance. The unmatched shield for element C was replaced by a housing with a matched shield for the second series tests.

Results of the second series of supersonic tests are shown in Figures 38 through 48. Predicted total temperatures, shown in Figures 38 through 40, are based on $C_C/C_B = 1.8$ (para. 4.3) and exhibit the same trends with earlier temperature predictions. In general, repeat data agrees for the three time intervals calculated.

A thermocouple was attached to the outside surface of sensor C housing at AEDC. Available shield surface temperature data are shown in Figure 41 for 400 and 600 psia pressure runs. The constant difference between element and shield surface temperatures throughout the run is indicative of close dynamic temperature matching between the element and inner radiation shield.

Comparisons of predicted temperatures and various parameters for first and second series of supersonic test runs are shown in Figures 42 through 47. Predicted temperatures, shown in Figures 42 and 43 for 400 and 900 psia pressure runs, are based on $C_C/C_B=1.6$ for comparison purposes. The second series of test runs involving the more realistic initial condition (model inject method), result in a 5 second earlier predicted temperature than the first series runs. Predicted temperature based on $C_C/C_B = 1.8$, also shown in Figures 42 and 43, illustrate the best justified predictions of the current study. Comparisons of sensor B time rates of temperature change, Figures 44 and 45, show the effect of different initial conditions; the heated outer surface of the sensor B housing in the first series of test (dashed curves) results in steeper (increased) temperature slopes for about 15 sec. into each run. Sensor C time rates of temperature change are essentially the same for both series of test runs. Time constant uniformity is increased for the second series test runs at 400 psia pressure, Figure 46. In general, Figures 46 and 47 indicate that the time constants for first and second series runs have much the same trends and magnitudes.

Predicted pressures, calculated for one 600 psia test run in the second series of tests, were based on equation (20) using predicted temperature variation, Figure 38. The constant "C" was calculated from equation (21) using calibration data, Figure 23, for each sensor. The "C" value must be corrected for the difference in air turbulence between the flow apparatus and the supersonic tunnel by the factor described in para. 5.2. The measured pressure, shown as the dashed curve in Figure 48, is the total pressure

behind the shock wave which was calculated from stagnation pressure data. Predicted pressures from a single sensor appear to be impractical at this stage of development due to excessive scatter of calculated results.

7. FINAL TOTAL TEMPERATURE SENSOR.

7.1 Final Design of Total Temperature Sensor.

Two pairs of high temperature, high altitude total temperature sensors, fabricated for the subject contract, were each designated as REC Models 107C-1 and 107C-2 (corresponding to prototype sensors B and C sensors, respectively). The sensors were designed for an internal flow of Mach 0.3. (Prototype sensors had internal flow of Mach 0.1.) Basic information on the Model 107C is presented in the REC Specification Drawing, Appendix B.

Model 107C incorporates changes and improvements over the prototype sensors, consisting of enlarging flow exit ports to accomodate the internal flow Mach number increase, increasing maximum operating temperature by redesign of the element stem, and improving the strength of the thermocouple lead wire junction at the base of the model by adding a wire support tube. The diameters of alumina insulators in the element stem were increased to eliminate the gold used for anchoring platinum wire spacers to the insulators. Thus the maximum operating temperature was increased from 1100°C to 1400°C. The increase of internal Mach number will provide improved performance for the intended flight applications.

7.2 Calibration of Final Total Temperature Sensors.

The four 107C total temperature sensors were calibrated in the internal flow apparatus at nominal test pressures of 4, 8, and 16 inches mercury, and at an average stepped temperature change from 77°F to 212°F. Figure 49 shows similar time constant results for units with the same configuration, within experimental accuracy. The experimental constants and their ratio are as follows:

Model 107C-1, serial numbers 1 and 2:

$$C_1 = 0.0071 \text{ ft}^2/^\circ\text{R}^{1/2}$$

Model 107C-2, serial numbers 1 and 2:

$$C_2 = 0.0125 \text{ ft}^2/^\circ\text{R}^{1/2}$$

Ratio of experimental constants:

$$C_1/C_2 = 0.57$$

C_1/C_2 is used in the equation for total temperature predictions shown on the 107C specification drawing, Appendix B. The experimental constant "C" is used for predicting total temperature or pressure using a single sensor as described in paragraph 5.2. (Note that "C" may require a correction factor to account for different levels of air turbulence between calibration and intended flight applications, as explained in paragraph 5.2. The ratio C_1/C_2 does not require a correction since turbulence effects cancel.)

Insufficient capacity of the internal flow apparatus necessitated reducing the sensor internal Mach number to assure sonic flow at the sensor exit ports. (The required downstream to upstream pressure ratio must be less than 0.528.) The sensors were calibrated with three of the four sensor exit flow ports covered with a metal sleeve. Calibration results at the low internal Mach number were corrected to the nominal internal Mach number of 0.3 as follows.

$$\tau(\text{sensor}) = \left[\frac{M\ (1 \text{ exit port open})}{M\ (4 \text{ exit ports open})}\right]^{1/2} \tau(\text{calibration})$$

Mach numbers were determined from area ratios calculated from measured sensor dimensions.

7.3 Predicted In-Flight Performance of Final Total Temperature Sensor.

Predicted in-flight performance of REC Models 107C-1 and 107C-2, based on the expected high Mach number operational trajectory and corresponding altitude variation (Figure 4 of Ref. 1), is shown in Figure 50. At subsonic Mach numbers no shock occurs ahead of the sensor and the design velocity cannot be maintained inside the shield. The Mach number inside the shield was then determined by using fictitious throats when the external flow was subsonic.

The in-flight performance results, Figure 50, are based on time constant calibrations of prototype sensors B and C. The calibrations for prototype seasors with internal flow of Mach 0.1 were corrected analytically for internal flow of Mach 0.3 for the final sensors by the method of fictitious throats (time constant varies inversely with the square root of internal Mach number).

The dynamic characteristics of a 2.0 mm. diameter (0.079 in.) sensing element, 0.333 internal Mach number, 0.5 mm. (0.020 in.) thick shield, and 25.0 mm (0.984 in.) distance of thermocouple from the sensor leading edge, is shown in Figure 3 (reproduced Figure 16, Ref. 1). In-flight performance, Figure 50, is based on the recovery temperature from Figure 3. The recovery temperature and the dynamic temperature response of the 2.0 mm diameter sensing element, curves A1 and A2, are reproduced in Figure 50 for comparison with predicted dynamic characteristics of Models 107C-1 and 107C-2. Numerical iterations for selected time increments were employed to evaluate the element temperatures.

8. CONCLUSIONS AND RECOMMENDATIONS.

Two prototype total temperature sensors, designated as sensors B and C, were designed and fabricated according to the criteria developed under the first phase investigation, Reference 1. Experiments were conducted in the REC internal flow apparatus and in a supersonic tunnel. Two pairs of total temperature sensors were fabricated and delivered to NASA under terms of the subject contract. The two sensor configurations are designated as REC Models 107C-1 and 107C-2 (see specification drawing, Appendix B).

Recommendations based on the subject study are as follows:

(1) The supplied Model 107C units should be tested for in-flight performance, perhaps on a flight vehicle such as the X-15.

(2) No further supersonic wind tunnel tests are necessary. Temperature step transients and turbulence associated with wind tunnel testing do not occur in actual flight operation. Sensor temperature stabilization before the temperature step is questionable and may influence test results. Based on available data, a minimum of about 10 seconds after the temperature step is necessary for obtaining an acceptable temperature prediction.

(3) Over the range investigated, test results of prototype sensors calibrated in the REC internal flow apparatus indicate uniform calibration results for sensor operation at total pressures down to 1/4 inch mercury (occurs at an altitude of about 60 km and flight Mach number 6). Calibration techniques at very low pressures and the associated rarefied gas effects could be investigated.

(4) Turbulence level influence on time constant and its effect on single sensor performance could be investigated. Reliable operation of sensors in pairs is expected, regardless of turbulence level.

9. REFERENCES.

1. DeLeo, R.V., Sreenivasan, K., and Thompson, D.I., "Study to Determine Suitable High Temperature - High Altitude Total Temperature Sensors", Final Summary Report, Contract No: NAS8-5274, REC, February 1964.

2. Hansen, C.F., "Approximations for the Thermodynamic and Transport Properties of High Temperature Air", NASA-TR-R-50 (1959).

3. The International Nickel Company, Inc., "Mechanical and Physical Properties of the Austenitic Chromium-Nickel Stainless Steels at Elevated Temperatures", New York, 1963.

4. Mallard, S.R., "Summary of the NASA-Rosemount High Temperature, High Altitude Total Temperature Sensing System Test in Tunnel E", LTR-AEDC-VKF-HS-5-64, AEDC, 1964.

5. Mallard, S.R., "Summary of the NASA-Rosemount Total Temperature Sensing System Test at Mach 8", LTR-AEDC-VKF-HS-2-65, AEDC, 1965.

6. S.A. Schaaf, University of California Institute Engineering Research Report HE-150-66, 1950.

10. NOMENCLATURE.

A - Area of surface of the element, ft^2

a - Velocity of sound ft/hr or ft/sec

C - Experimental or geometric constant for sensor, $ft^2/°R^{1/2}$

Cp - Specific heat of sensing element material, Btu/lb - °R

D - Diameter of sensing element, ft

e - Napierian base for natural logarithms, 2.718

Exp - Exponent

F - Radiation configuration factor; also, angle factor

H - Temperature dependent parameter of sensing element material properties, $\rho Cp = f(Tw)$, $Btu/ft^3 - °F$

h - Convective heat transfer coefficient of the fluid, $Btu/hr-ft^2-°R$

k - Thermal conductivity of air, Btu/hr.-ft-°F

L - Length of sensing element, ft.

M - Mach number of flow inside shield

Nu - Nusselt number, dimensionless

p - Pressure, lb/ft^2 or atmospheres

Pr - Prandtl number of air, dimensionless

Q - Temperature dependent parameter of air properties, $(a/\mu\ T)^{1/2}\ Pr^{1/3}\ k = f\left[(T_o + T_w)/2\right]$, $Btu/lb^{1/2} - °R^{1.5}-hr.$

q_c - Convective heat loss, $Btu/hr-ft^2$

q_R - Radiation loss, $Btu/hr. - ft^2$

R - Gas constant of air, ft/°F

Re - Reynolds number, dimensionless

St - Stanton number, dimensionless

T - Temperature, °R

t - Time, hr

T_a - Ambient temperature, °R

T_o - Total temperature, °R

Tr - Recovery temperature of sensing element, °R

Tw - Temperature of sensing element (wall temperature), °R

V - Velocity, ft/hr

w - Mass of sensing element, lbs.

x - Distance from the element leading edge, ft.

Z - Modified Reynolds number, $(Re\ Pr)^{1/2}/2.63M$

$\dot{T}$ - Time rate of change in sensing element temperature, dT/dt, °R/hr

ϵ - Emissivity of the surface, = 0.68

θ - Temperature excess, or difference between element and ambient temperatures, $T-T_a$, °F

θ_o - Temperature excess at time zero, °F

μ - Viscosity of air, lb/ft-hr or lb/ft-sec

ρ - Density of sensing element material, lb/ft^3

σ - Stefan-Boltzmann constant = .1713 x 10^{-8} Btu/hr $-ft^2-°R$

τ - Time constant, hr. or sec.

Subscripts

$()_o$ - Total condition, or initial condition

$()_B$ - Applies to sensor B

$()_C$ - Applies to sensor C

$()_1$ - Applies to Model 107C-1

$()_2$ - Applies to Model 107C-2

TABLE I: DYNAMIC RESPONSE OF THE SENSING ELEMENT

Parallel flow D = 2.0 mms. M = 0.3; x = 37.5 mms.

Low Mach Number

Altitude Kms	T_r °R	T_i °R	T_i^* °R
0			
[illegible]	522.0	522.0	
5.08	498.1	522.0	
8.88	489.1	508.5	
12.6	479.0	499.5	
19.8	504.0	494.6	
26.2	674.3	531.2	
29.8	822.3	589.1	
38.1	977.8	626.8	
47.8	1298.7	707.9	
59.4	1668.4	787.9	
72.3	1759.3	852.1	851.2
85.0	1574.6	885.6	884.5
	1458.4	894.6	894.3

High Mach Number

Altitude Kms	T_r °R	T_i °R	T_i^* °R
0	522.0	522.0	
6.56	572.2	522.0	
9.90	617.0	549.	
14.20	777.6	605.7	
19.60	1094.9	725.6	
30.20	1897.2	1042.0	
39.20	2678.6	1368.0	
44.20	3119.9	1552.3	
55.90	3057.1	1844.0	
66.60	3571.2	2029.0	
76.90	3186.0	2122.7	2121.5
86.30	3292.2	2168.1	2166.5
95.00	3713.4	2187.0	2187.5

T_r = Recovery Temperature

T_i = Dynamic Response of the sensing element using continuum flow relations.

T_i^* = Dynamic Response of the sensing element using slip-flow relations.

TABLE II: 'ρC_p' of Annealed Austenitic Stainless Steels at Various temperatures.

Temperatures °F	ρC_p B/ft. °F		
	Type 321	Type 316	Type 347
68	55.85	55.62	55.50
200	57.58	57.55	57.05
400	62.15	61.[illegible]7	60.64
600	64.68	64.05	63.6
800	66.[illegible]1	65.[illegible]2	65.[illegible]1
1000	67.21	[illegible]	66.7[illegible]
1200	68.20	67.[illegible]5	68.06
1400	70.[illegible]	[illegible].1[illegible]	70.55
1600	72.46	75.41	74.76
1800	75.72	7[illegible].[illegible]	[illegible].71

Values taken from ASTM Spec. Tech. Pub. No. 1[illegible],1952, p. 10. Garofalo, F., Malenock, P.R., and Smith, G.V. "The Influence of Temperature on the Elastic Constants of Some Commercial Steels."

TABLE III: [illegible]ATERIALS [illegible] ON [illegible]

T (°F)	T (°R)	ρC_p (B/ft^3-°F) for 347 SST	a (ft/sec)	Pr	$\mu \times 10^5$ (lb$_m$/ft-sec)	k (B/hr-ft-°F)	$(\frac{\rho}{\mu T})^{[illegible]}$ (Pr)$^{[illegible]}$ k (B/lb$^{0.5}$-°F$^{1.5}$-hr)	[illegible] (sec [illegible]) M=0.[illegible]	[illegible]
68	528	53.30	1127	.73[illegible]	1.219	0.01[illegible]4	5.047	[illegible].45	17.[illegible]
100	560	54.40	1160	.731	1.275	.0142	5.156	9.45	[illegible]
200	660	57.05	1259	.733	1.442	.0164	5.394	9.47	[illegible]
300	760	59.00	1349	.735	1.596	.0186	5.609	9.42	[illegible]
400	860	60.64	1432	.737	1.739	.0208	5.811	9.35	[illegible]
500	960	62.40	1510	.739	1.875	.0227	5.943	9.40	[illegible]
600	1060	63.68	1592	.741	2.005	.0246	6.095	9.36	[illegible]
700	1160	64.42	1653	.743	2.124	.0264	6.195	9.31	[illegible]
800	1260	65.21	1718	.745	2.239	.0280	6.276	9.30	[illegible]
900	1360	65.[illegible]	1784	.747	2.345	.0296	6.362	[illegible].28	[illegible]
1000	1460	66.71	1842	.749	2.450	.0312	6.428	9.29	[illegible]
1100	1560	67.60	1902	.751	2.549	.0327	6.500	9.31	[illegible]
1200	1660	68.66	196[illegible]	.753	2.650	.0342	6.569	9.36	[illegible]
1300	1760	69.60	2014	.755	2.744	.0356	6.610	9.4[illegible]	[illegible]
1400	1860	70.55	2064	.757	2.843	.0369	6.643	9.51	[illegible]
1600	2060	74.76	216[illegible]	.760	3.025	.0396	6.736	9.94	[illegible]
1800	2260	81.71	2261	.763	3.19[illegible]	.0422	6.831	10.[illegible]1	[illegible]
2000	2460	81.80	[illegible]	.765	3.350	.0448	6.92[illegible]	10.57	[illegible]
2200	2660	82.76	2445	.767	3.505	.0472	6.992	10.60	[illegible]
2400	2860	85.70	25[illegible]	.766	3.65[illegible]	.0496	7.066	10.80	[illegible]
2600	3060	87.25	26[illegible]	.760	3.792	.0520	7.113	10.99	20.[illegible]
[illegible]800	[illegible]	88.80	[illegible]	.750	3.930	.0558	7.330	10.[illegible]	[illegible]
3000	3460	89.[illegible]	2746	.736	4.[illegible]	.0618	7.791	10.25	[illegible]
3200	[illegible]	[illegible].66	2802	.718	[illegible].197	.0835	1[illegible].101	[illegible]7.9[illegible]	[illegible]
[illegible]400	3860	90.15	[illegible]	.694	[illegible].323	.1244	14.409	5.60	[illegible]
[illegible]	4060	91.05	2897	.663	4.450	.1650	18.215	4.48	[illegible]

TABLE LII (Continued)

T (°F)	$\frac{\theta}{d\theta/dt}$ (sec) (Average Values) for p = 1.0 atm	
	M = 0.333	M = 0.1
68	6.42	11.73
100	6.42	11.72
200	6.44	11.75
300	6.40	11.68
400	6.35	11.59
500	6.39	11.66
600	6.36	11.61
700	6.33	11.55
800	6.32	11.54
900	6.31	11.51
1000	6.31	11.53
1100	6.33	11.55
1200	6.29	11.61
1300	6.41	11.70
1400	6.46	11.79
1600	6.76	12.33
1800	7.28	13.28
2000	7.18	13.12
2200	7.20	13.15
2400	7.38	13.47
2600	7.47	13.63
2800	7.37	13.45
3000	6.95	12.69
3200	5.40	9.85
3400	3.81	6.95
3600	3.04	5.55

TABLE IV

SUMMARY OF WIND TUNNEL TEST RUNS AT MACH 8

Group No. -Run No.	M	Nominal p_t (psig)	Nominal T_o (°F)	Average p_t (psia)	Average T_o (°R)	Average p_t' ("Hg)	Re/ft_{-6} x 10^{-6}
1-1	7.89	900	880	891.4	1316.2	16.39	4.12
2-2	7.79	500	840	499.8	1297.5	9.73	2.48
3-3	7.77	400	835	400.7	1282.5	7.89	2.01
4-4	7.77	400	900	405.6	1358.0	7.95	1.87
5-5	7.77	400	900	401.3	1353.0	7.93	1.86
6-5	7.77	400	900	399.8	1354.9	7.88	1.86
7-6	7.79	500	900	500.8	1342.6	9.73	2.34
8-6	7.79	500	900	500.2	1357.0	9.74	2.31
9-7	7.89	900	900	894.6	1351.5	16.43	3.94
10-7	7.89	900	900	897.4	1350.0	16.56	3.97

TABLE V:

SUMMARY OF MAY 20, 21 MACH 8 WIND TUNNEL RUNS AT AEDC

Run No.	M	Average P_t (psia)	Average T_o (°R)	$Re/ft \times 10^{-6}$	P_o' ("Hg)
15	7.89	898	1351	4.02	16.52
16	7.82	604	1350	2.78	11.56
17	7.89	900	1345	4.06	16.55
18	7.82	601	1347	2.77	11.50
19	7.77	403	1343	1.89	7.94
20	7.77	403	1340	1.90	11.58
21	7.82	605	1350	2.80	11.58
22	7.77	403	1350	1.88	7.94

FIGURE I: Comparison of heat loss of the sensing element by convection and radiation

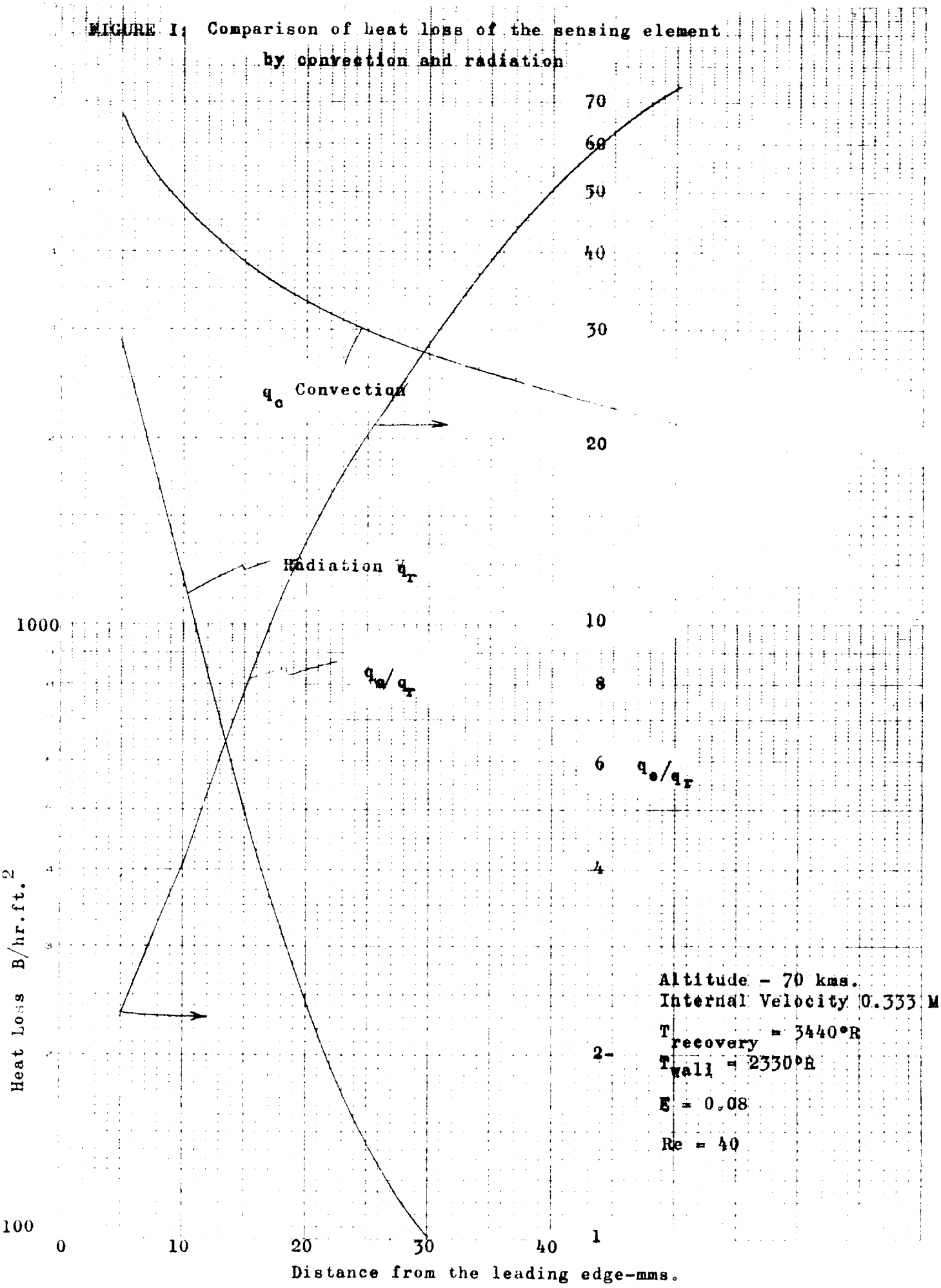

FIGURE 2: A cross plot of experimental data (from Figure 22 of Ref. 1) showing the variation of air gap conduction with distance from the leading edge. Reynolds number inside the shield is 40.

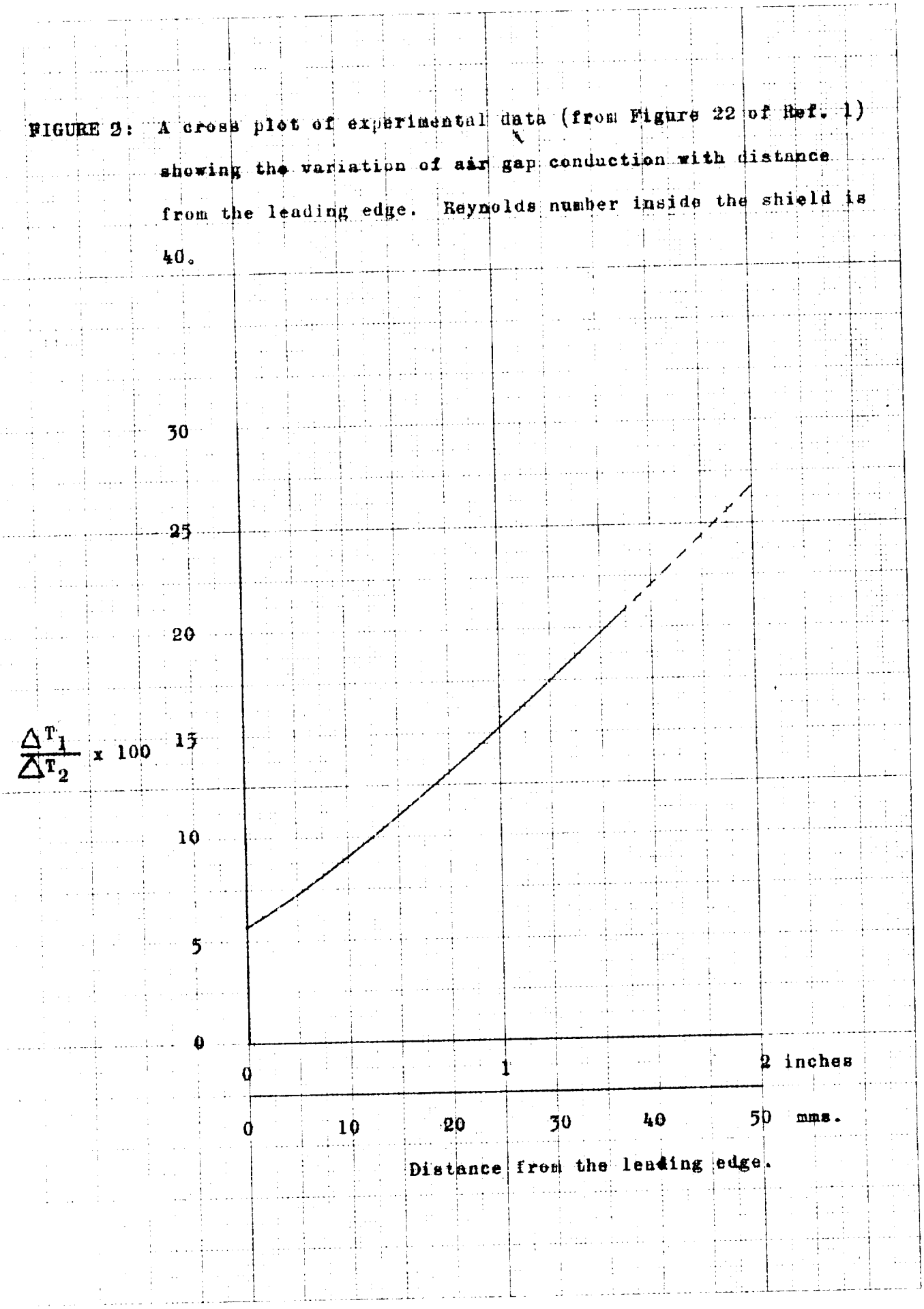

FIGURE 3

Dynamic Characteristic of the Sensing Element, Parallel Flow

D = 2.0 mms
M = 0.333
x = 25 mms
s = 0.5 mm

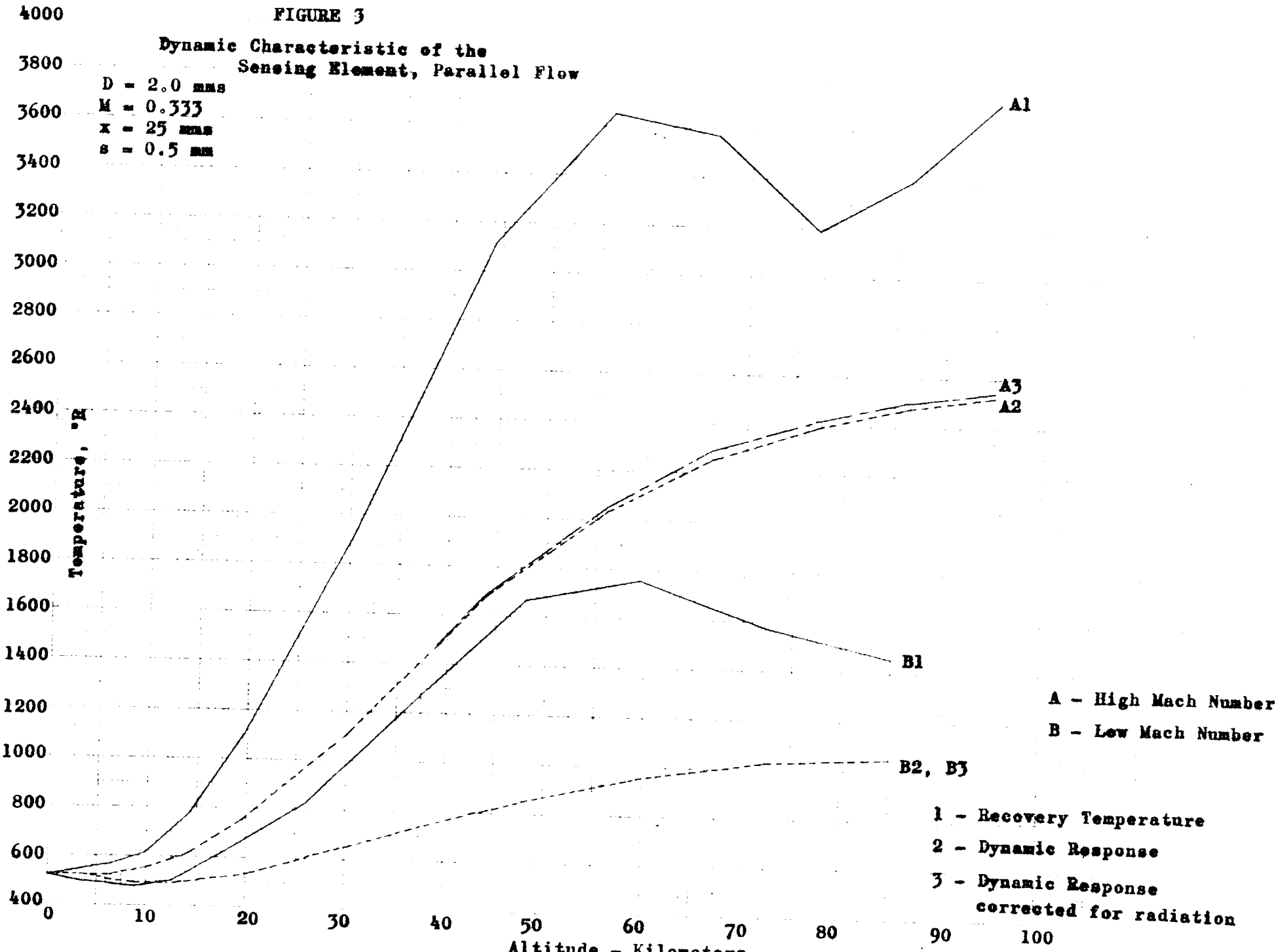

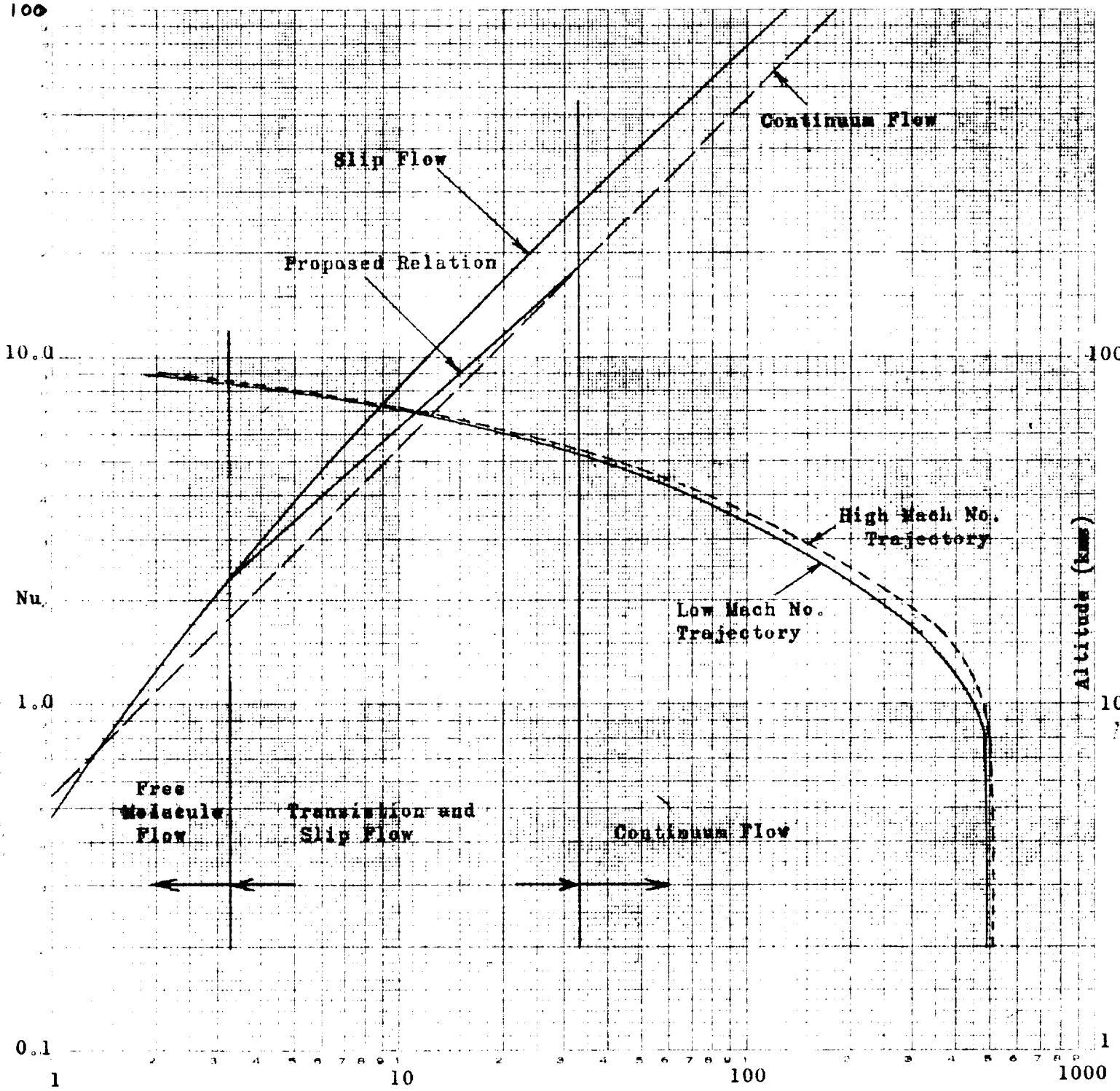

FIGURE 4: Variation of Nusselt number with Z

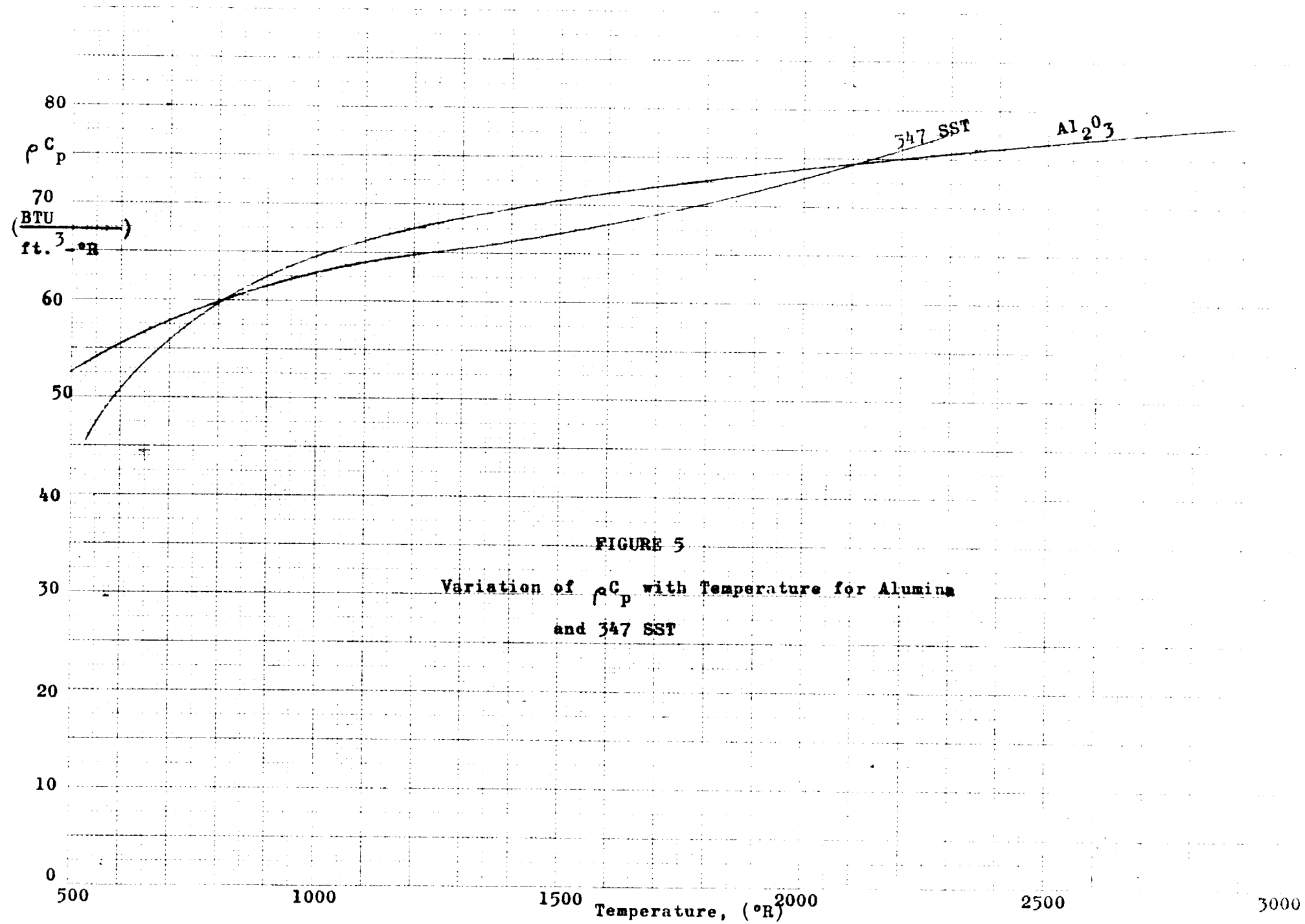

FIGURE 5

Variation of ρC_p with Temperature for Alumina and 347 SST

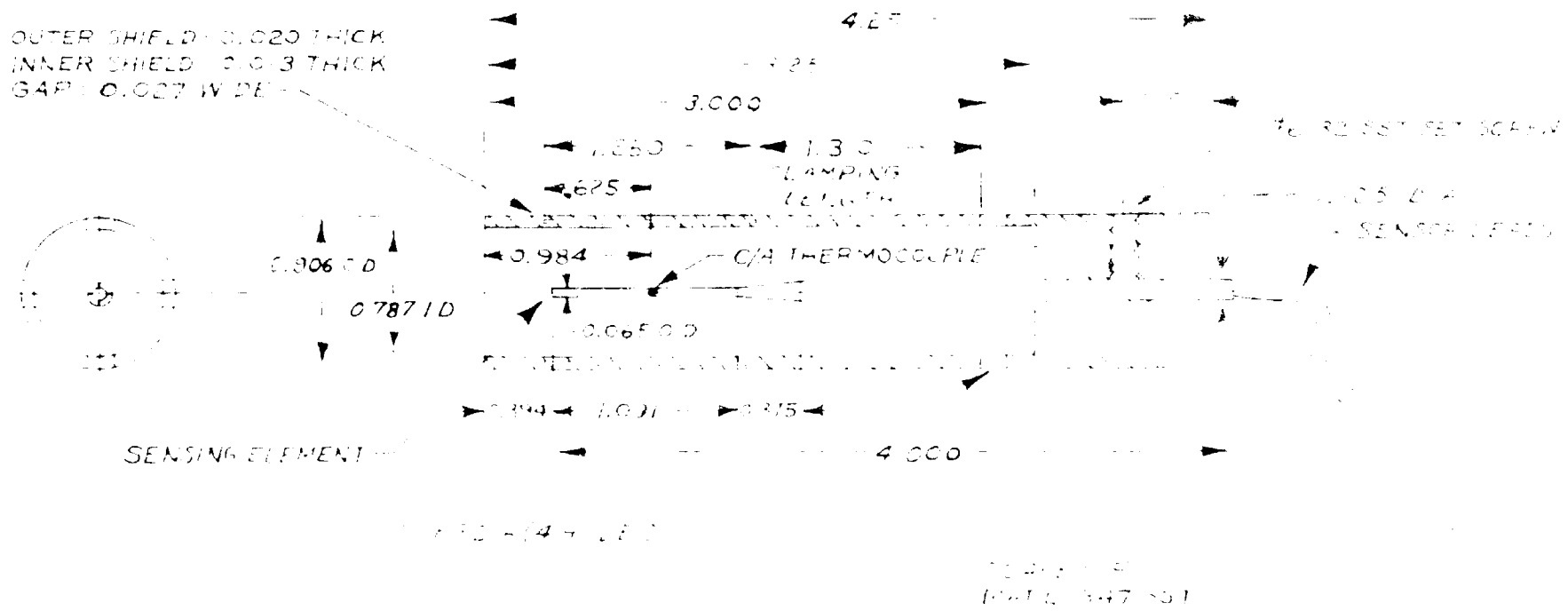

HIGH TEMPERATURE - HIGH ALTITUDE TOTAL TEMPERATURE SENSOR

FIGURE

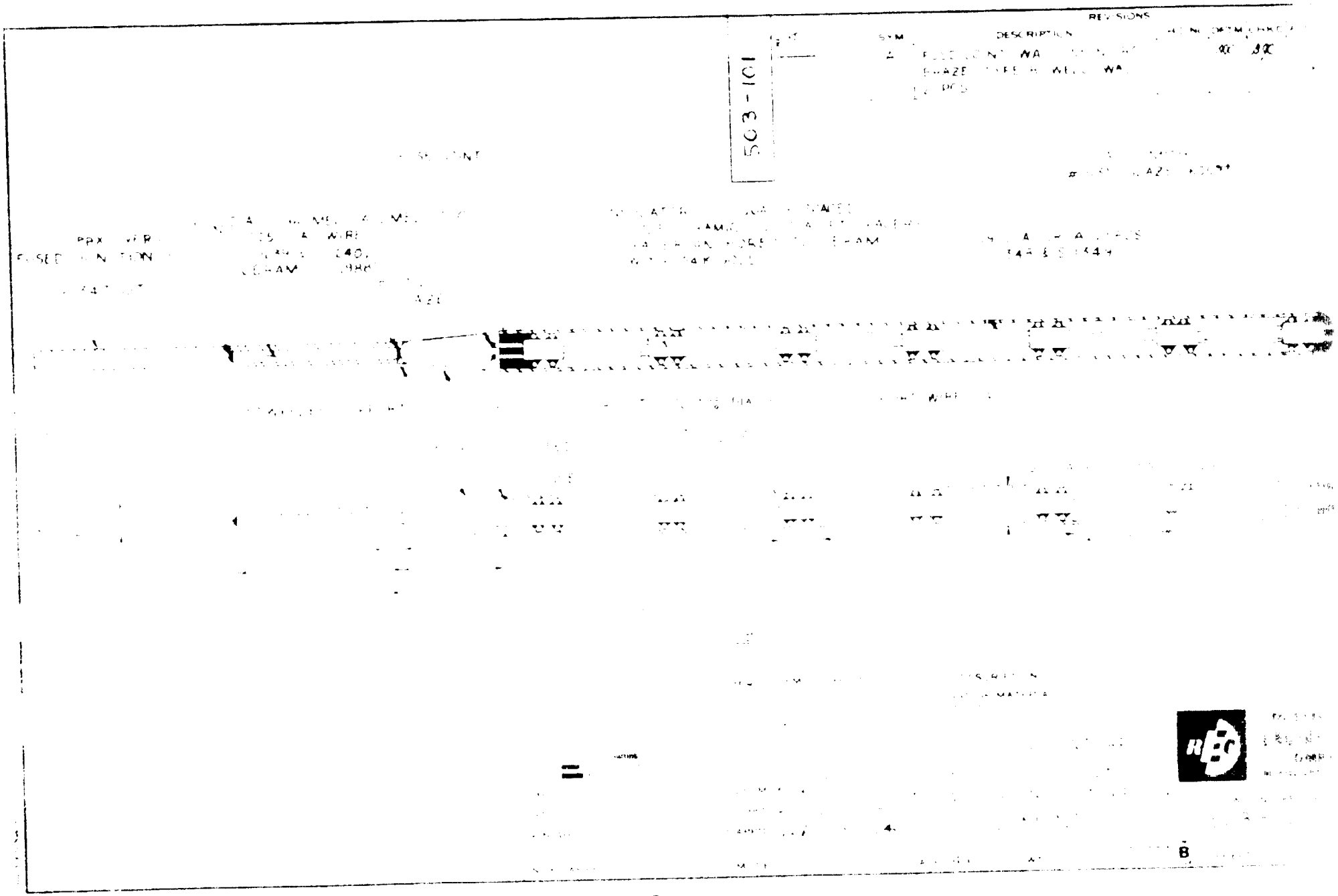

Figure 7

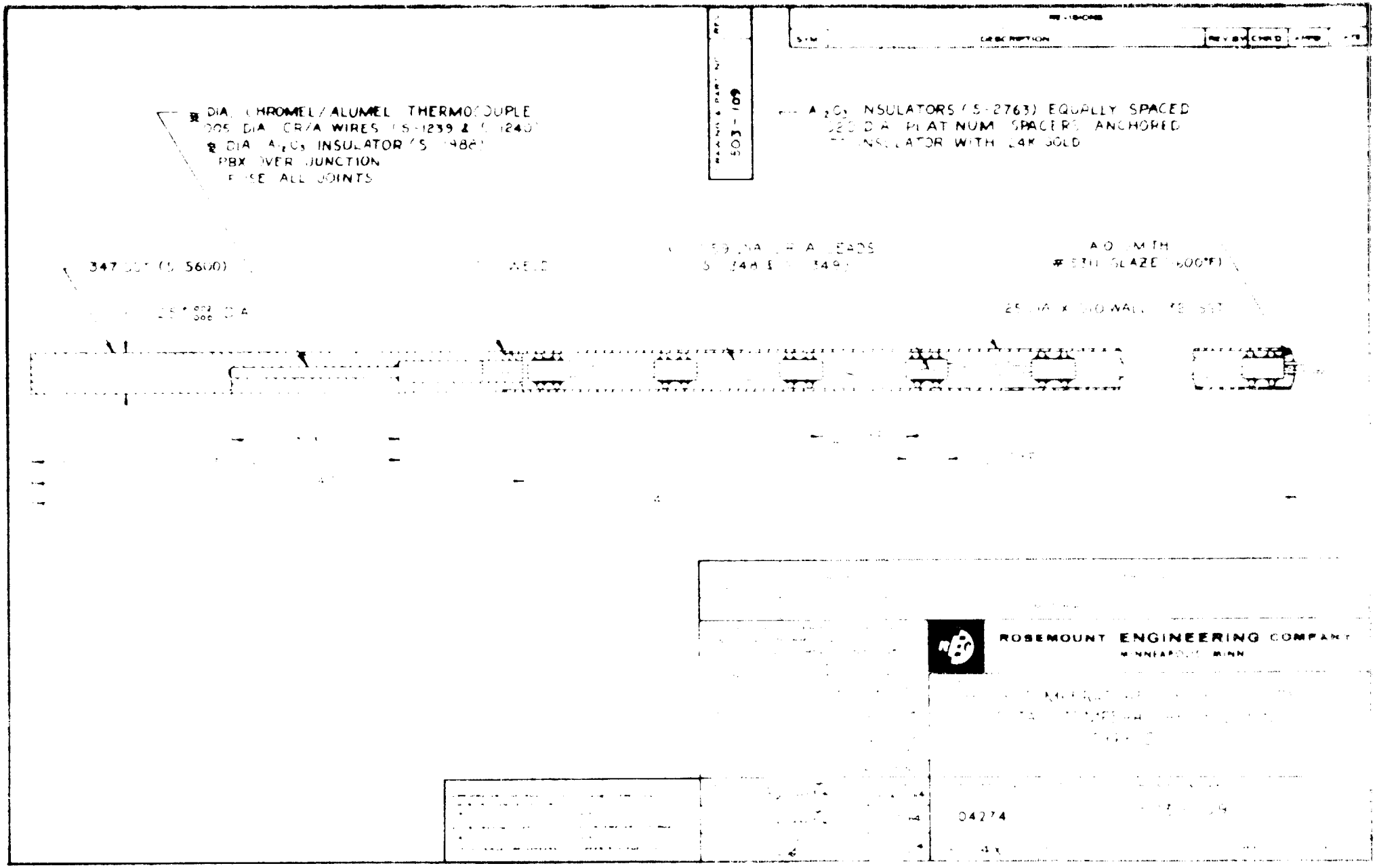
DIA CHROMEL/ALUMEL THERMOCOUPLE
DIA CR/A WIRES
DIA A_2O_3 INSULATOR
PBX OVER JUNCTION
A_2O_3 INSULATORS EQUALLY SPACED
DIA PLATINUM SPACERS ANCHORED
INSULATOR WITH 24K GOLD
ROSEMOUNT ENGINEERING COMPANY
04274

Figure 8

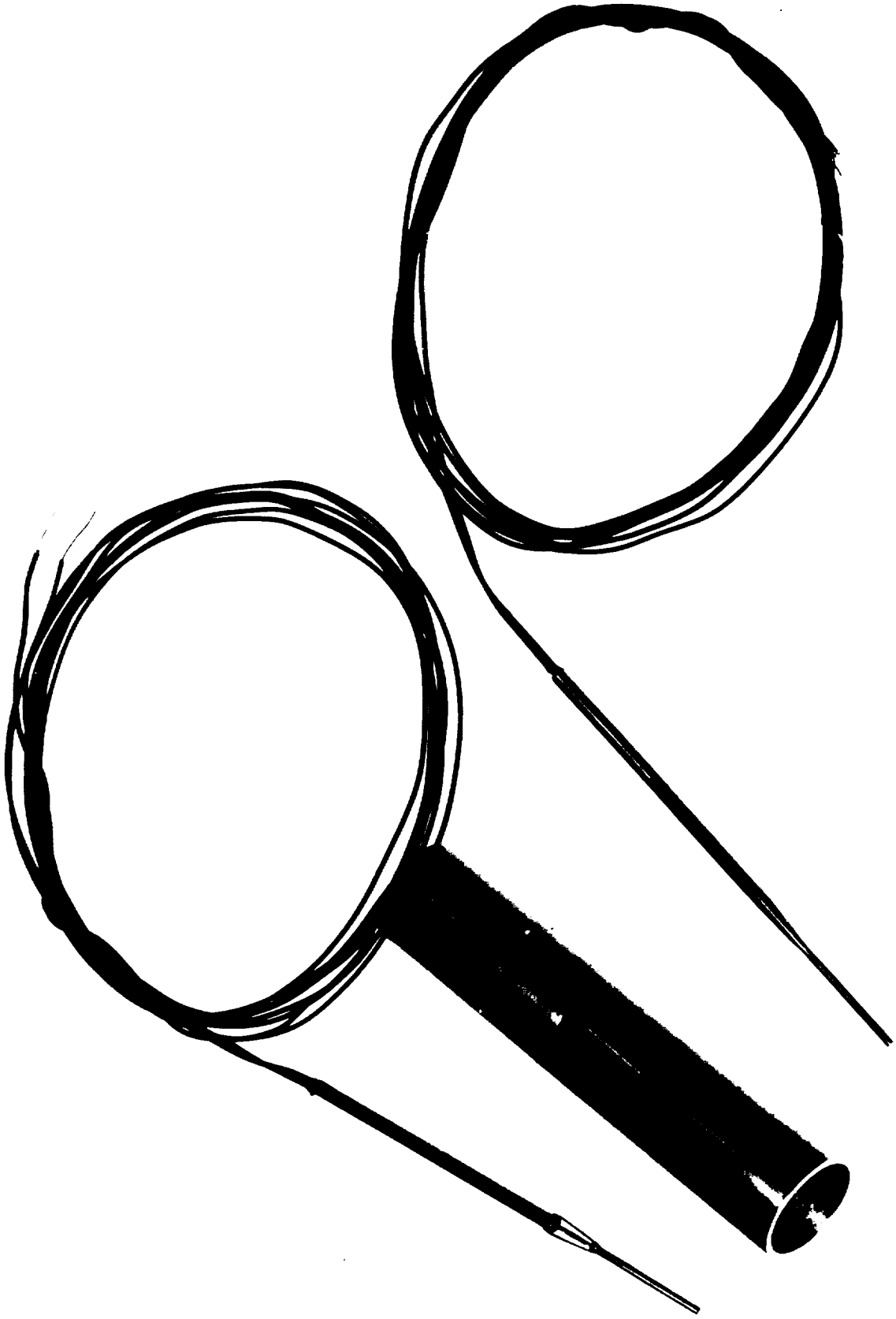

Figure 9: Photograph of Sensor Shield and Elements, Type A (Left) and Type B

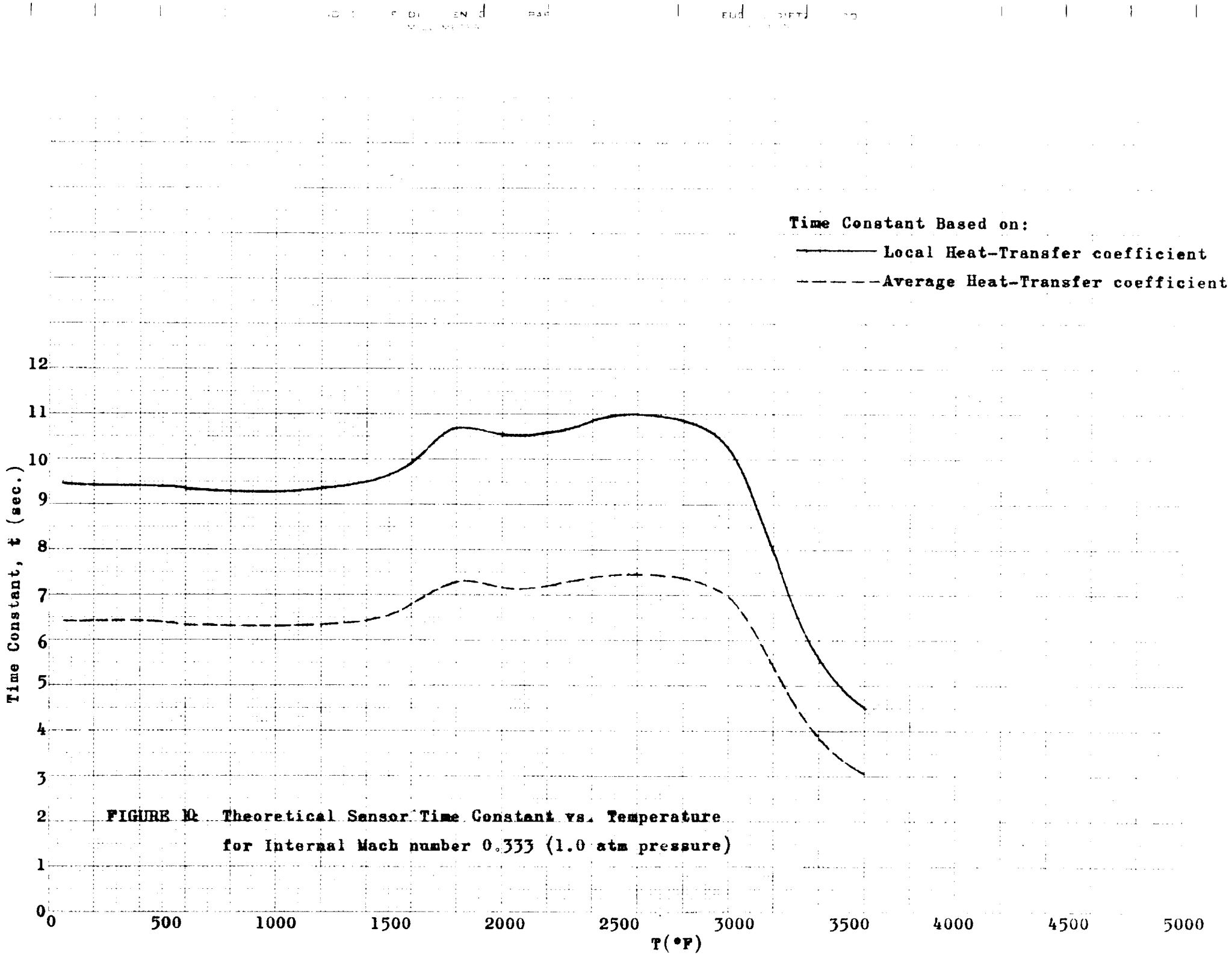

FIGURE 10 Theoretical Sensor Time Constant vs. Temperature for Internal Mach number 0.333 (1.0 atm pressure)

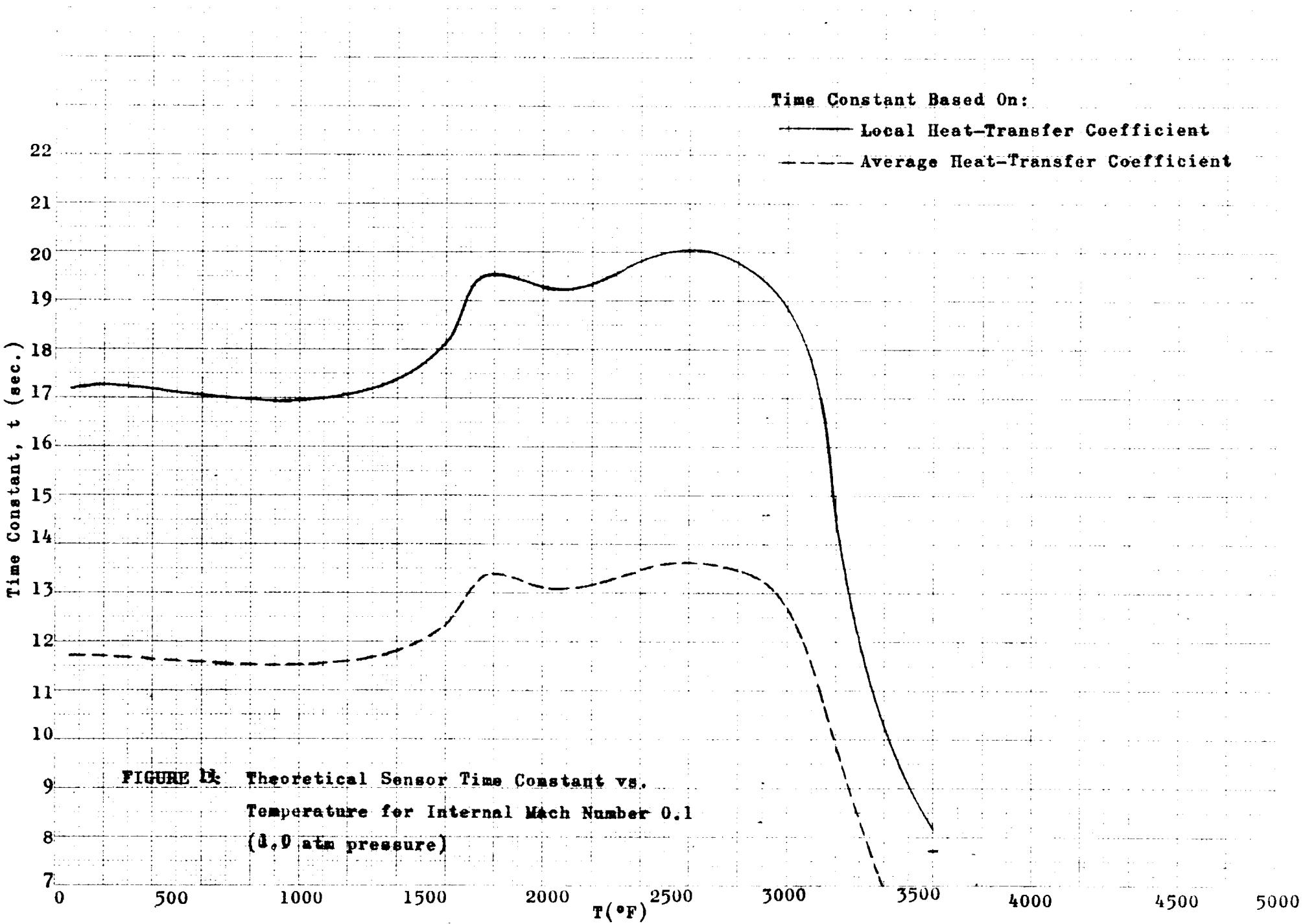

FIGURE 11: Theoretical Sensor Time Constant vs. Temperature for Internal Mach Number 0.1 (1.0 atm pressure)

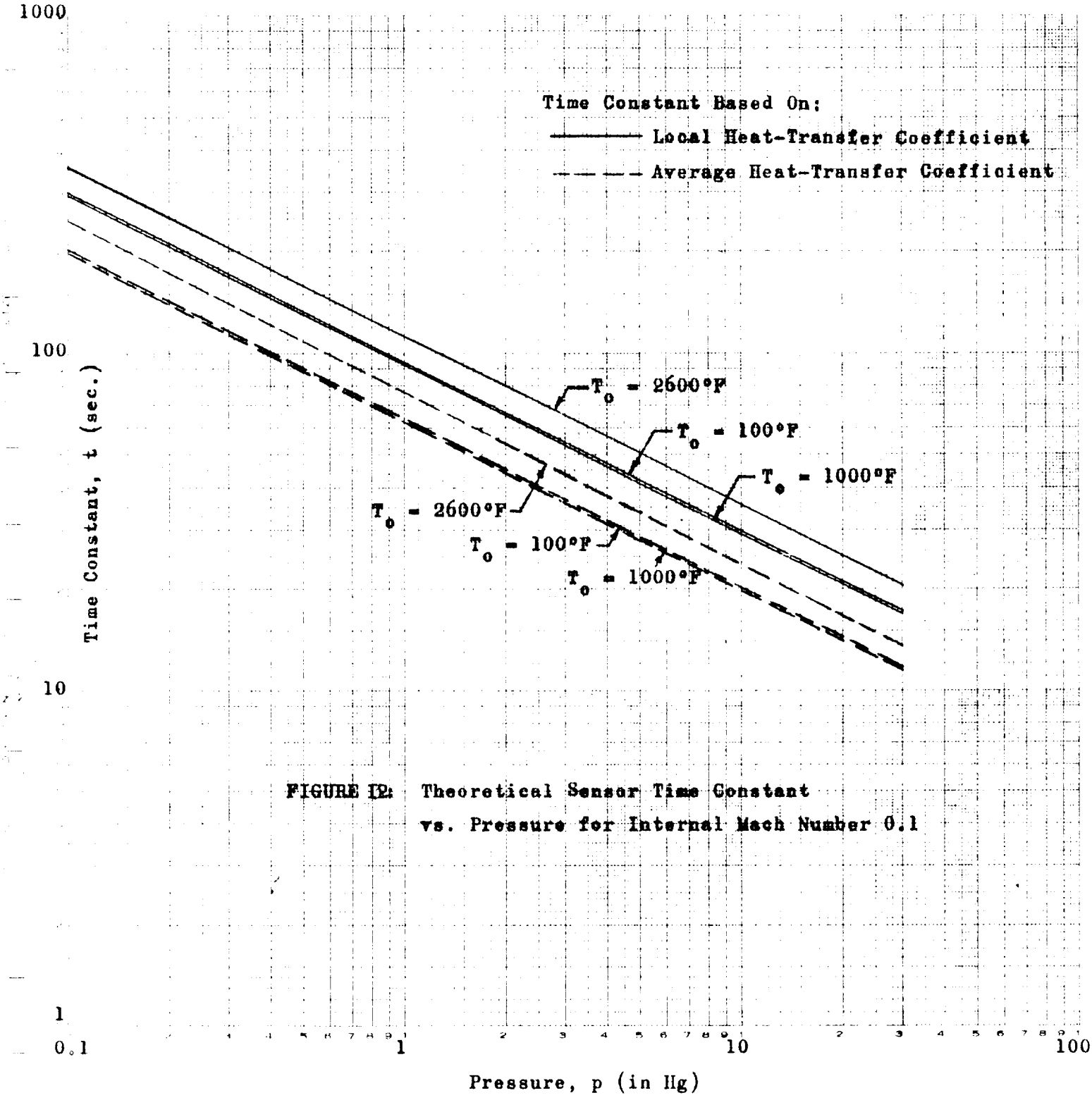

FIGURE 12: Theoretical Sensor Time Constant vs. Pressure for Internal Mach Number 0.1

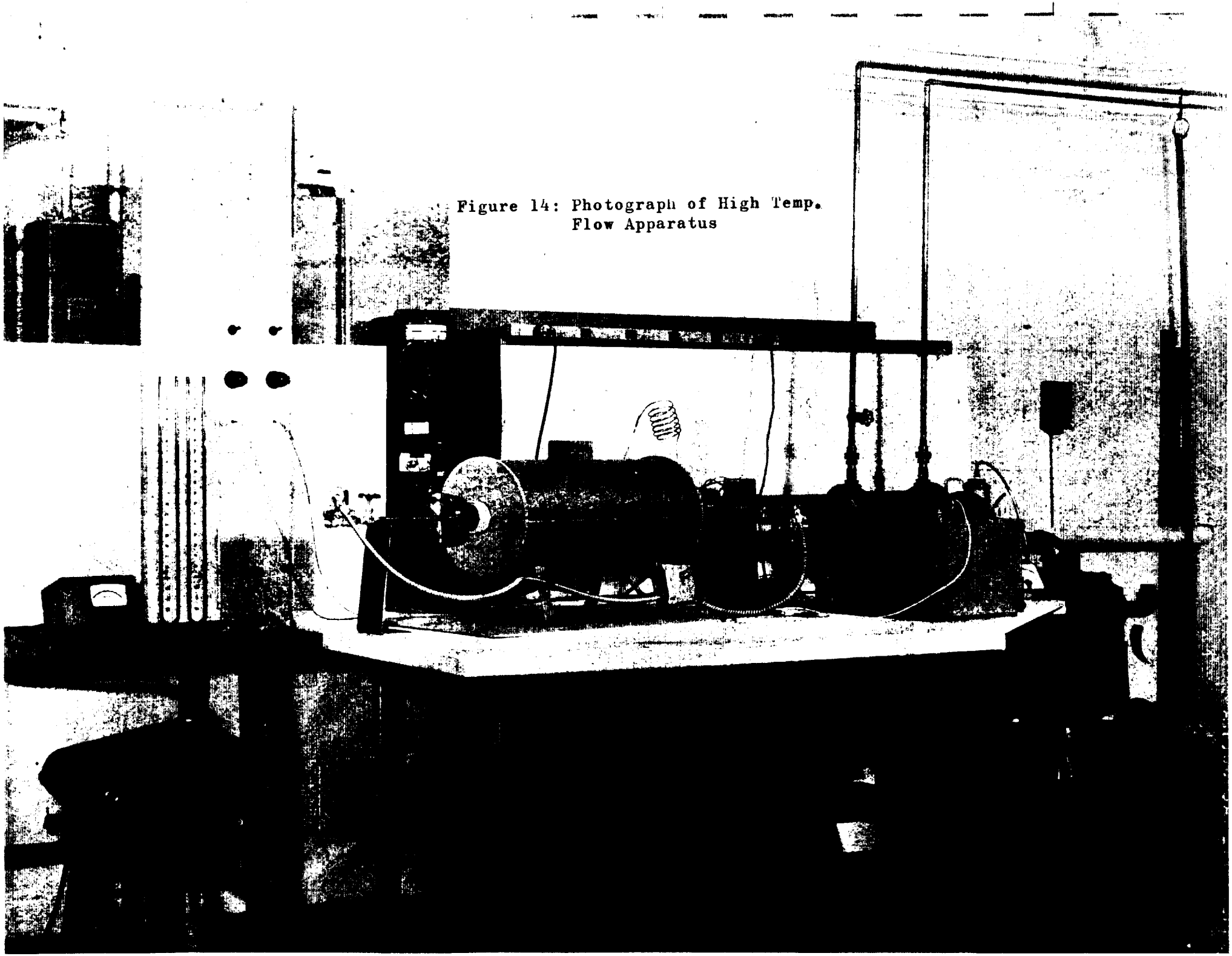

Figure 14: Photograph of High Temp. Flow Apparatus

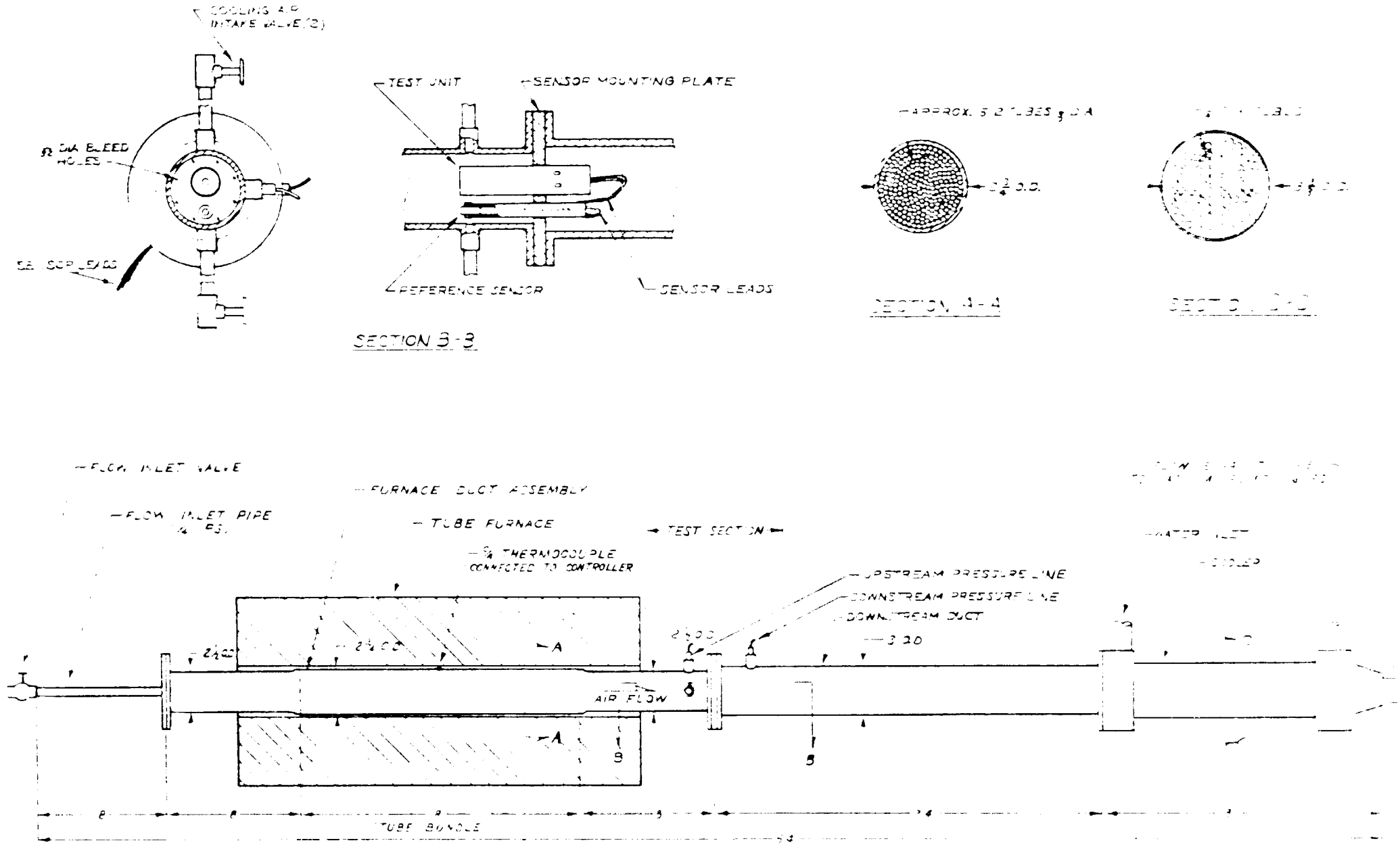

HIGH TEMPERATURE FLOW APPARATUS

FIGURE 13

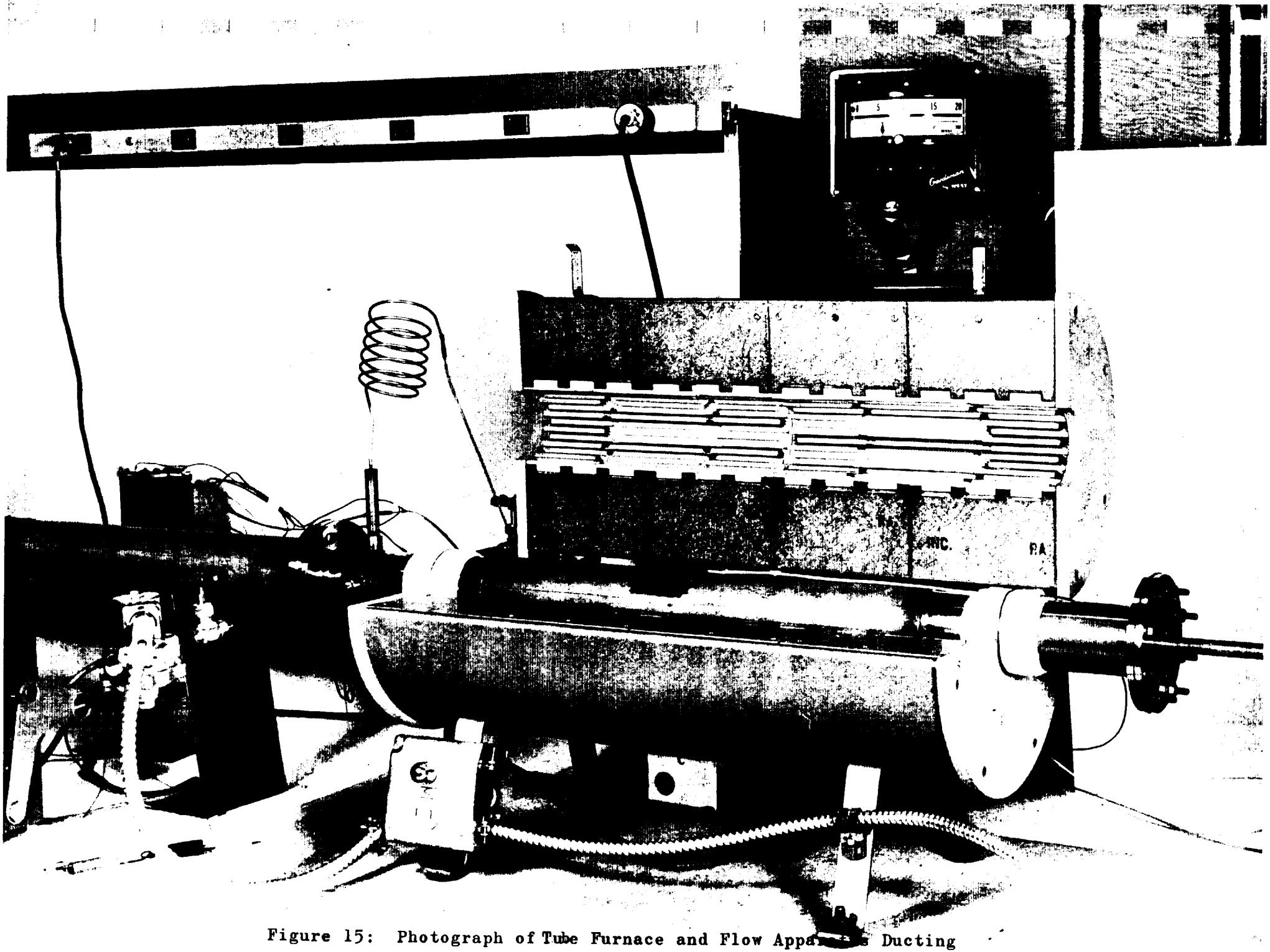

Figure 15: Photograph of Tube Furnace and Flow Appa[illegible] Ducting

Figure 16: Photograph of Test Sensor and Reference Sensor Installed in Mounting Flange

FIGURE 17 TYPICAL TOTAL TEMPERATURE OUTPUT TRACE FOR TIME CONSTANT DETERMINATION

Time Constant = Time t at 63.5% of ΔT

or

Time t at intersection of initial slope with final temperature

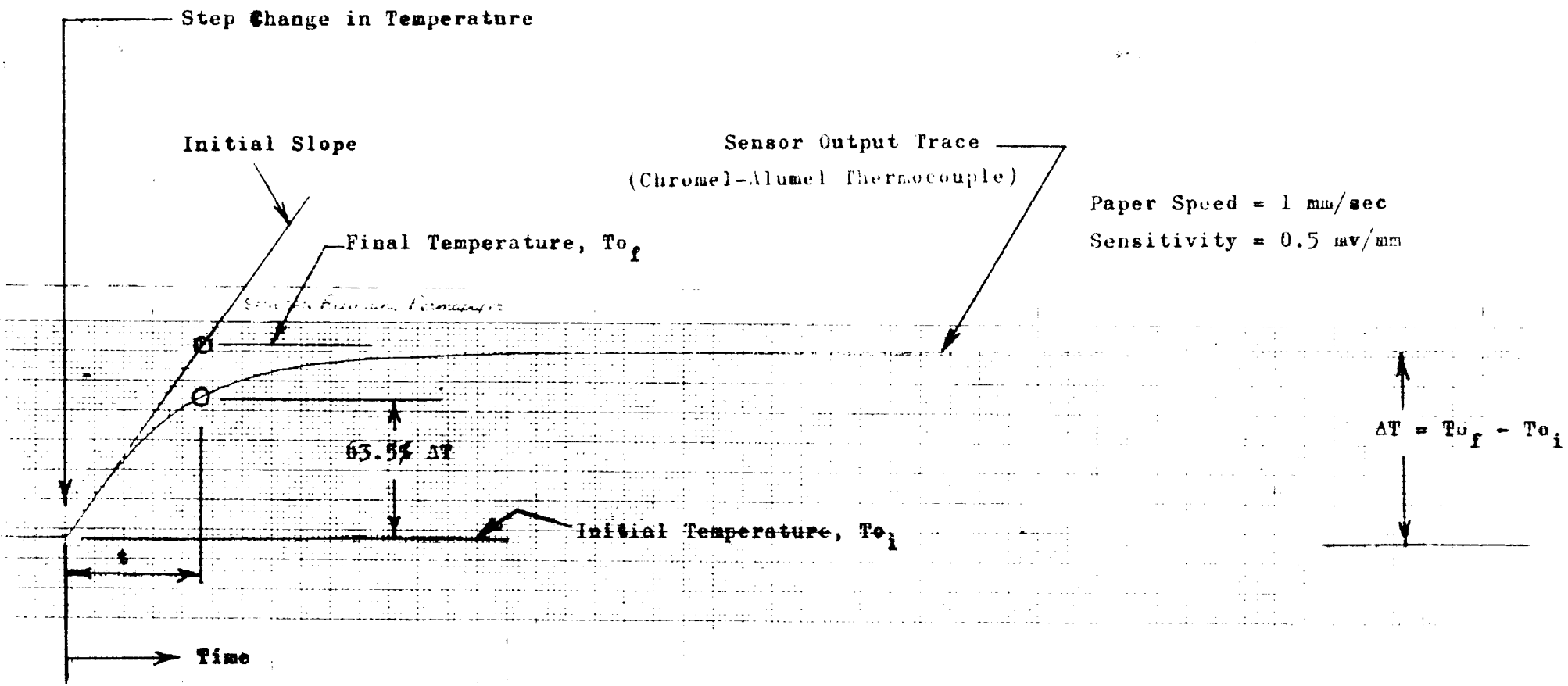

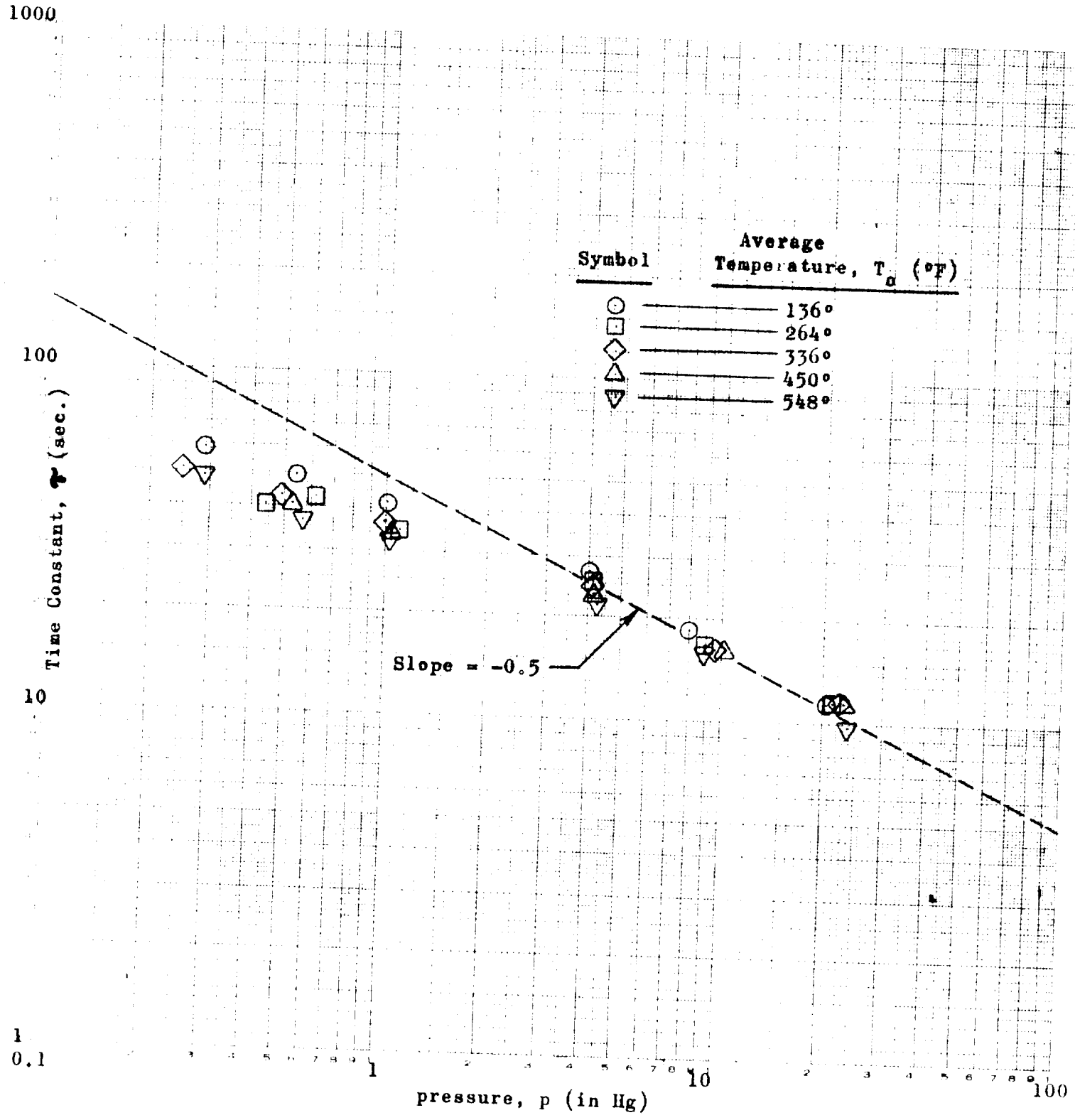

FIGURE 18: Time Constant vs. Pressure for Type A Sensing Element

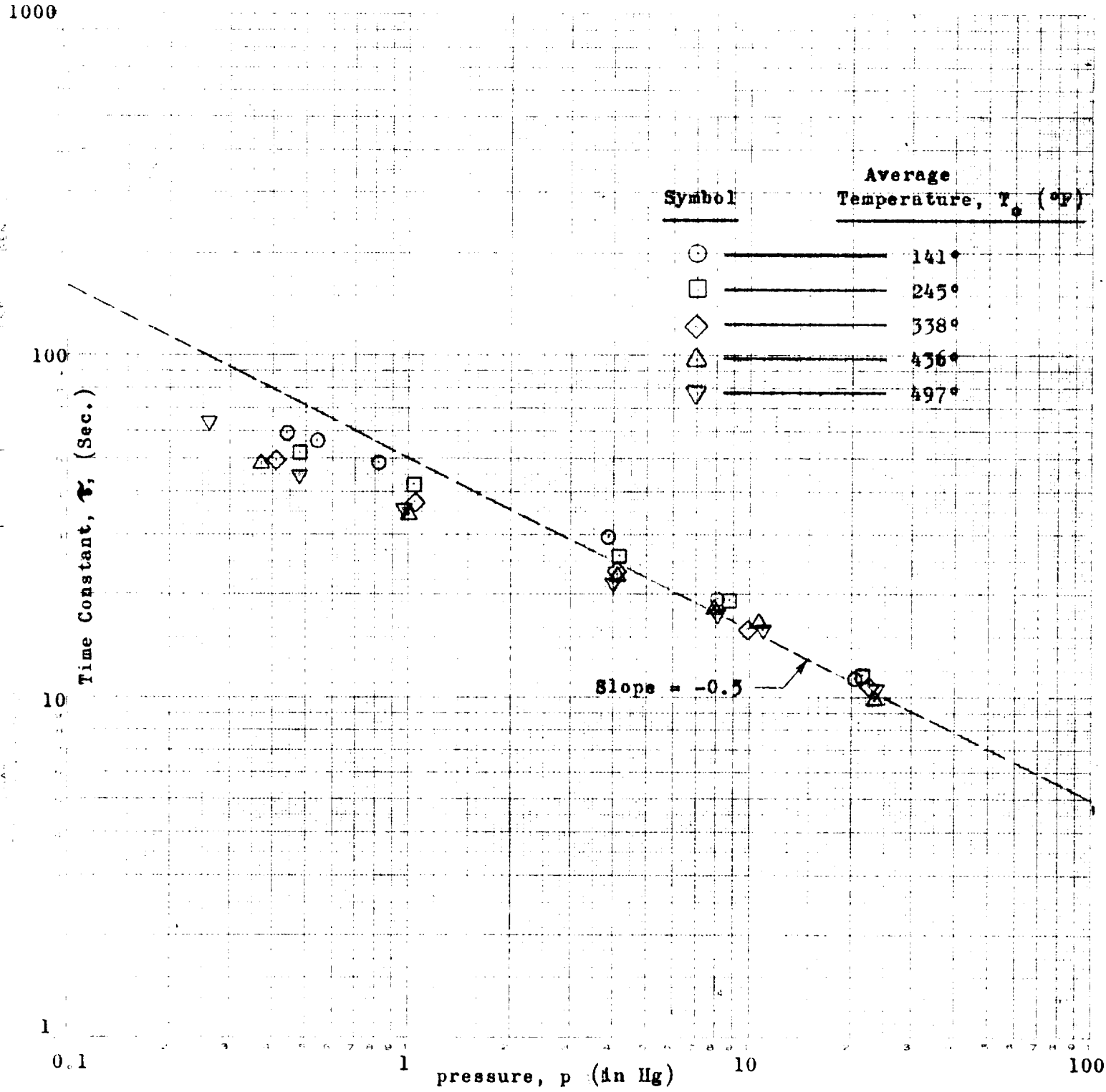

FIGURE 19 Time Constant vs. Pressure for Type B Sensing Element

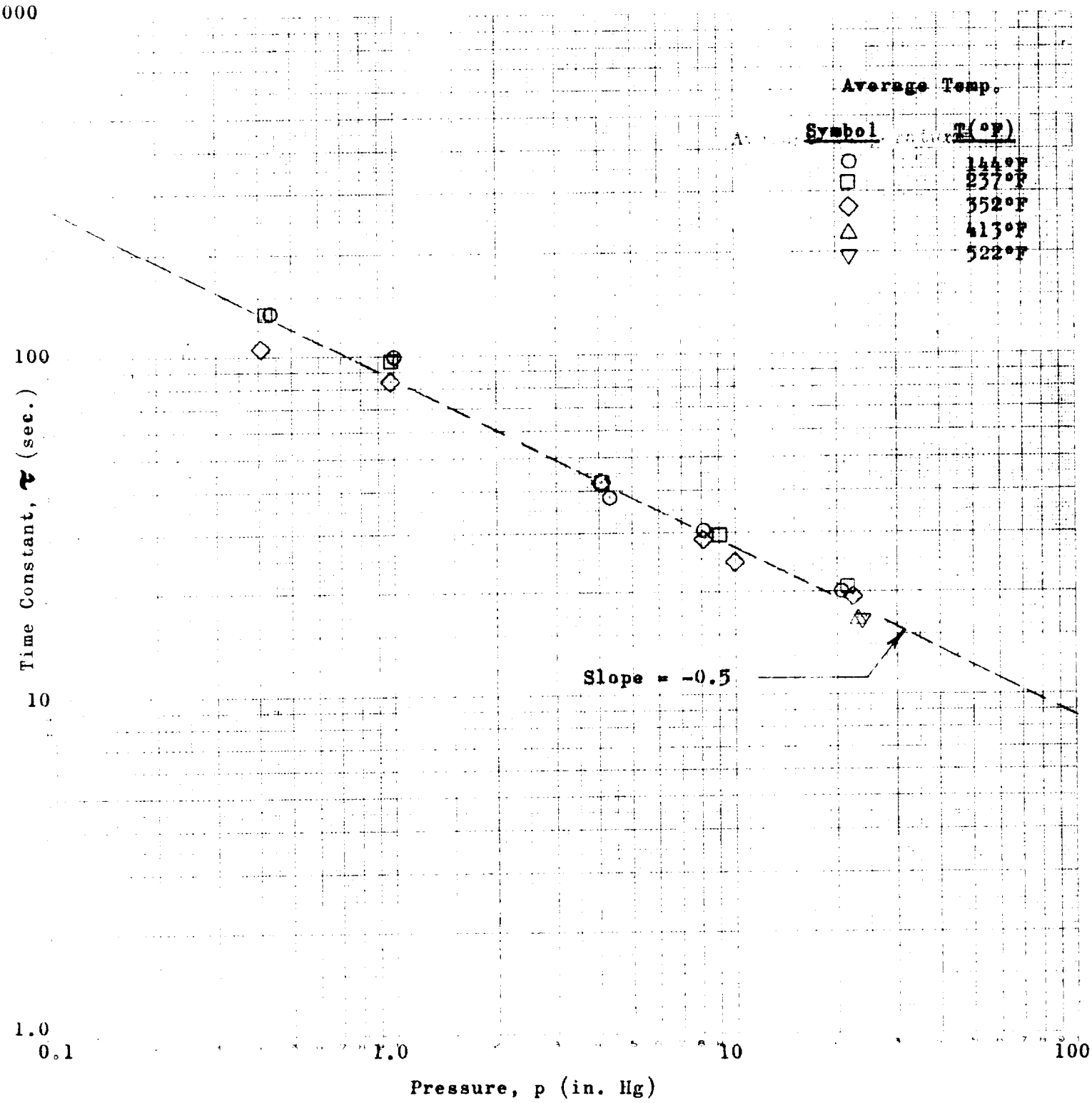

FIGURE 20 Time Constant vs. Pressure for Type C Sensing Element

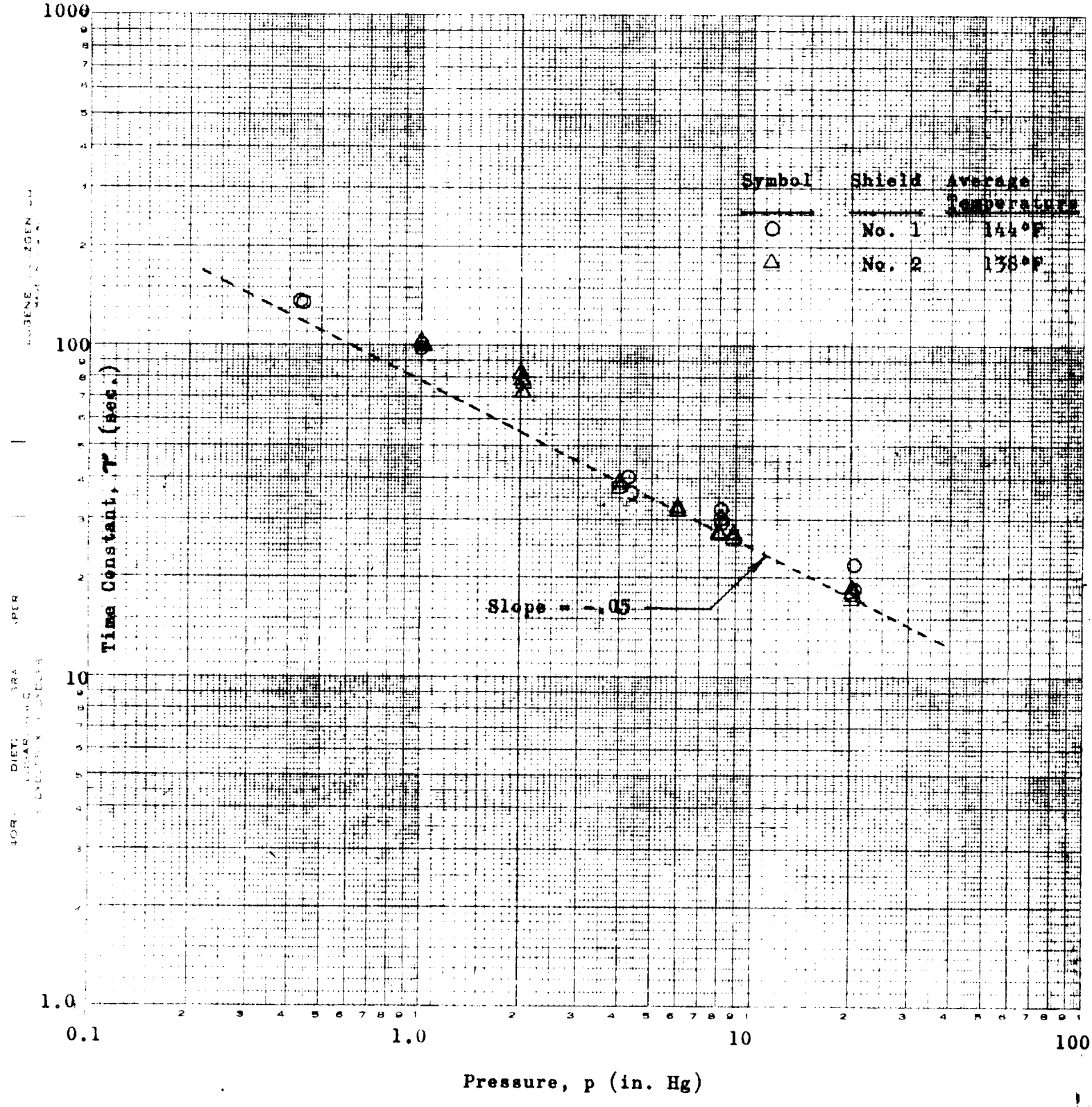

FIGURE 21: Time Constant vs. Pressure for Type C Sensing Element Installed in Two Radiation Shields

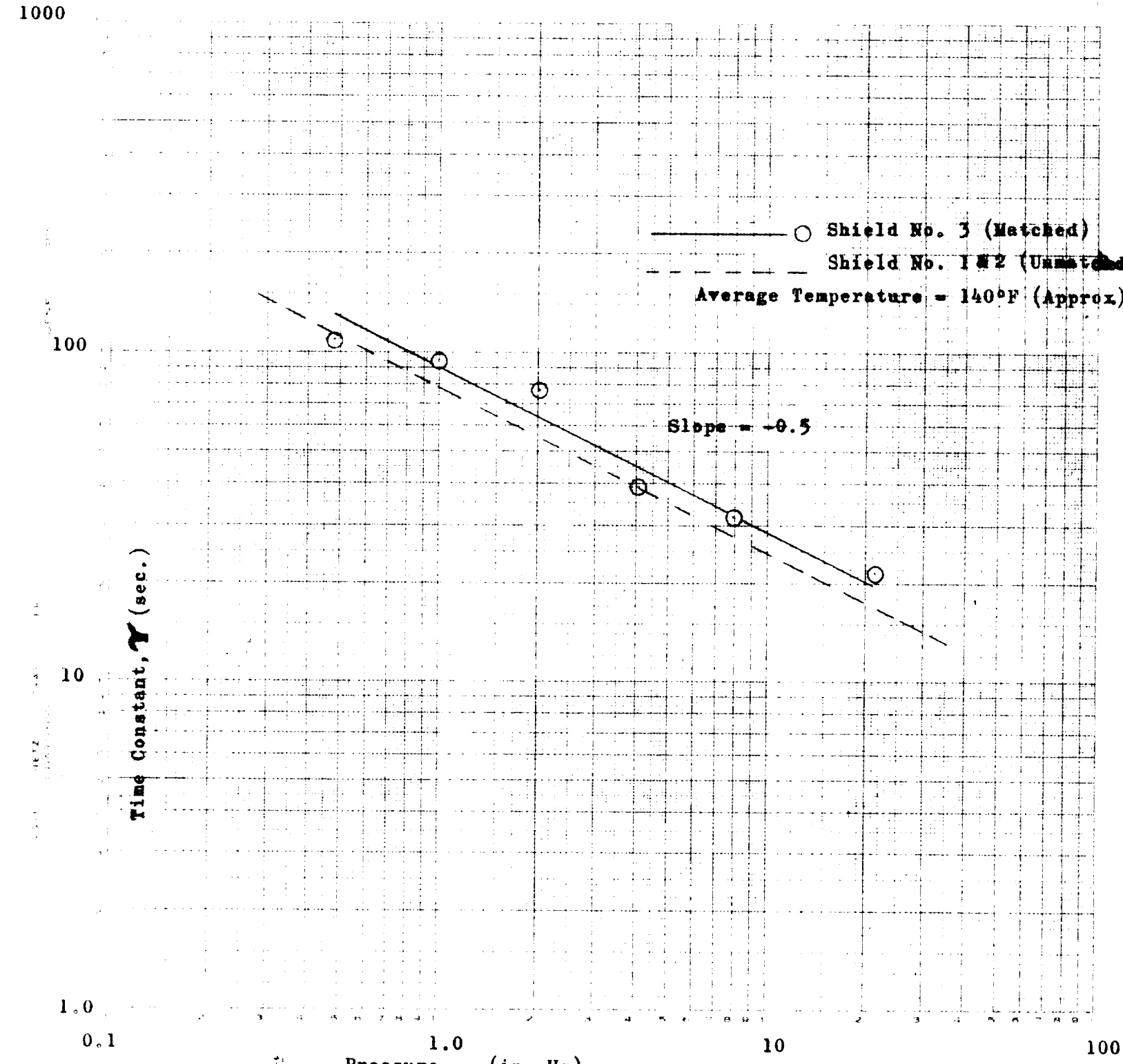

Figure 22 Time Constant Calibration For Type C Sensing Element Installed In Two Radiation Shield Configurations

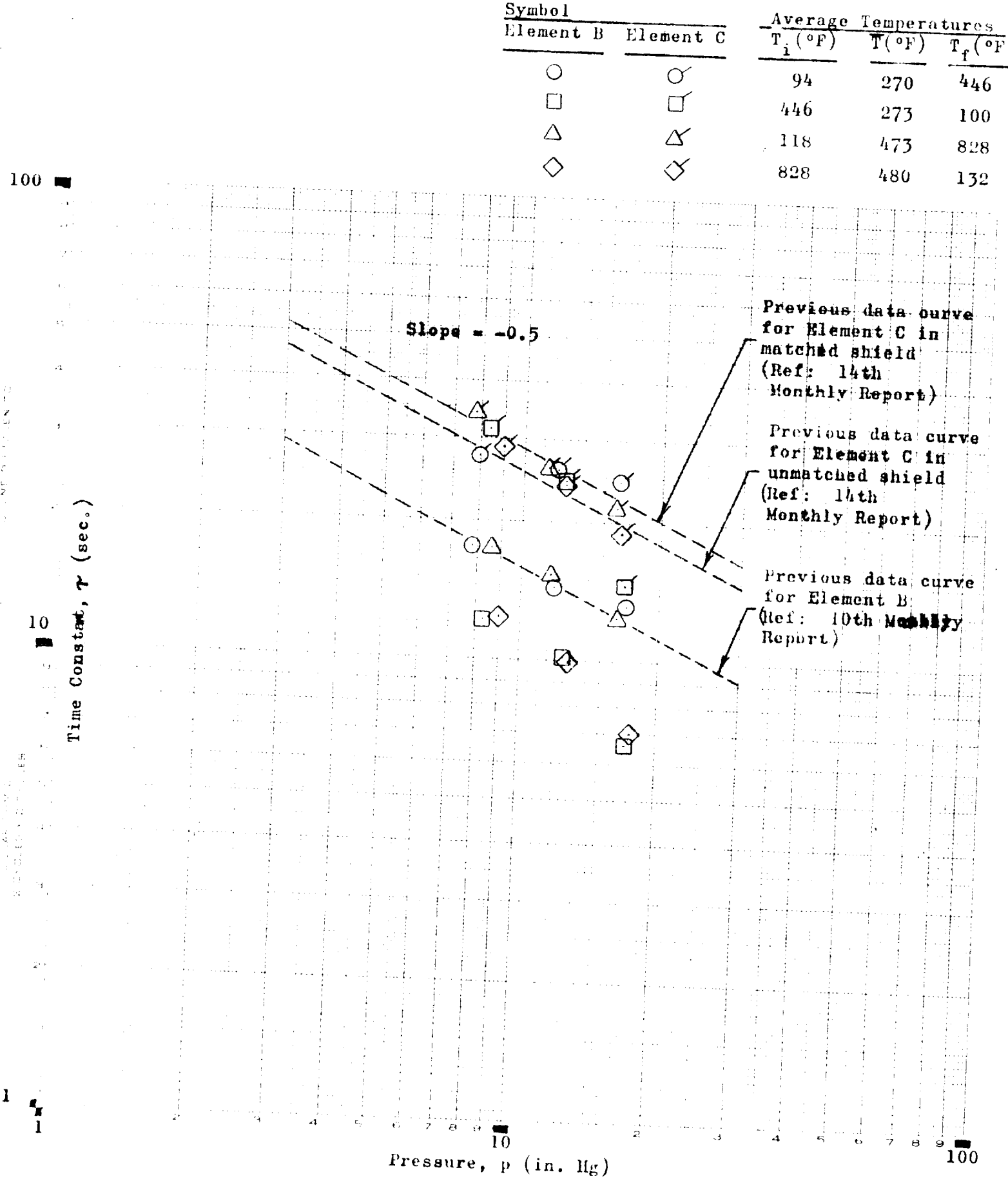

Figure 23 Calibration of Sensing Elements B and C

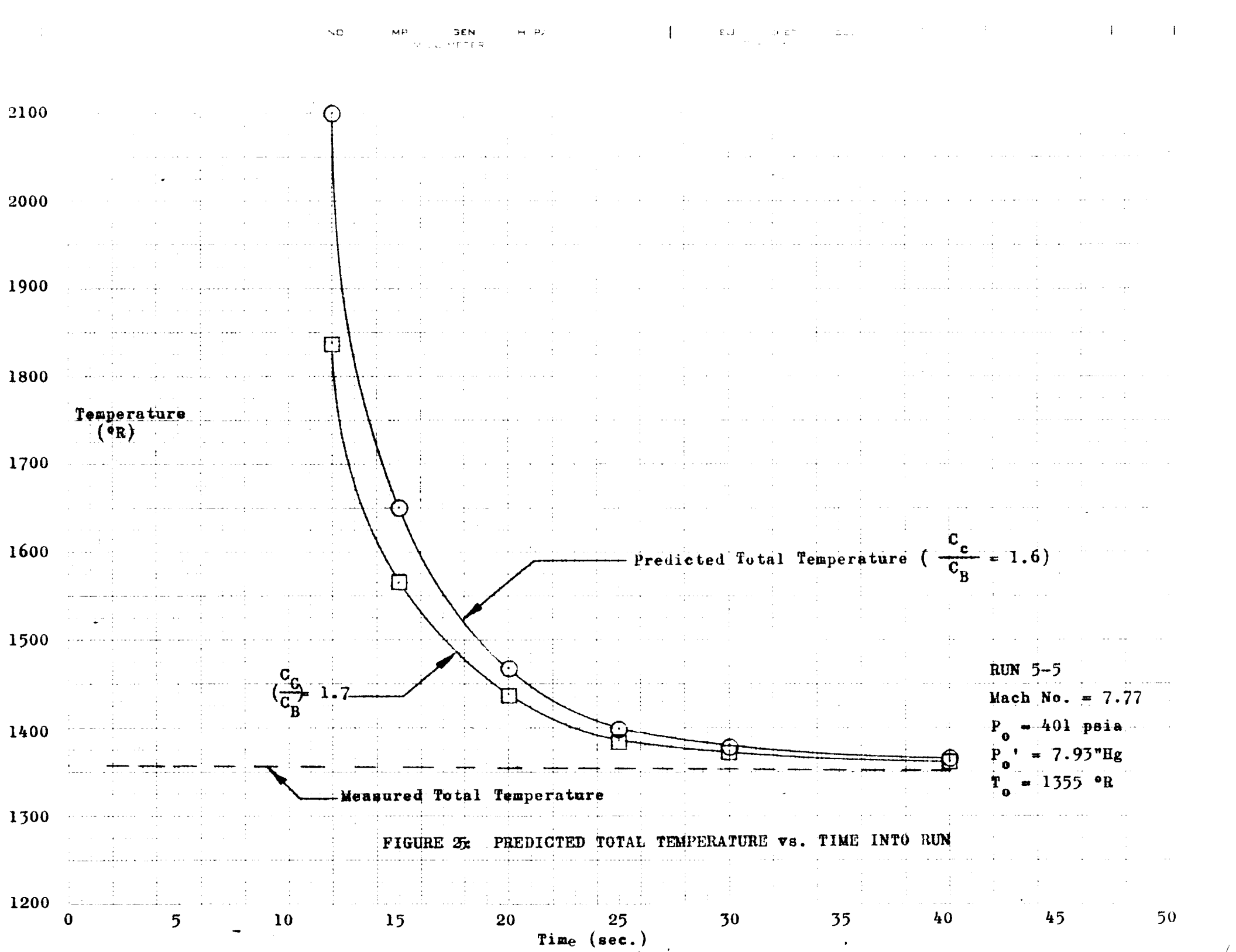

FIGURE 25: PREDICTED TOTAL TEMPERATURE vs. TIME INTO RUN

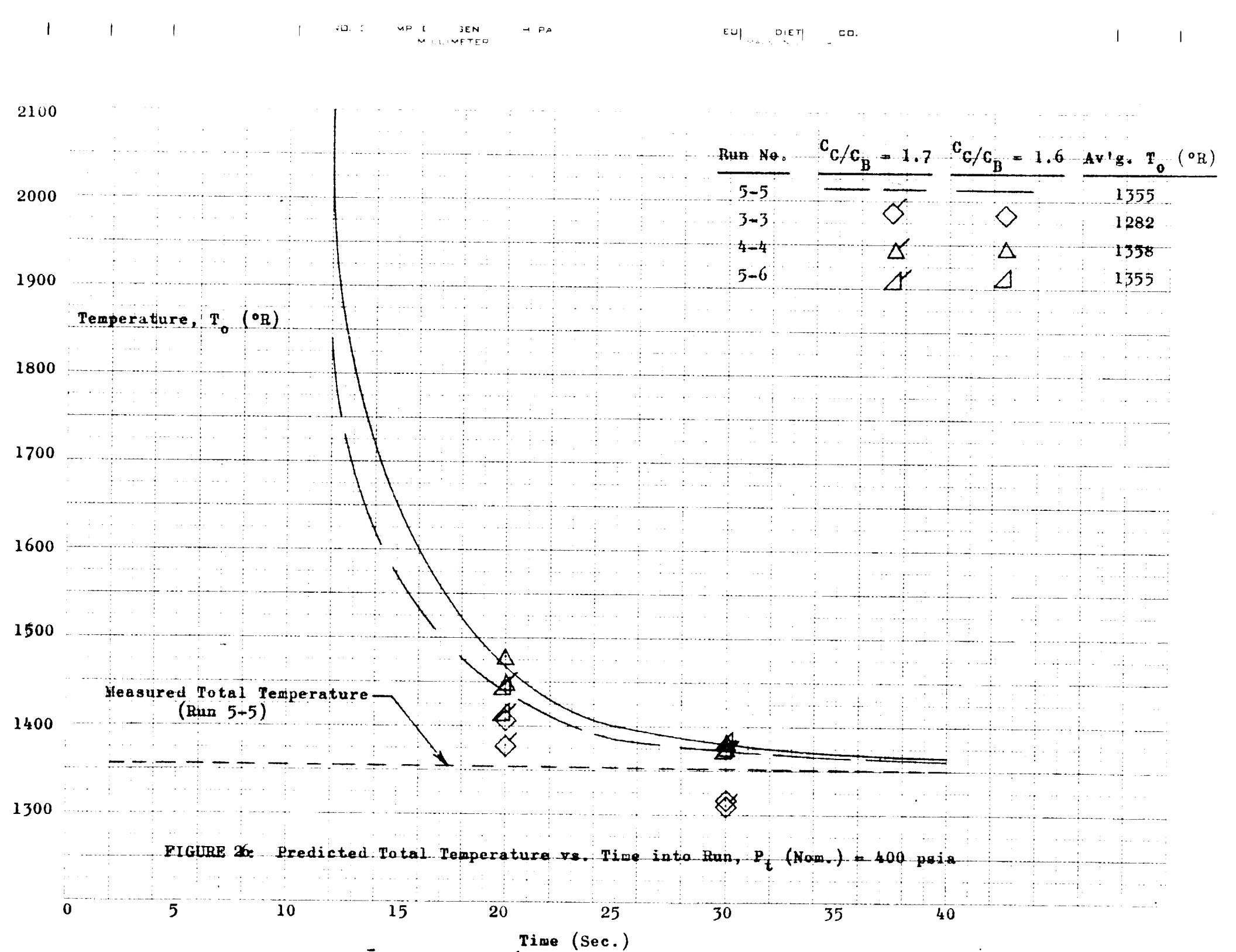

FIGURE 26. Predicted Total Temperature vs. Time into Run, P_t (Nom.) = 400 psia

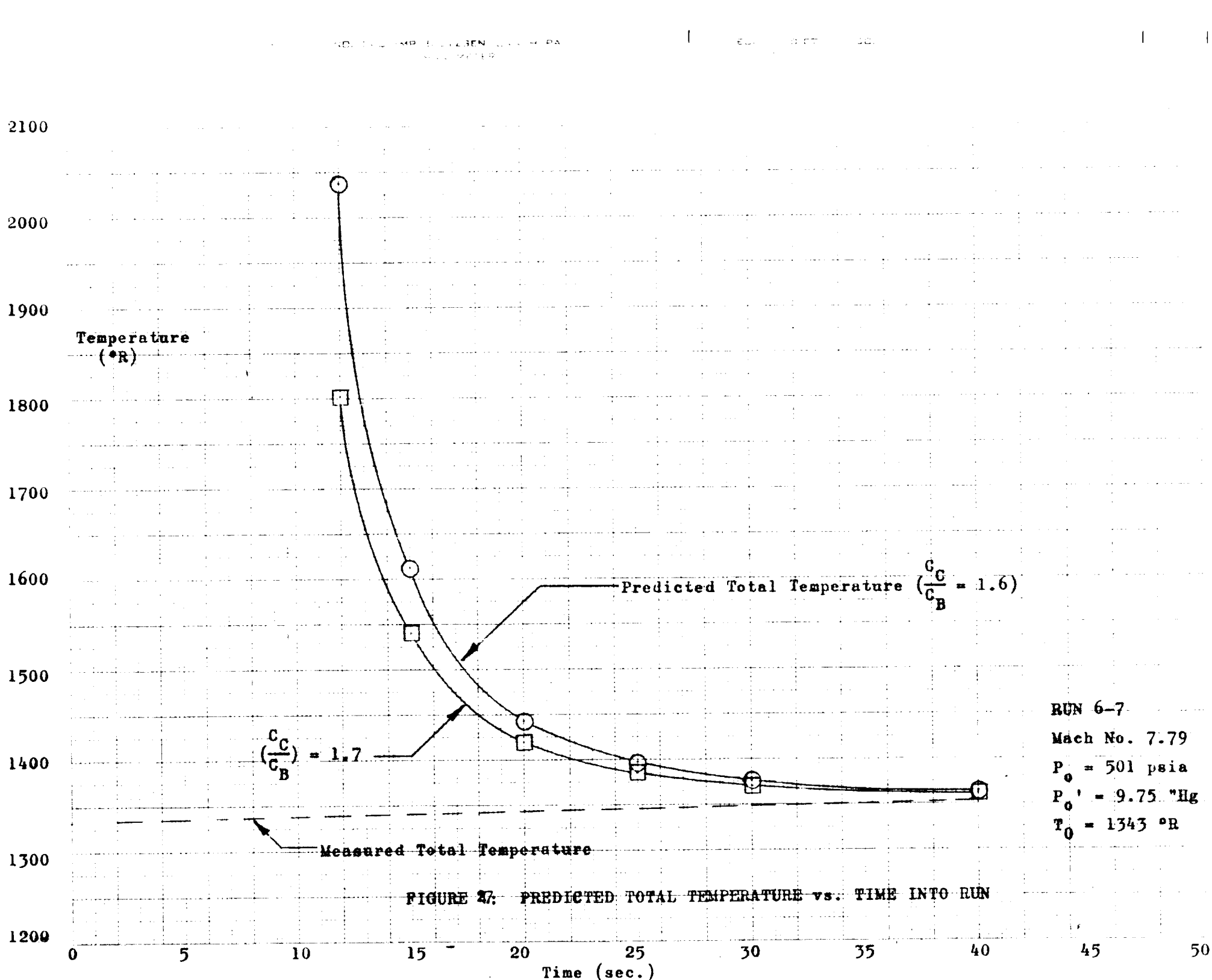

FIGURE 27: PREDICTED TOTAL TEMPERATURE vs. TIME INTO RUN

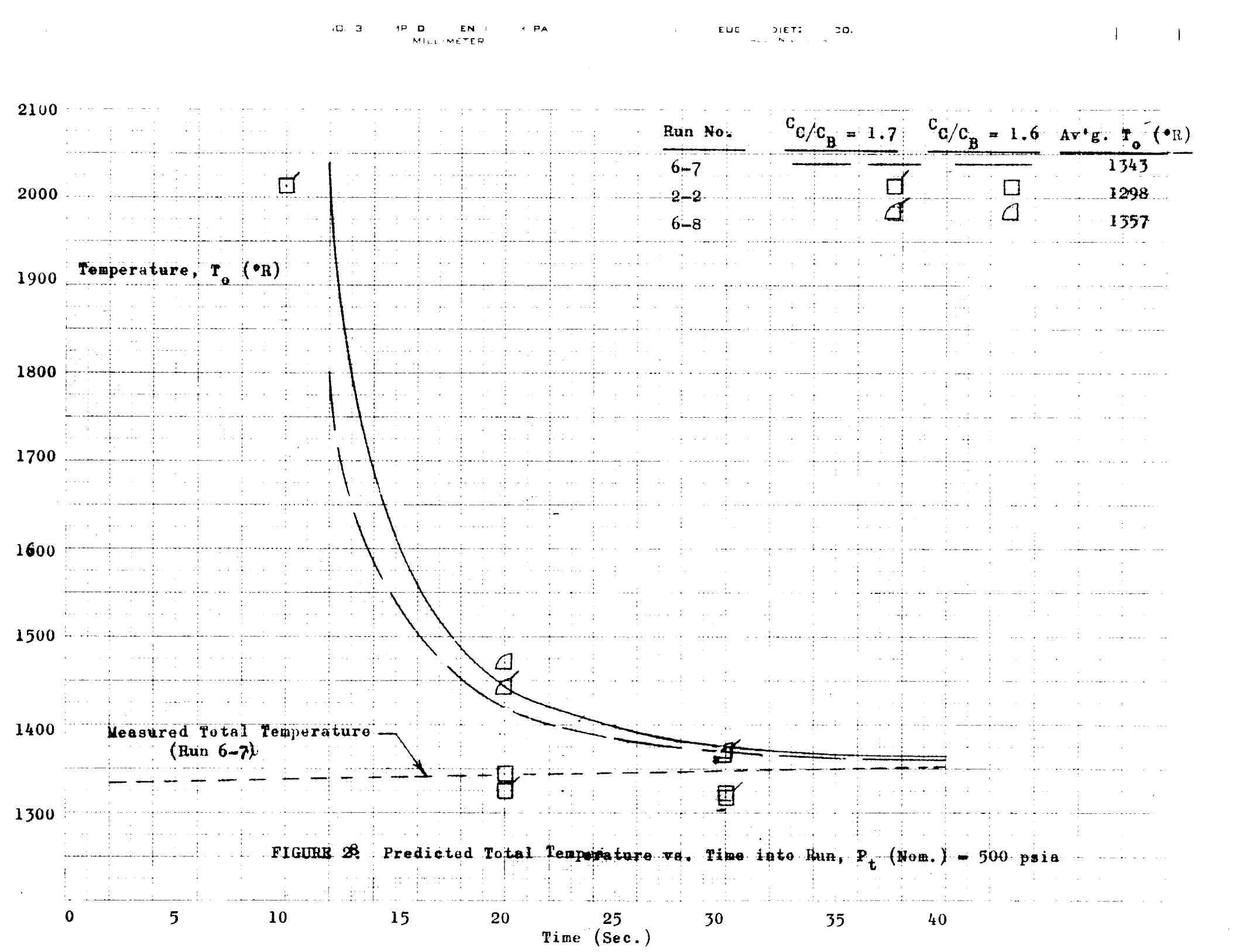

FIGURE 28. Predicted Total Temperature vs. Time into Run, P_t (Nom.) = 500 psia

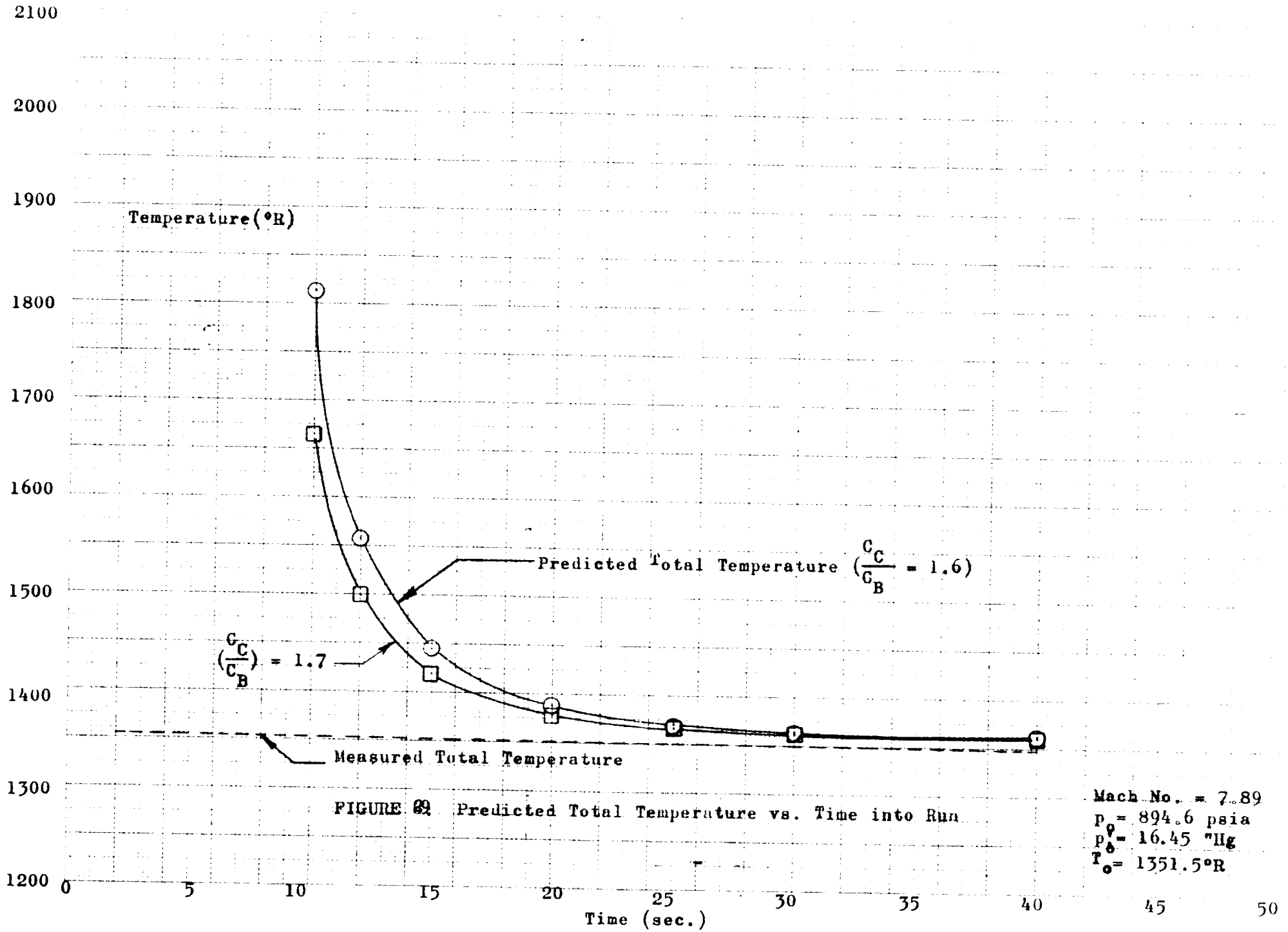

FIGURE 89 Predicted Total Temperature vs. Time into Run

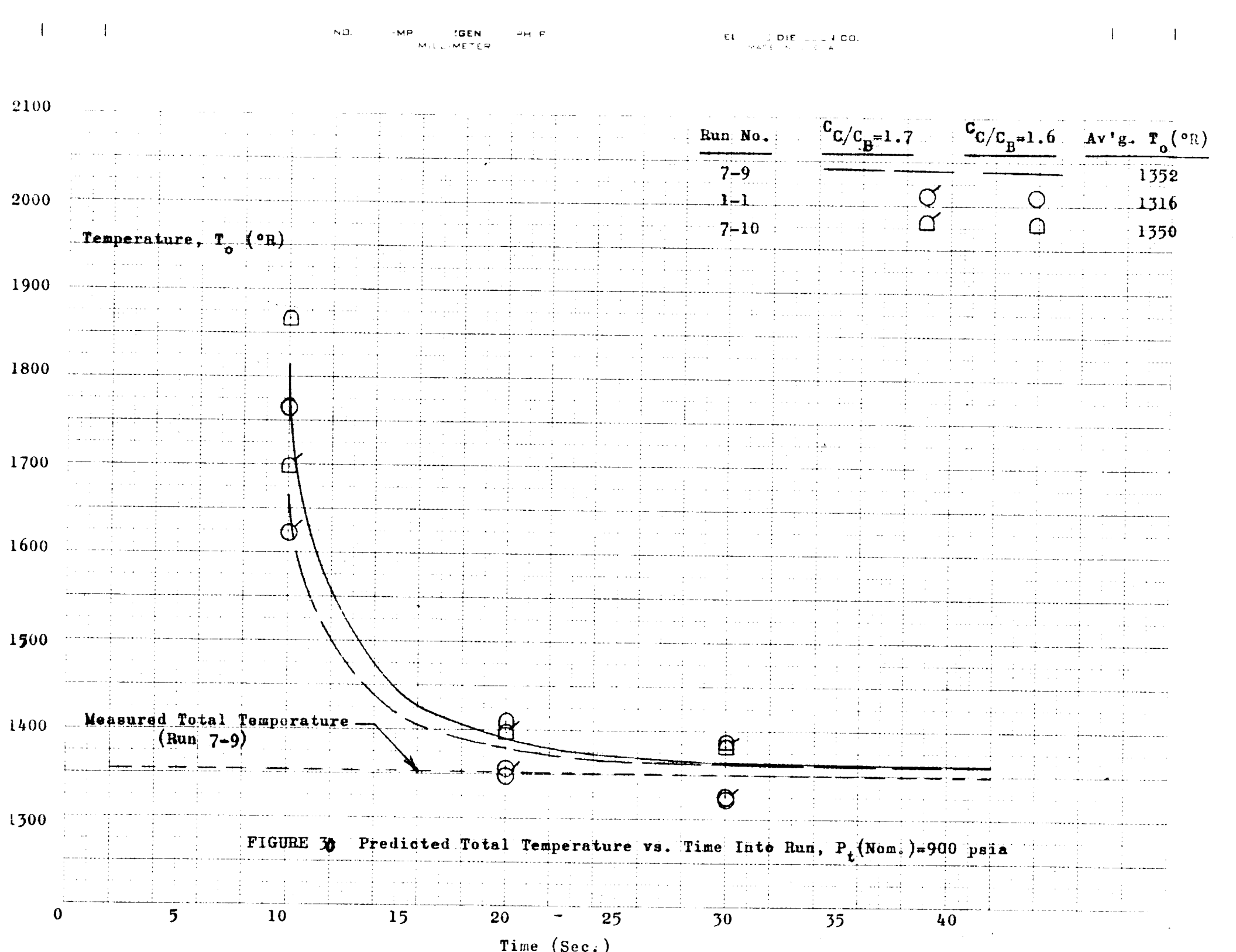

FIGURE 30 Predicted Total Temperature vs. Time Into Run, P_t(Nom.)=900 psia

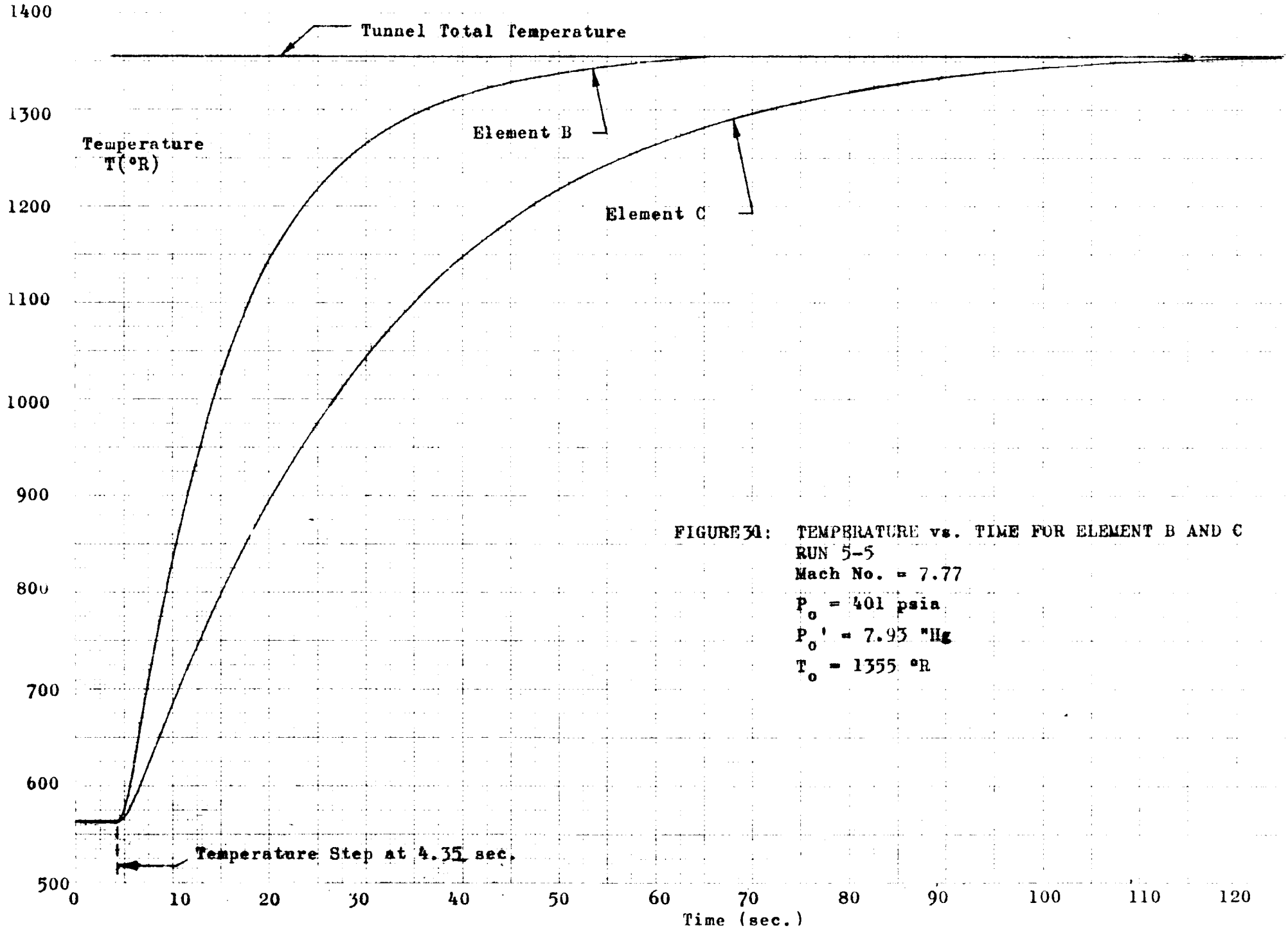

FIGURE 31: TEMPERATURE vs. TIME FOR ELEMENT B AND C
RUN 5-5
Mach No. = 7.77
P_o = 401 psia
P_o' = 7.93 "Hg
T_o = 1355 °R

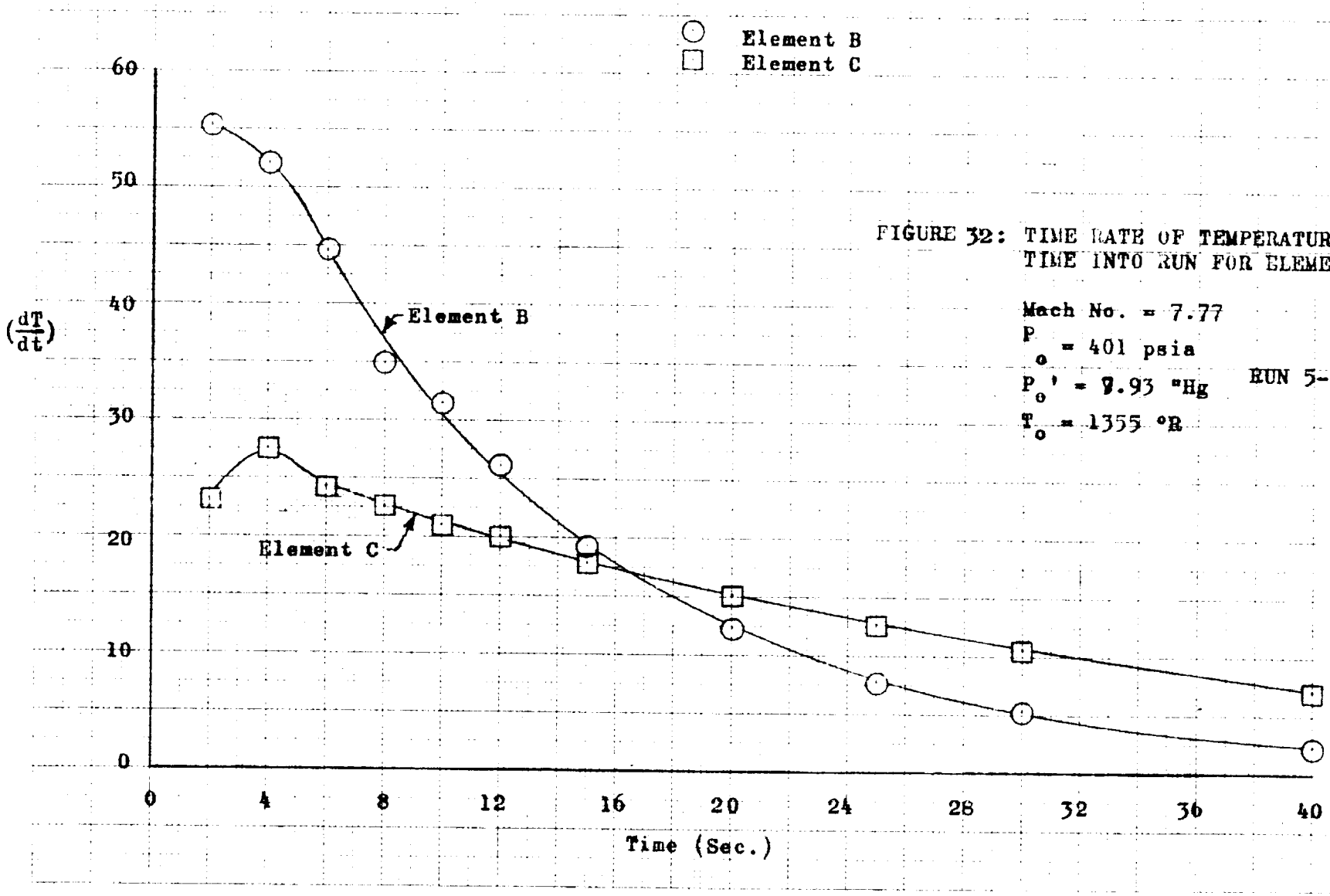

FIGURE 32: TIME RATE OF TEMPERATURE CHANGE vs. TIME INTO RUN FOR ELEMENT B AND C

Mach No. = 7.77
P_o = 401 psia
P_o' = 7.93 "Hg RUN 5-5
T_o = 1355 °R

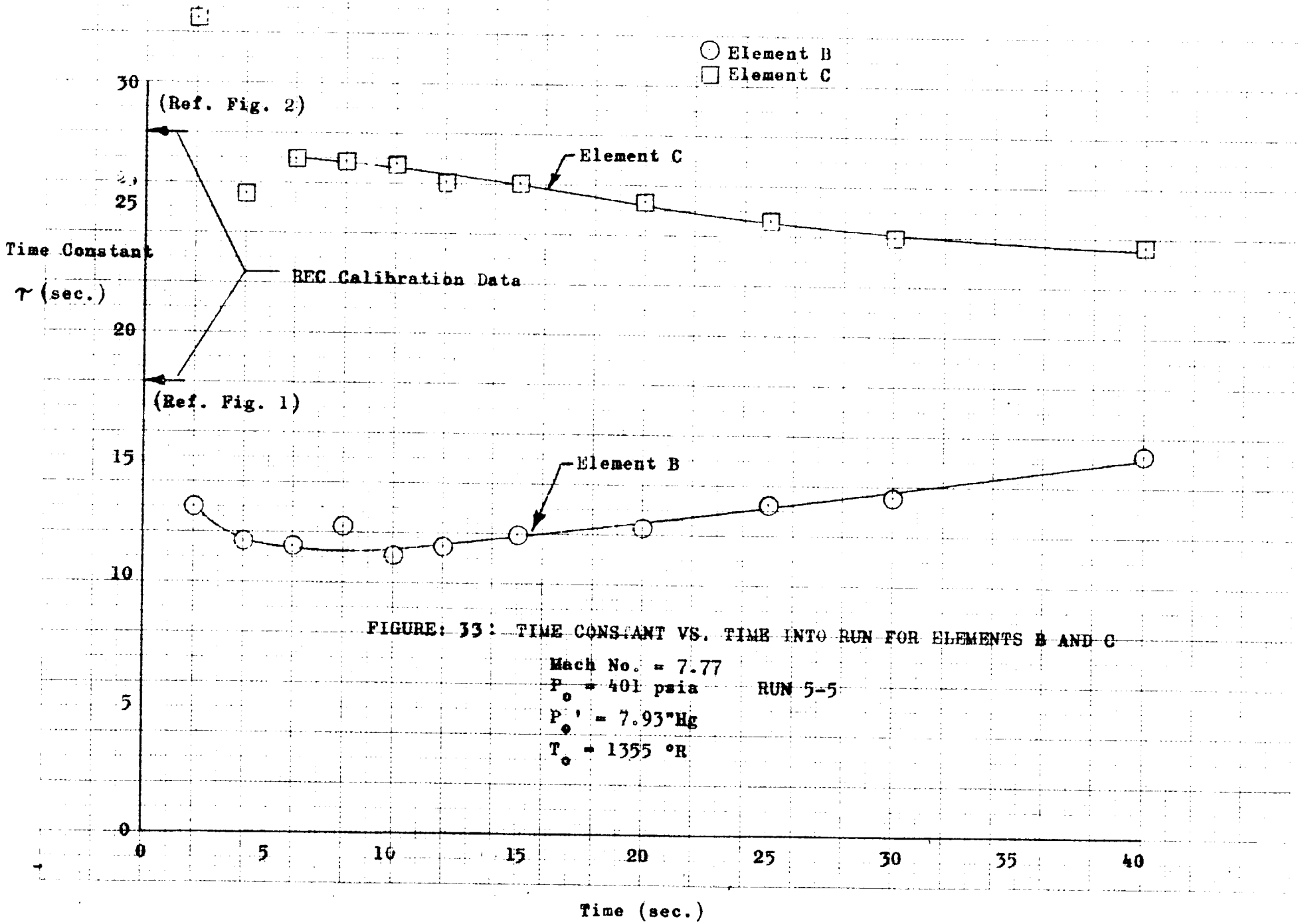

FIGURE: 33 : TIME CONSTANT VS. TIME INTO RUN FOR ELEMENTS B AND C

Mach No. = 7.77
P_o = 401 psia RUN 5-5
P_o' = 7.93"Hg
T_o = 1355 °R

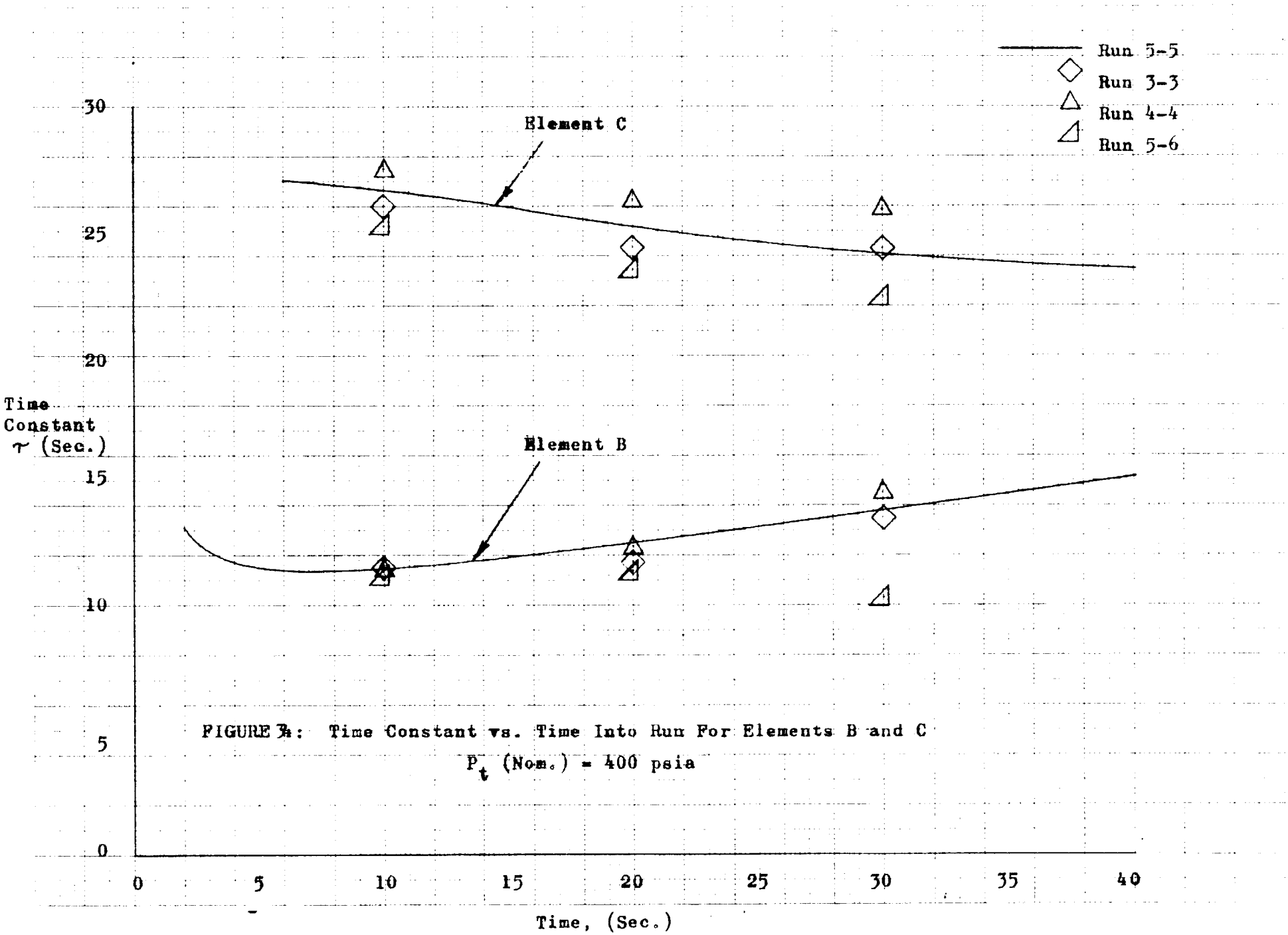

FIGURE 3a: Time Constant vs. Time Into Run For Elements B and C

P_t (Nom.) = 400 psia

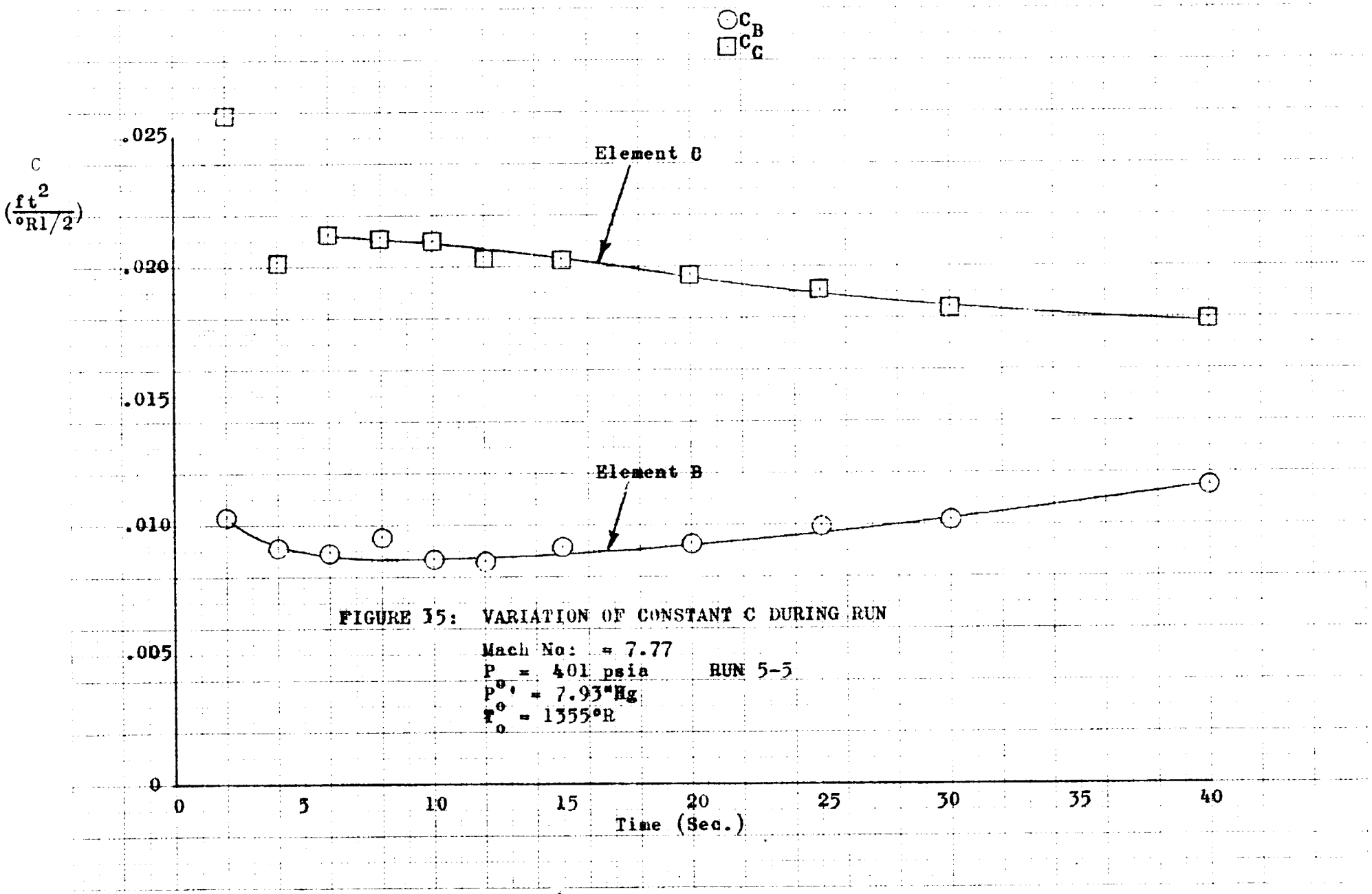

FIGURE 35: VARIATION OF CONSTANT C DURING RUN

Mach No: = 7.77
P_o = 401 psia RUN 5-5
P^o_o = 7.93"Hg
T^o_o = 1355°R

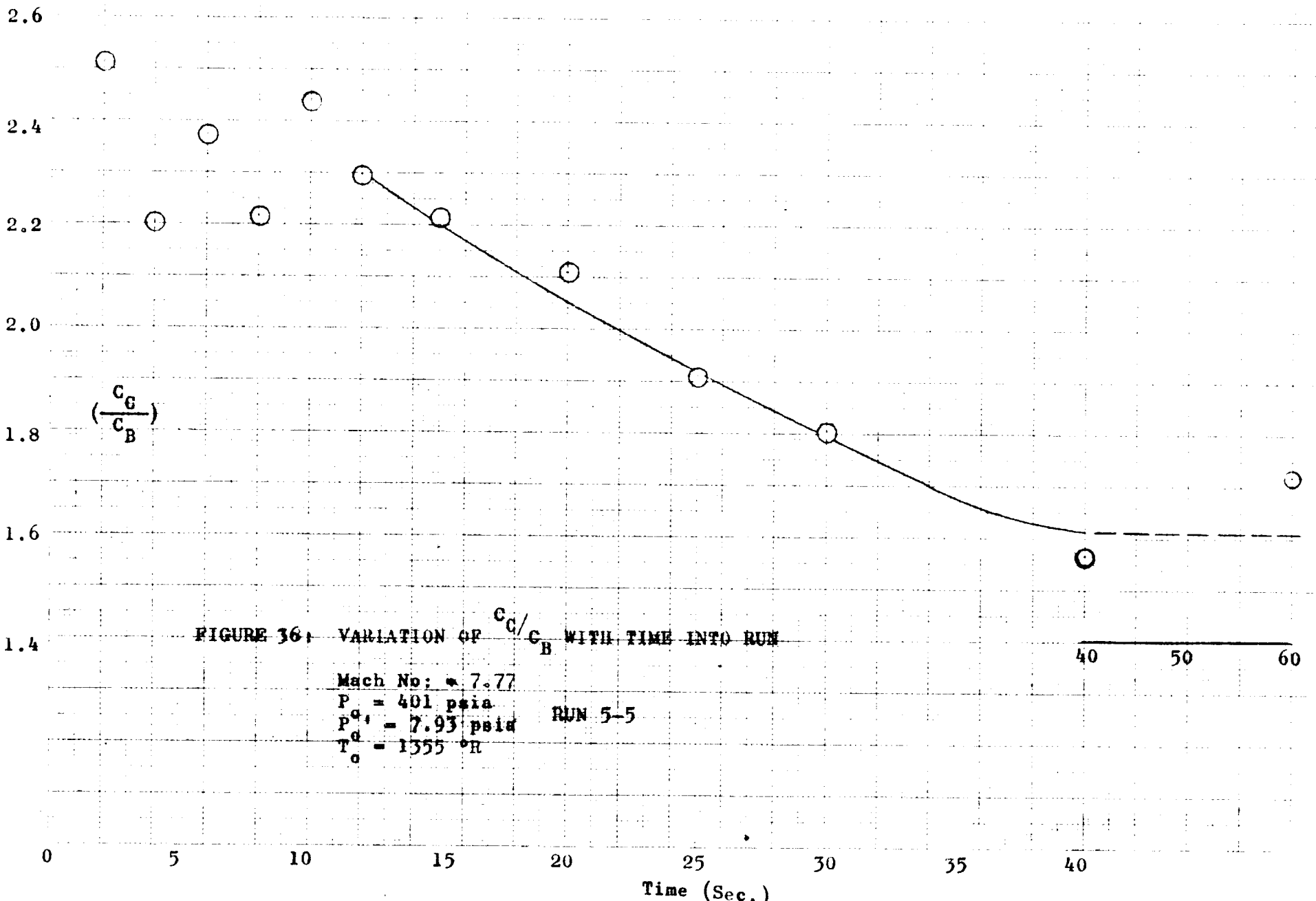

FIGURE 36: VARIATION OF C_C/C_B WITH TIME INTO RUN

Mach No: = 7.77
P_o = 401 psia
P^o_t = 7.93 psia RUN 5-5
T_o = 1355 °R

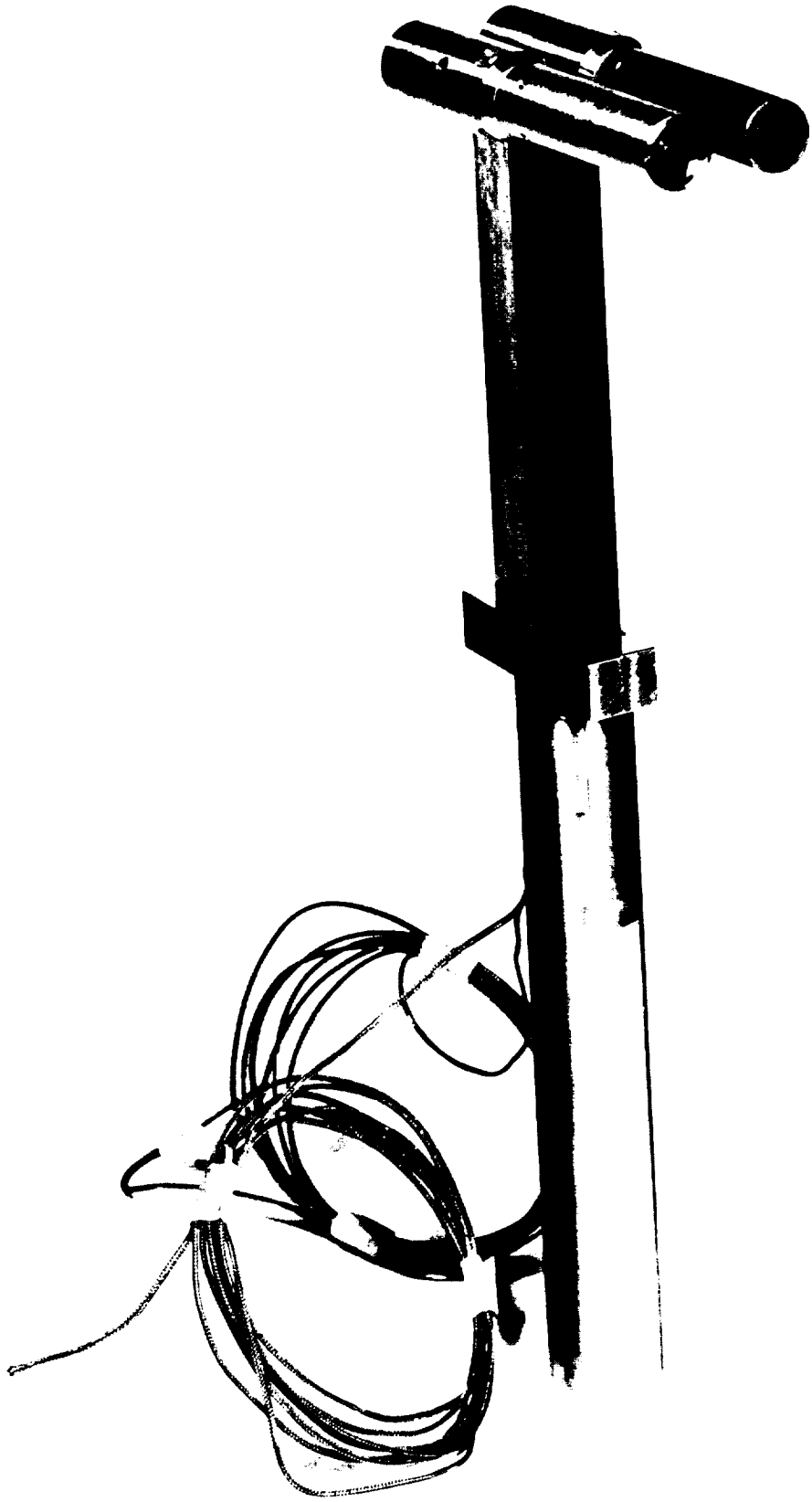

Figure 37: Photograph of Sensors B and C in Dual Sensor Wind Tunnel Mount

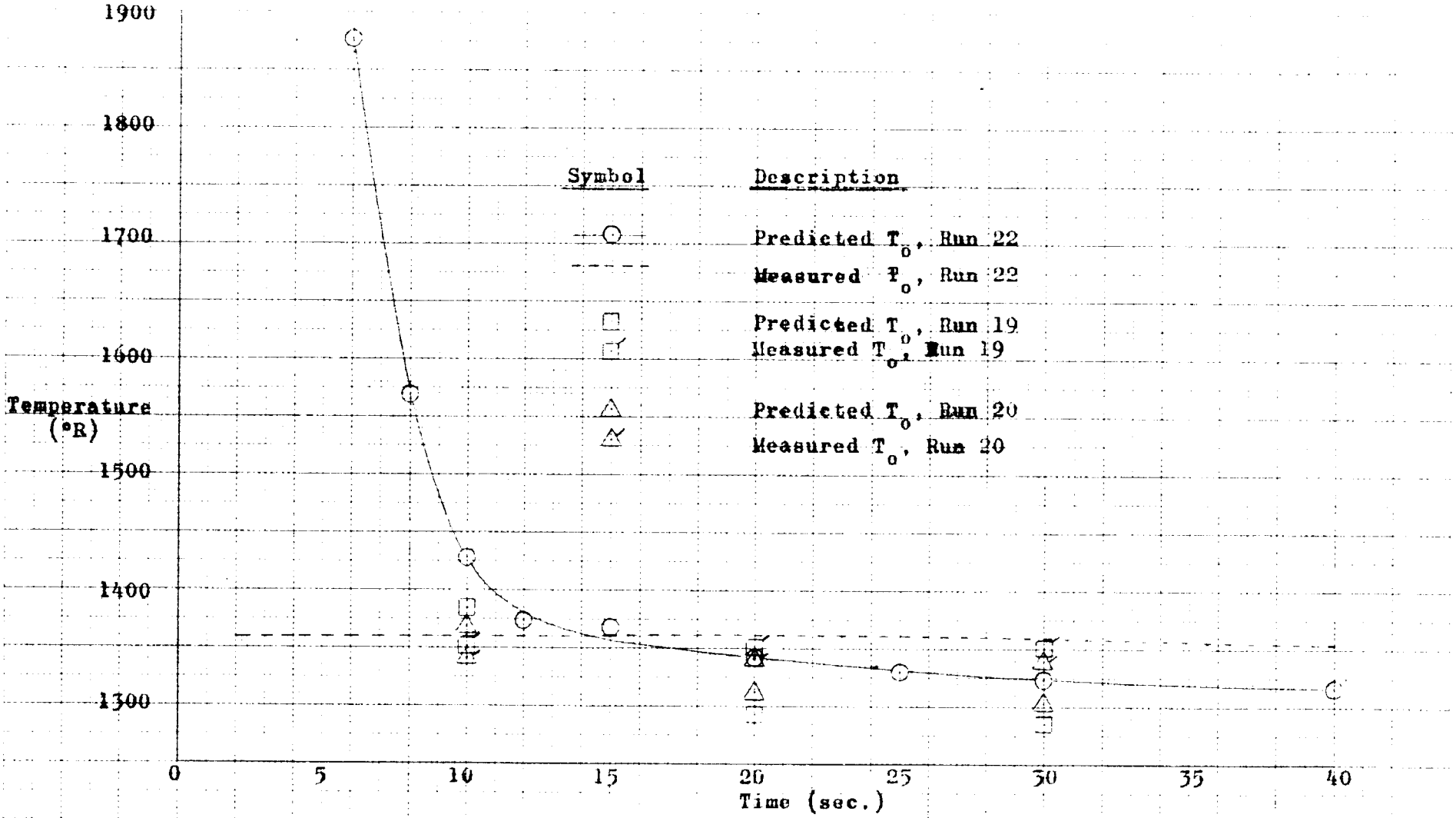

Figure 38 Predicted Total Temperature vs. Time into Run $C_C/C_B = 1.8$

Mach No. = 7.77

P_o = 400 psia (Nominal)

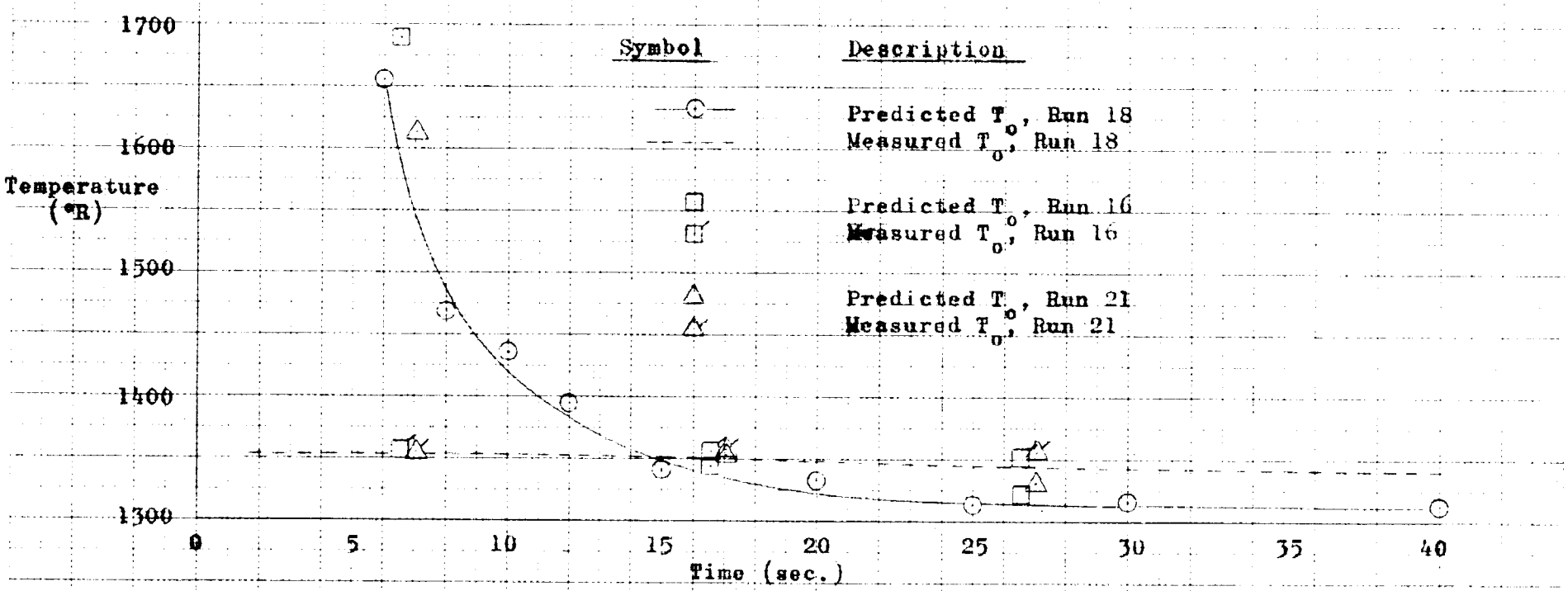

Figure 39 Predicted Total Temperature vs. Time into Run $C_C/C_B = 1.8$

Mach No. = 7.82
p_o = 600 psia (Nominal)

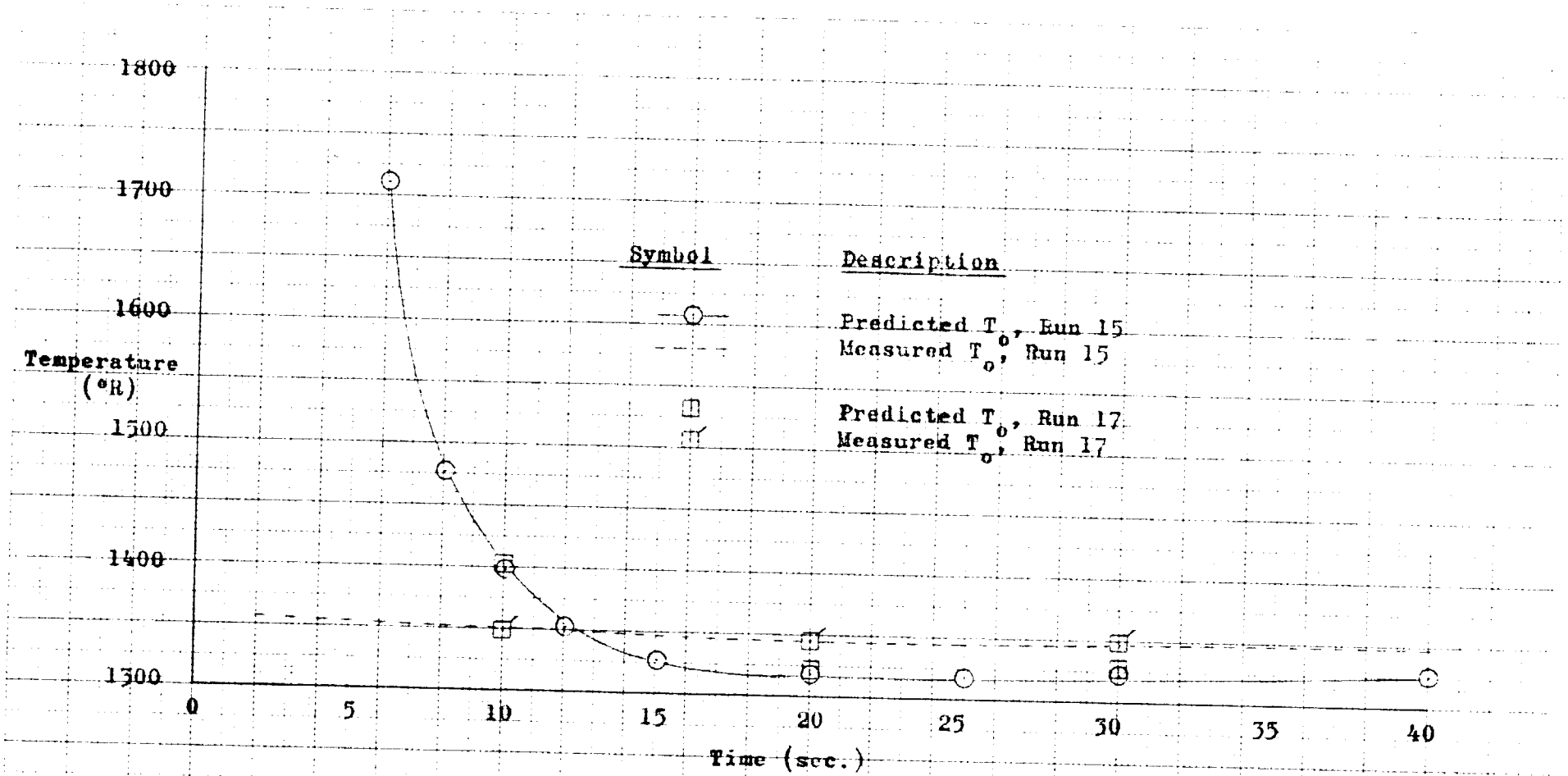

Figure 40. Predicted Total Temperature vs. Time into Run C_C/C_B=1.8

Mach No. = 7.89
P_o = 900 psia (Nominal)

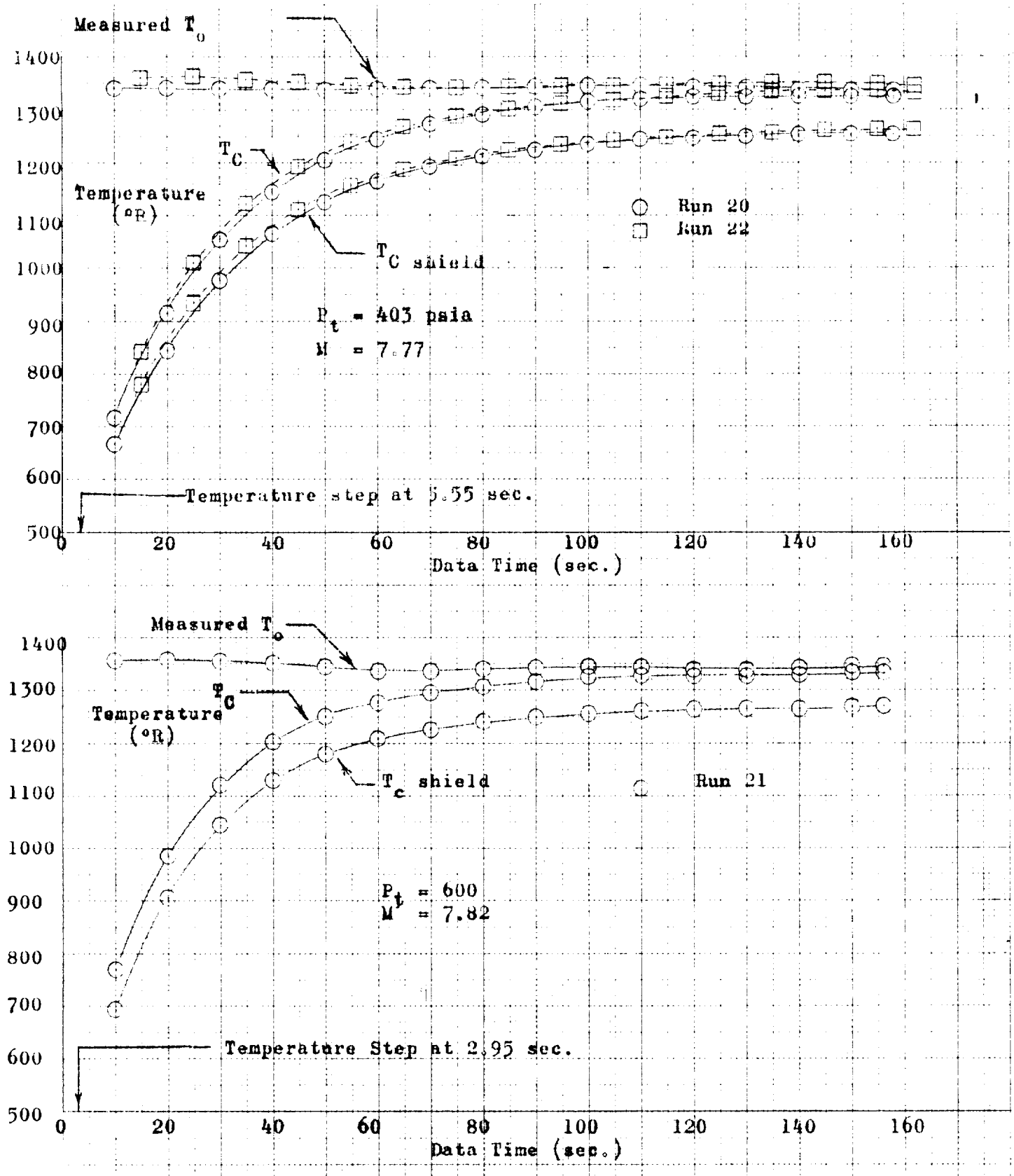

Figure 41 Comparison of Shield Surface Temperatures with Element Temperatures and Measured T_o for Sensor C, Mach 8 Wind Tunnel Runs.

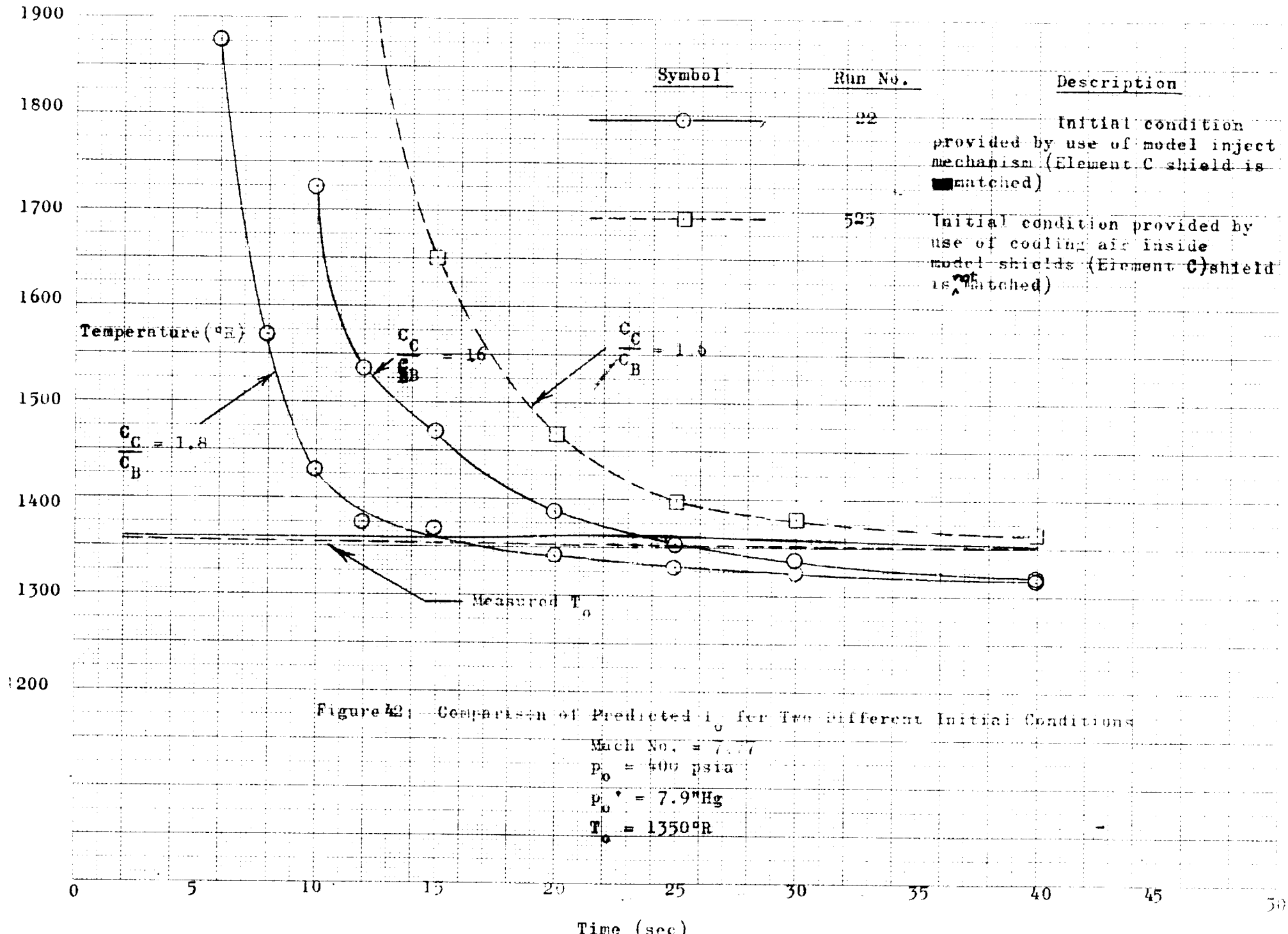

Figure 42. Comparison of Predicted i_o for Two Different Initial Conditions

Mach No. = 7.77

p_o = 400 psia

p_o' = 7.9"Hg

T_o = 1350°R

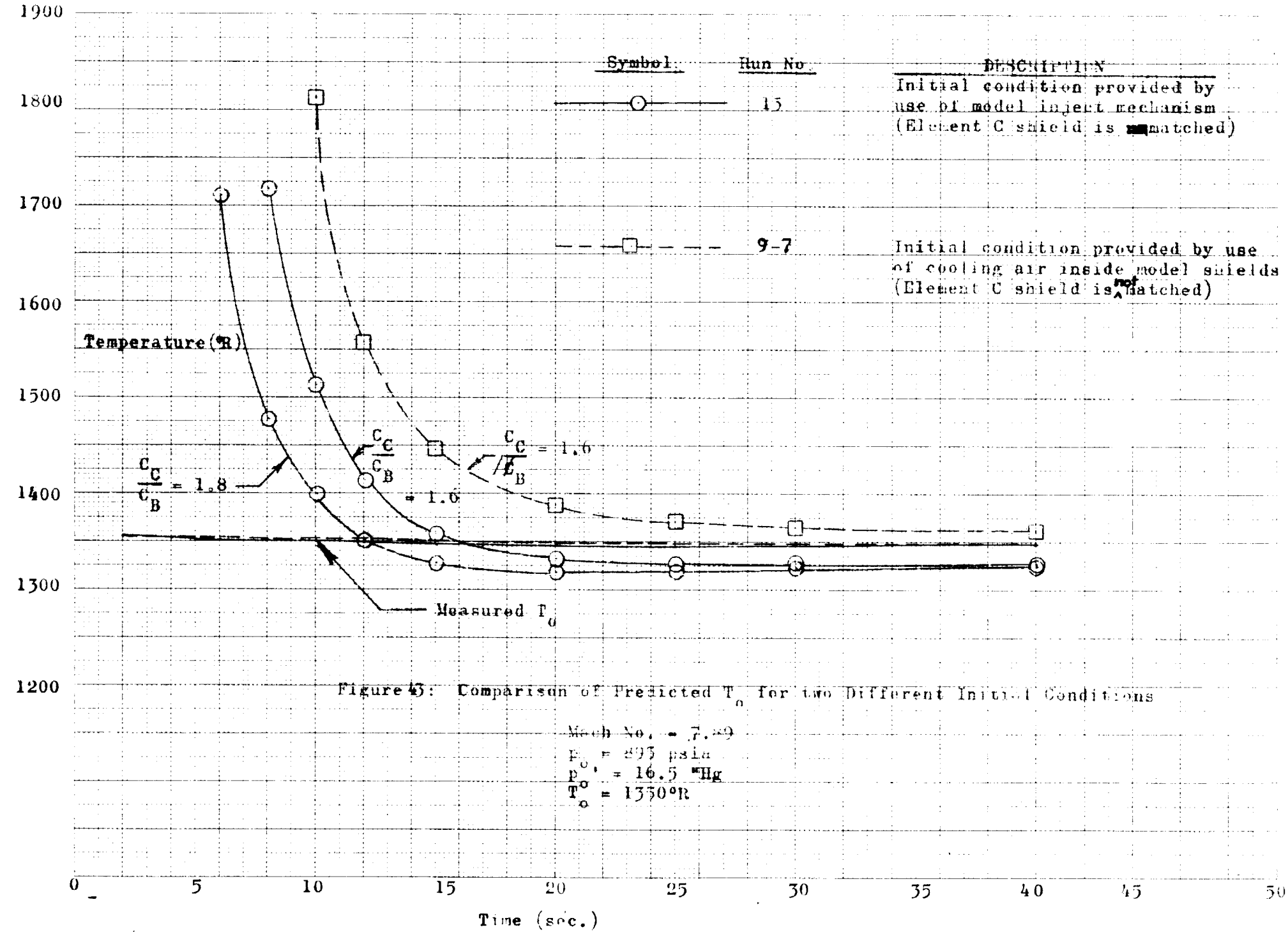

Figure 43: Comparison of Predicted T_o for two Different Initial Conditions

Mach No. = 7.89
P_o = 893 psia
p_o' = 16.5 "Hg
T_o = 1330°R

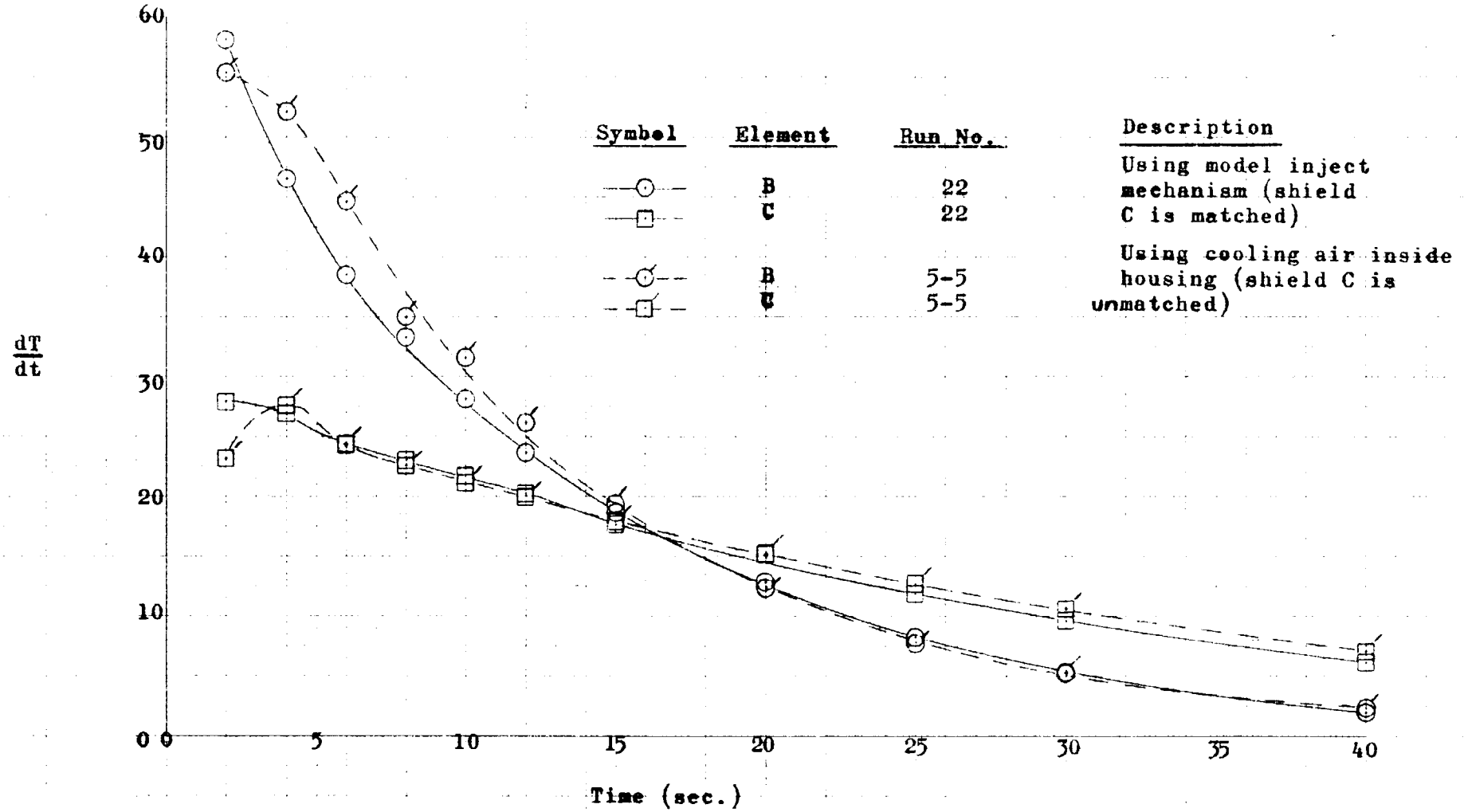

Figure 44: Comparison of Time Rate of Temperature Change for Two Different Initial Conditions, p_t = 400 psia

Nominal M = 8

Nominal T_o=1350°R

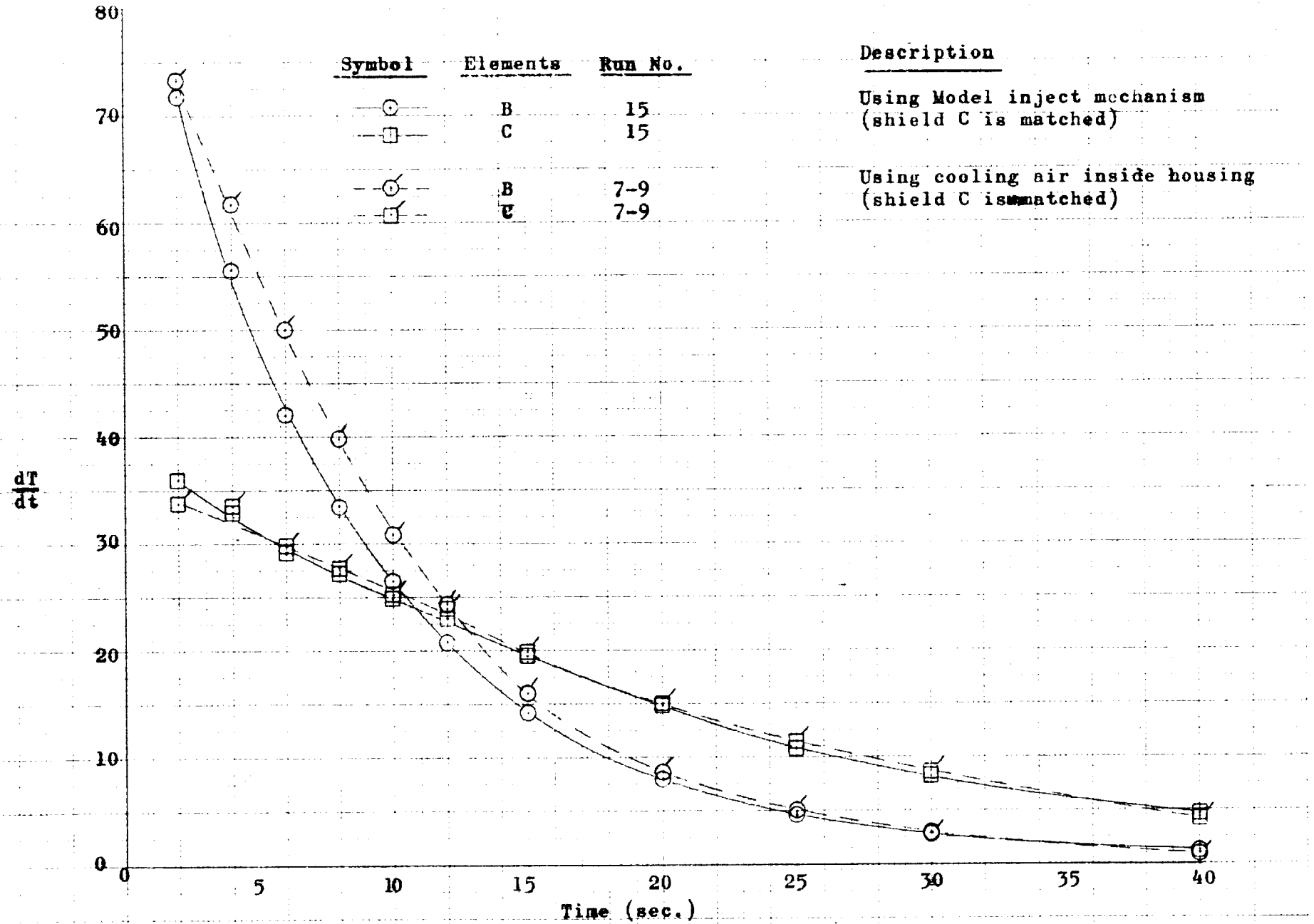

Figure 45: Comparison of Time Rate of Temperature Change for Two Different Initial Conditions, p_t = 900 psia
Nominal M = 8, Nominal T_o = 1350°R

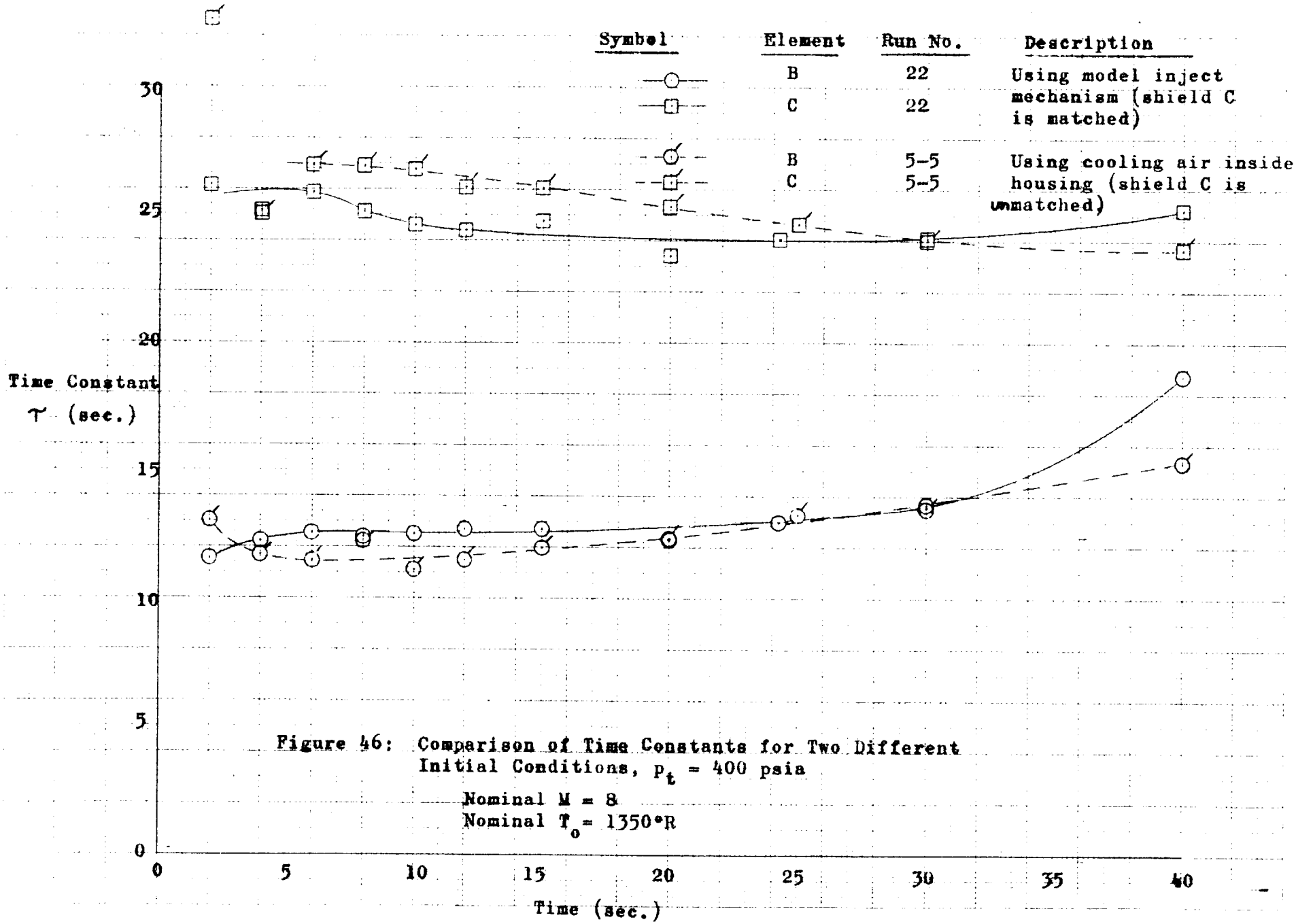

Figure 46: Comparison of Time Constants for Two Different Initial Conditions, p_t = 400 psia

Nominal M = 8
Nominal T_o = 1350°R

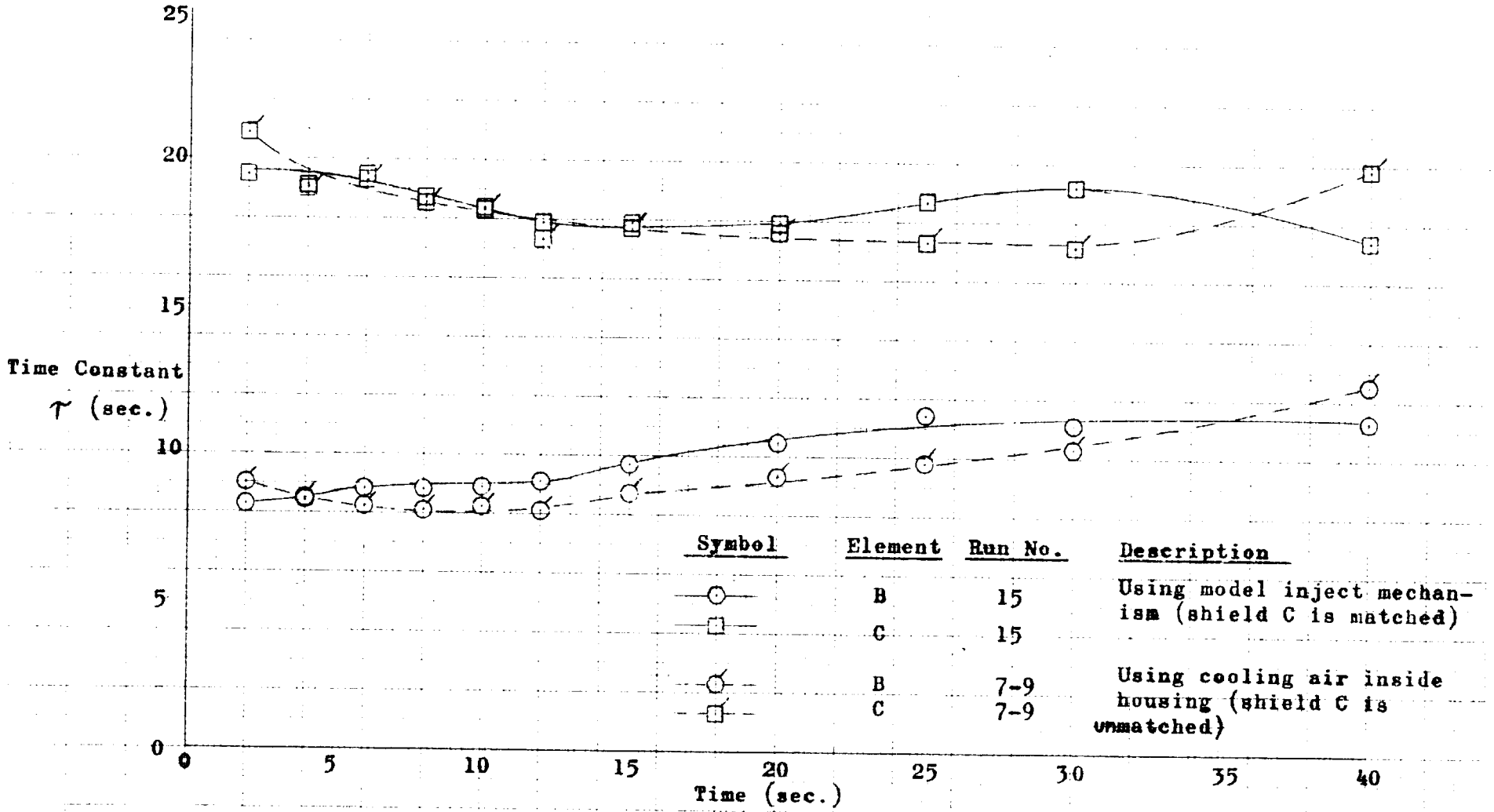

Figure 47: Comparison of Time Constants for Two Different Initial Conditions, p_t = 900 psia

Nominal M = 8

Nominal T_o = 1550°R

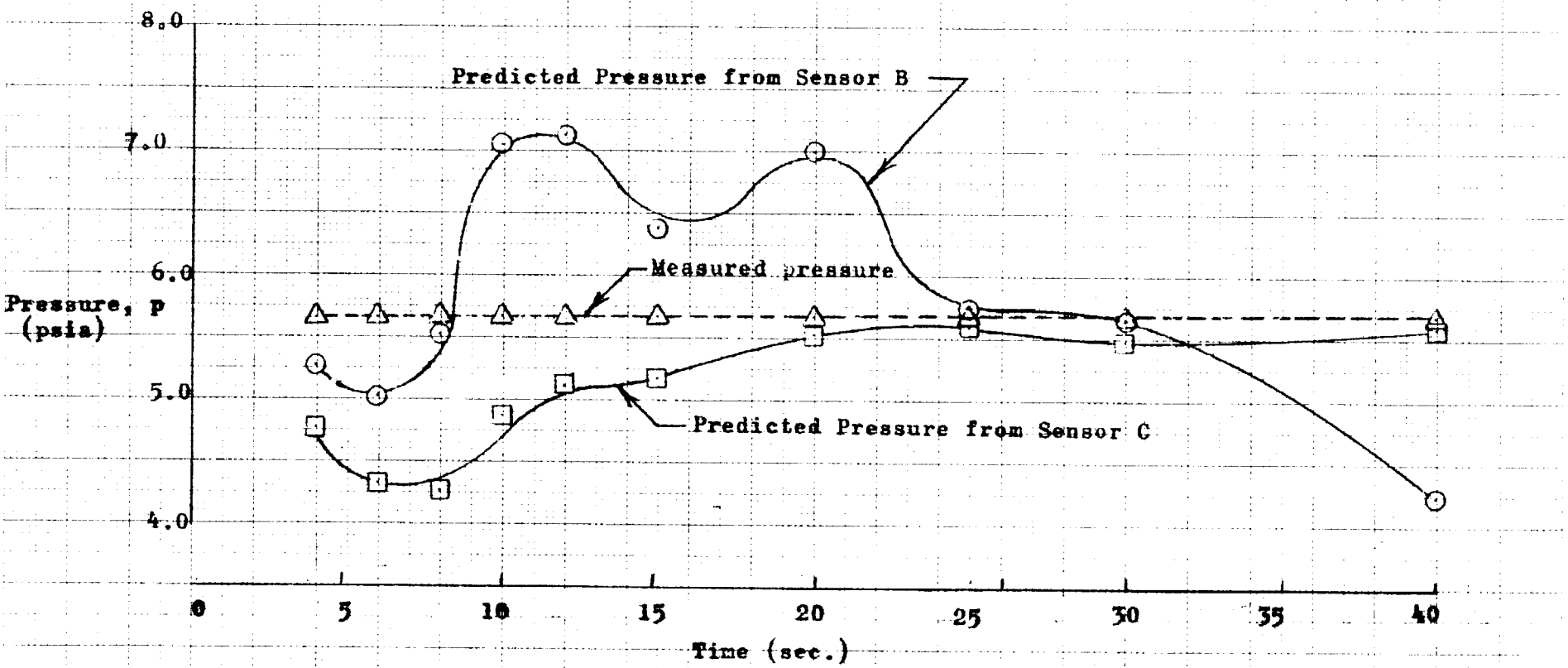

FIGURE 48

Predicted Pressure for Sensors B and C using Predicted Temperature and $C_C/C_B = 1.8$.

Run 18

M = 7.82

P_{t_1} = 601 psia (average)

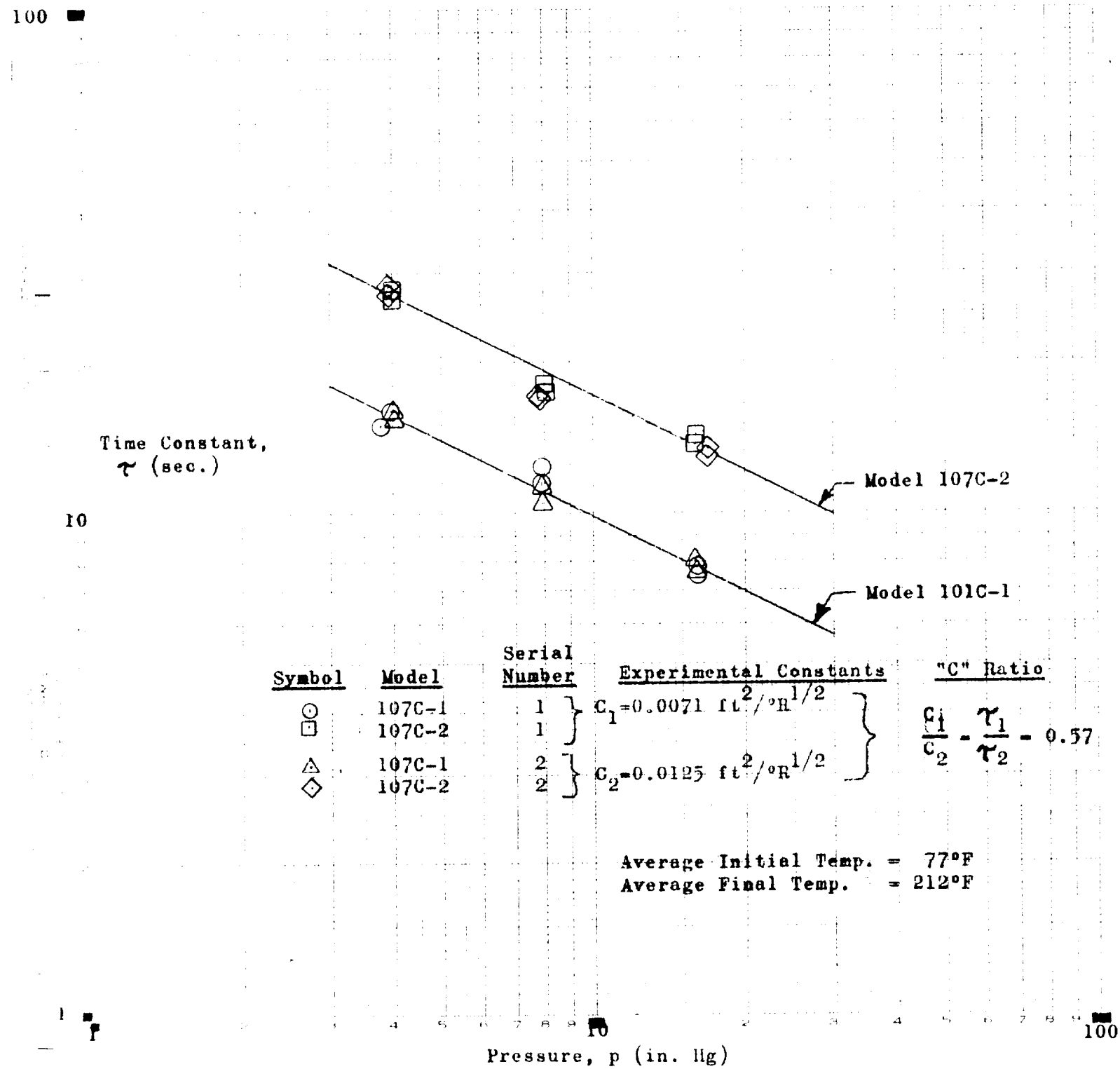

Figure 49: Calibration Data for Four Final Total Temperature Sensors

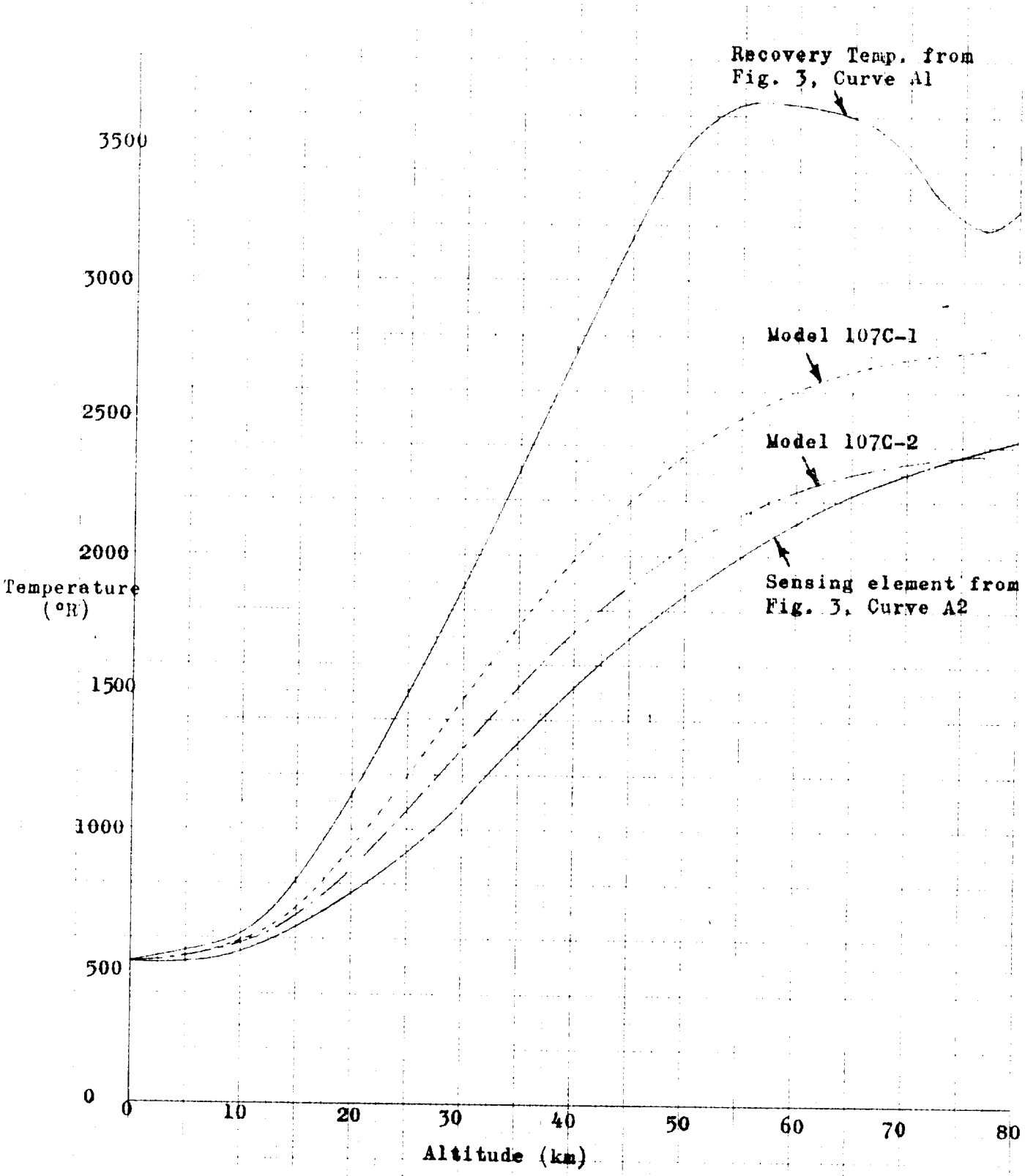

Figure 50: Predicted Dynamic Characteristics of REC Models 107C-1 and 107C-2

APPENDIX A

CALCULATION OF HEAT TRANSFER TO THE SENSING ELEMENT

The configuration factor between the sensing element and the open end of the shield, should first be calculated to evaluate the heat transfer. The configuration considered is shown in Figure 1A. It is assumed that the diameter of the sensing element is much smaller than the diameter of the shield.

The differential angle factor between the sensing element and dA_2 can be written as:

$$dF_{1-2} = \frac{\cos\beta_1 \cos\beta_2}{\pi S^2} dA_2$$

But $$\beta_1 + \beta_2 = \frac{\pi}{2}$$

Expressing $\cos\beta_1$ and $\cos\beta_2$ in terms of distances, we get:

$$dF_{1-2} = \frac{1}{\pi S^2}\left[\frac{a}{S}\ \frac{r}{S}\right] r dr d\theta$$

$$= \frac{a}{\pi}\left[\frac{r^2 dr}{S^4}\right] d\theta$$

$$= \frac{a}{\pi}\left[\frac{r^2 dr}{a^2+r^2}\right] d\theta$$

where $$S^2 = a^2 + r^2$$

To obtain the angle factor between the one half of the sensing element and half the open end we integrate dF_{1-2} as follows:

$$F_{1-2} = a \int_0^R \frac{r^2 dr}{(a^2+r^2)^2} \int_0^{\pi} \frac{d\theta}{\pi}$$

$$= a \int_0^R \frac{r^2 dr}{(a^2+r^2)^2}$$

$$= 1/2 \left[\tan^{-1} \frac{R}{a} - 1/2 \sin \left(2 \tan^{-1} \frac{R}{a} \right) \right]$$

By symmetry the other face of the sensing element has the same angle factor with the other half of the sensing element. Therefore, the total angle factor F can be written as:

$$F = \tan^{-1} \frac{R}{a} - 1/2 \sin \left(2 \tan^{-1} \frac{R}{a}\right)$$

Now the radiation heat loss from the sensing element can be written as:

$$q_R = \sigma \epsilon F \left(\frac{T}{100}\right)^4 \text{ Btu/hr. ft.}^2$$

where q_R = Radiation loss, Btu/hr. ft.^{2}

ϵ = Emissivity of the surface, = 0.08

σ = Stefan-Boltzman constant

= 0.1713×10^{-8} Btu/hr. ft.^{2} (°R)

T = Absolute temperature of the sensing element, °R

The value of F for values of a, in this range 5 to 50 mms. were calculated and thus q_R evaluated at each value of a.

Convective Heat Transfer: The convective heat transfer to the sensing element q_c is given by:

$$q_c = h(t_r - t_w)$$

where q_c = convective heat loss, Btu/hr. ft.^{2}

t_r = Recovery Temperature inside the shield, °F

t_w = Wall temperature, °F

h = heat transfer coefficient, Btu/hr. ft^2 °F

The value of h for various values of the distances from the leading edge, in the range 5-50 mms, were calculated and hence q_c evaluated.

Finally, the ratio q_c/q_R was calculated for each value of a. The results are shown graphically in Figure 1.

The values of t_r and t_w correspond to an actual flight condition at an altitude of 70 Kms. These values were taken from Figure 3.

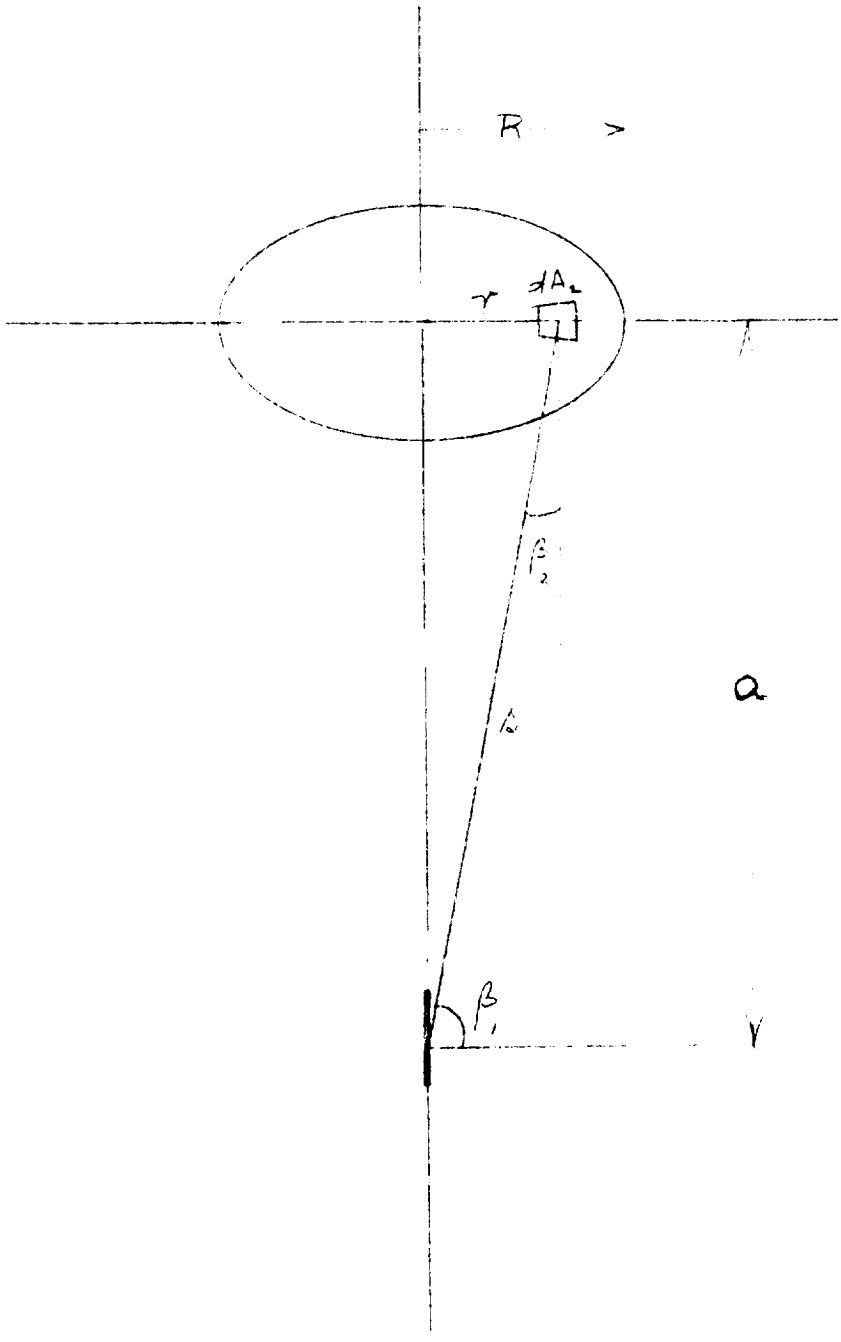

FIGURE A: Geometrical Configuration Considered

DRAWING & PART NO	REV
107C	

REVISIONS					
SYM	DESCRIPTION	REV BY	CHK'D	APP'D	DATE

SPECIFICATIONS

1. **SCOPE**. The Model 107C series of total temperature sensors are normally used in pairs which are necessary for total temperature predictions, and are designed for operation in the earth's atmosphere for flight applications to Mach number 5.0 and to altitude of 200,000 feet.

2. **GENERAL DESCRIPTION**. The Model 107C total temperature sensor has a chromel versus alumel thermocouple located within a cylindrical 347 SST sensing element. The element is shielded by a 347 SST housing consisting of inner and outer radiation shields which are separated by an enclosed circumferential gap. The sensor is designed for maximum temperature of 1400° C. Model 107C-1 and Model 107C-2 constitute the pair of sensors required for total temperature predictions. Model 107C-2 sensing element diameter is about double that of Model 107C-1.

3. **EQUATIONS FOR TEMPERATURE PREDICTIONS**. The following equation is based on dynamic temperature responses of a pair of Model 107C sensors, and is required for temperature predictions:

$$T_o = \frac{T_{w1} - T_{w2}\,(\dot{T}_1/\dot{T}_2)(C_1/C_2)}{1 - (\dot{T}_1/\dot{T}_2)(C_1/C_2)}$$

where: T_o is the predicted total temperature in °R, subscripts 1 and 2 pertain to Models 107C-1 and 107C-2, respectively; T_w is the measured element temperature; $\dot{T}$ is the time rate of temperature change, dT/dt; and C_1/C_2 is a calibration constant.

In addition to temperature predictions with a pair of sensors, pressure predictions are possible with a single Model 107C provided temperature is known. Conversely, temperature predictions are possible with a single sensor provided pressure is known.

4. **TYPICAL CALIBRATION DATA**. Typical experimental time constants measured near the beginning of the transient response to a stepped temperature change are shown in Figure 1 for Models 107C-1 and 107C-2. The calibration ratio, C_1/C_2, is the ratio of the time constants determined at the same test conditions. A typical value for $C_1/C_2 = 0.57$.

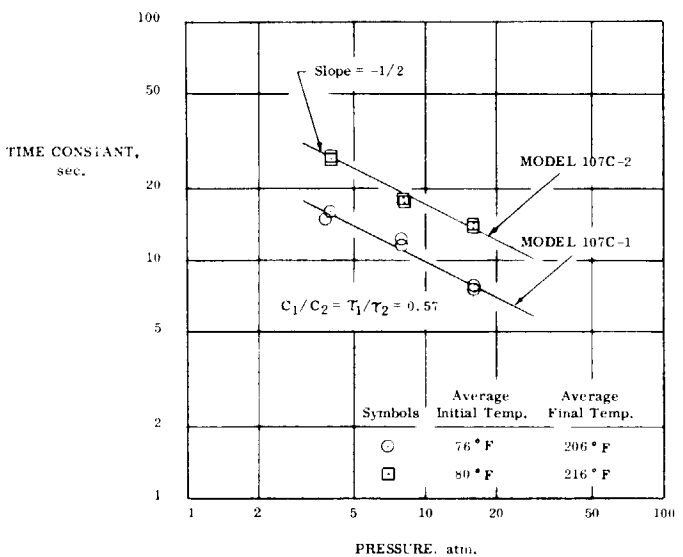

FIGURE 1: TYPICAL SENSOR CALIBRATION DATA

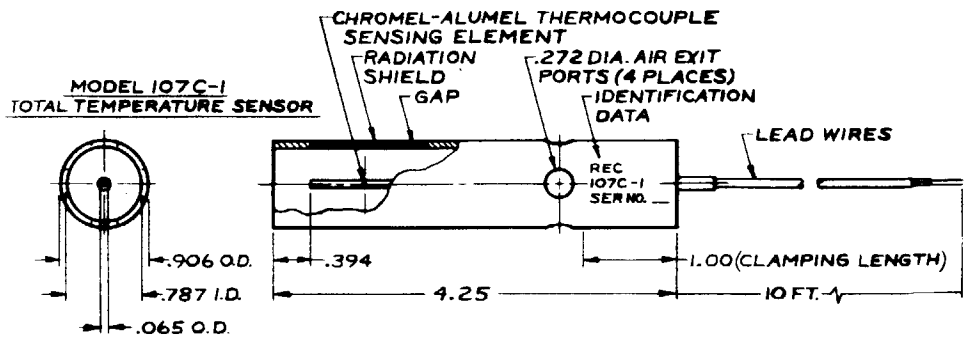

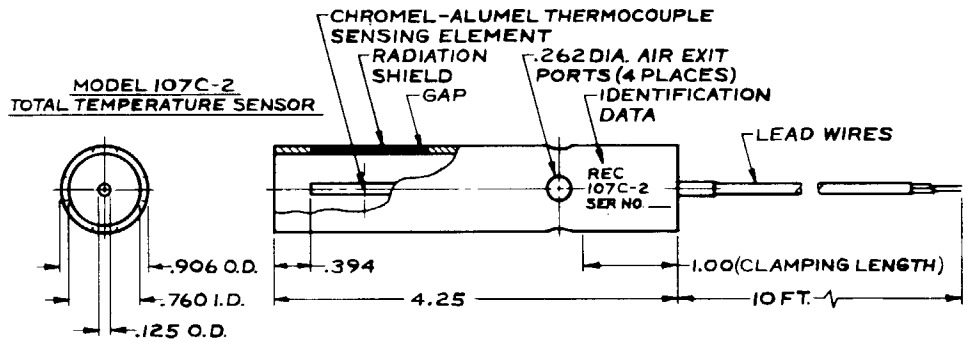

QUANTITY REQD	PART NO	ITEM NO	DESCRIPTION
			LIST OF MATERIAL

UNLESS OTHERWISE SPECIFIED
REMOVE ALL BURRS AND SHARP EDGES
MACHINE SURFACE FINISH 125
TOLERANCES:
DECIMALS: X ± 1; XX ± 02; XXX ± 010
FRACTIONS: ± 1/32
ANGLES: ± 2
HOLES: .0135 to .125 +.004 -.001; .126 to .250 +.005 -.001; .251 to .500 +.006 -.001
DO NOT SCALE PRINT

ROSEMOUNT ENGINEERING COMPANY
MINNEAPOLIS, MINN.

TITLE: SPECIFICATION DRAWING
SENSOR, TOTAL TEMPERATURE, HIGH TEMPERATURE-HIGH ALTITUDE

DR BY	DATE	CODE IDENT NO	SIZE	DRAWING & PART NO	REV
R. THORSFELDT	9-27-65	04274	C	107C	
CHK'D A. SAARI	11-2-65				
APP'D		SCALE FULL	WT	SHEET 1 OF 1	

PROPRIETARY INFORMATION IS CONTAINED HEREIN AND IS TO BE HANDLED ACCORDINGLY
DATE
DRAWING DOES NOT CONTAIN PROPRIETARY INFORMATION
DATE
IF SIGNATURE APPEARS THE UPPER STATEMENT APPLIES

APPENDIX B